INFLUENCE OF THE NONLINEAR BEHAVIOR OF SEMI-RIGID CONNECTIONS ON THE ANALYSIS OF LOW-RISE STEEL FRAMED STRUCTURES

A THESIS SUBMITTED TO
THE GRADUATE SCHOOL OF NATURAL AND APPLIED SCIENCES
OF
MIDDLE EAST TECHNICAL UNIVERSITY

BY

ZAFER KARAKAŞ

IN PARTIAL FULFILLMENT OF THE REQUIREMENTS
FOR
THE DEGREE OF MASTER OF SCIENCE
IN
CIVIL ENGINEERING

JANUARY 2017

Approval of the thesis:

INFLUENCE OF THE NONLINEAR BEHAVIOR OF SEMI-RIGID CONNECTIONS ON THE ANALYSIS OF LOW-RISE STEEL FRAMED STRUCTURES

submitted by **ZAFER KARAKAŞ** in partial fulfillment of the requirements for the degree of **Master of Science in Civil Engineering Department, Middle East Technical University** by,

Prof. Dr. Gülbin Dural Ünver
Dean, Graduate School of **Natural and Applied Sciences** _____

Prof. Dr. İsmail Özgür Yaman
Head of Department, **Civil Engineering** _____

Assoc. Prof. Dr. Afşin Sarıtaş
Supervisor, **Civil Engineering Department, METU** _____

Examining Committee Members:

Prof. Dr. Cem Topkaya
Civil Engineering Department, METU _____

Assoc. Prof. Dr. Afşin Sarıtaş
Civil Engineering Department, METU _____

Assoc. Prof. Dr. Özgür Kurç
Civil Engineering Department, METU _____

Assist. Prof. Dr. Ozan Cem Çelik
Civil Engineering Department, METU _____

Assist. Prof. Dr. Saeid Kazemzadeh Azad
Civil Engineering Department, Atılım University _____

Date: 27/01/2017

I hereby declare that all information in this document has been obtained and presented in accordance with academic rules and ethical conduct. I also declare that, as required by these rules and conduct, I have fully cited and referenced all material and results that are not original to this work.

Name, Last Name: ZAFER KARAKAŞ

Signature :

ABSTRACT

INFLUENCE OF THE NONLINEAR BEHAVIOR OF SEMI-RIGID CONNECTIONS ON THE ANALYSIS OF LOW-RISE STEEL FRAMED STRUCTURES

Karakaş, Zafer
M.S., Department of Civil Engineering
Supervisor : Assoc. Prof. Dr. Afşin Sarıtaş

January 2017, 94 pages

In this thesis, the influence of several parameters to hysteretic behavior of semi-rigid connections on general response of low-rise special moment resisting frames (SMRF) is investigated. Two different types of low-rise structures, which are presented in SAC steel project, are taken into account. 1997 NEHRP (FEMA 1997a) and 1997 AISC provisions compliant flexible (lower bound) and rigid (upper bound) frames are selected to examine the influence of nonlinear behavior of connections on structural system response. Perimeter moment frames carry all of the seismic loads. OpenSees software is used in the analyses performed as part of this study. Beams and columns are modeled using nonlinear force-based beam-column frame elements. Semi-rigid connections are modeled using zero length rotational spring elements with hysteretic material response. In order to include P-Δ effects of gravity frames in the analysis, an additional imaginary bay with a leaning dummy column is added. Stiffness and strength

due to this additional bay is negligible because leaning dummy column is pin connected at the ends and the beams are considered as rigid trusses. Nonlinear geometric effects are included by utilizing corotational transformation. Shear effect of the elements is accurately taken into consideration in the structural models. Modal, nonlinear static (pushover) and nonlinear time history analyses are conducted. The combined influences of connection's rotational stiffness, yield moment and peak moment, mild or severe pinching and presence of strength loss or no strength loss are investigated in this study. Two sets of twenty ground motion records scaled to match seismic hazard levels of 10% and 2% probability of exceedance in 50 years are used for the nonlinear time history analyses. In terms of mean and median of interstory drift ratios (IDR), low-rise SMRF with semi-rigid connections do not reach collapse prevention (CP) limit of 5%. In 84th percentile of IDR, lower bound frames exceed the limit when connections are partial strength and have severe pinching with strength loss. In 95th percentile of IDR, all frames exceed the limit.

Keywords: Semi-Rigid Connections, Nonlinear Analysis, Steel Special Moment Resisting Frames, Pinching Effect, Hysteretic Behavior

ÖZ

YARI RİJİT BAĞLANTILARIN DOĞRUSAL OLMAYAN DAVRANIŞININ AZ KATLI ÇELİK YAPILARIN ANALİZLERİ ÜZERİNDEKİ ETKİSİNİN ARAŞTIRILMASI

Karakaş, Zafer
Yüksek Lisans, İnşaat Mühendisliği Bölümü
Tez Yöneticisi : Doç. Dr. Afşin Sarıtaş

Ocak 2017 , 94 sayfa

Bu tezde, yarı rijit bağlantıların histeretik davranışına etkiyen birkaç parametrenin, az katlı özel moment dayanımlı çerçevelerdeki genel etkisi araştırılmıştır. SAC çelik projesinde sunulan iki farklı az katlı yapı türü dikkate alınmıştır. Aynı zamanda 1997 NEHRP (FEMA 1997a) ve 1997 AISC şartnamelerine de uyan bu esnek (alt limit) ve rijit (üst limit) çerçeveler, bağlantıların doğrusal olmayan davranışının yapısal sistem tepkisi üzerindeki etkisini araştırmak amacıyla seçilmiştir. Moment aktaran dış çerçeve tüm sismik yükleri taşımaktadır. Bu çalışmanın bir parçası olarak OpenSees yazılımı analizlerde kullanılmıştır. Kolon ve kirişler, doğrusal olmayan kuvvet temelli kolon-kiriş çerçeve elemanları kullanılarak modellenmiştir. Yarı rijit bağlantılar, histeretik malzeme davranışı olan noktasal dönme yay elemanları kullanılarak modellenmiştir. Moment aktarmayan çerçevelerin P-Δ etkilerini analize dahil etmek için, fiktif bir kolon içeren

bir açıklık eklenmiştir. Bu hayali açıklığa bağlı rijitlik ve dayanım ihmal edilebilir, çünkü fiktif kolon uçlarda sabit mesnetle bağlanmıştır ve kirişler de rijit çubuklar olarak kabul edilmiştir. Doğrusal olmayan geometrik etkiler, analizlere korotasyonel formülasyon kullanılarak dahil edilmiştir. Elemanların kesme etkisi gerçekçi bir şekilde modellemede dikkate alınmıştır. Hem statik itme analizi hem de zaman tanım alanında doğrusal olmayan analiz yapılmıştır. Bu çalışmada, bağlantının rotasyonel rijitlik, akma momenti ve en yüksek momenti, az ya da çok seviyede daralma, ve dayanım düşüşü olması ya da olmaması durumlarının müşterek etkileri araştırılmıştır. Zaman tanım alanında doğrusal olmayan analiz için, 50 yılda %10 aşılma olasılığı ve 50 yılda %2 aşılma olasılığı ile ölçeklendirilmiş yirmişer deprem kaydı bulunan iki set kullanılmıştır. Modal analiz, statik itme analizi ve zaman tanım alanında doğrusal olmayan analizler sonrasında elde edilen sonuçlar sunulmuştur.

Anahtar Kelimeler: Yarı Rijit Bağlantılar, Doğrusal Olmayan Analiz, Çelik Özel Moment Çerçeveler, Daralma Etkisi, Histeretik Davranış

To my family

Gönül Karakaş, M. Şefik Karakaş, Önder Karakaş and Nadiye Karakaş

ACKNOWLEDGMENTS

I would like to express my gratitude to my supervisor, Assoc. Prof. Dr. Afşin Sarıtaş, whose immense knowledge, understanding, and patience contributed to my development as a graduate student. Without his continuous support, guidance, motivation, and encouragement, this research would not be possible. It was a great honor to work with him.

Besides my supervisor, I would like to thank the committee members, Prof. Dr. Cem Topkaya, Assoc. Prof. Dr. Özgür Kurç, Assist. Prof. Dr. Ozan Cem Çelik, Assist. Prof. Dr. Saeid Kazemzadeh Azad, for their time and contributions on this thesis. Their insightful comments and suggestions, along with hard questions directed me to broaden my perspectives for the research.

This study is supported by the Scientific and Technological Research Council of Turkey (TÜBİTAK) with the project number of 113M223. I would like to express my gratitude to TÜBİTAK for their support and funding in this study.

I would like to thank Yiğit Özçelik for guidance and contributions in this thesis.

I would also like to thank fellow graduate students; Alper Aldemir, Beyazıt B. Aydın, Murat Bayraktar, Erhan Budak, İ. Ozan Demirel, Furkan Gökmen, H. Fırat Özel, Ali Can Tatar, Erman Toraman, Ertürk Tuncer and M. Burak Yeşilyurt, and my friends; Ali E. Arslan, Mustafa Çelikkaya, Candan Doğan, Berksu Erkal, Mert Kaya, Efe Orhan, Onur Özcan, Buket Şahin, Osman Taştekin and Oytun Yüksel for their support and contribution in this study.

Finally, I must express my profound gratitude to my family for providing me with continuous support and encouragement throughout my studies. This accomplishment would not be possible without them.

TABLE OF CONTENTS

LIST OF TABLES

TABLES

LIST OF FIGURES

FIGURES

LIST OF ABBREVIATIONS

β	Ratio of Peak Moment Capacity of Connection to Plastic Moment Capacity of Connecting Beam
λ	Ratio of Connection's Initial Stiffness to Flexural Rigidity of Connecting Beam
θ_s	Rotation of a Connection at Service Loads
A	Area of a Steel Section
A_v	Shear Area of a Steel Section
b_f	Flange Width of a Steel Section
d	Depth of a Steel Section
d_w	Web Depth of a Steel Section
K_c	Rotational Stiffness of Connection
K_s	Secant Stiffness of a Connection at Service Loads
M_{ch}	Post-Yielding Stiffness of Connection
M_{cp}	Peak Moment Capacity of Connection
M_{cy}	Yield Moment of Connection
M_n	Maximum Moment that a Connection Is Able to Carry
M_p^{beam}	Plastic Moment Capacity of a Beam
M_s	Moment of a Connection at Service Loads
R_μ	Ductility Reduction Factor
R_o	Overstrength Reduction Factor
t_f	Flange Thickness of a Steel Section
t_w	Web Thickness of a Steel Section
ATC	Applied Technology Council
CLE	Contingency Level Earthquake
CP	Collapse Prevention
CUREE	California Universities For Research In Earthquake Engineering
FEMA	Federal Emergency Management Agency
FR	Fully Restrained

IDR	Interstory Drift Ratio
IMF	Intermediate Moment Frames
IO	Immediate Occupancy
LB	Lower Bound
LS	Life Safety
MCE	Maximum Considered Earthquake
MRF	Moment Resisting Frame
N/A	Not Available
NEHRP	National Earthquake Hazards Reduction Program
PGA	Peak Ground Acceleration
PR	Partially Restrained
SAC	SAC Joint Venture
SEAOC	Structural Engineers Association of California
SFRS	Seismic Force Resisting System
SMF	Special Moment Frames
SMRF	Special Moment Resisting Frames
UB	Upper Bound
UBC	Uniform Building Code

CHAPTER 1

INTRODUCTION

1.1 General

Steel structural framing systems are widely used especially in developed countries. There are numerous reasons for the use of steel in construction sectors all around the world; including rapid design, fabrication and erection cycle with structural steel, useful and practical shapes globally available in the market, high strength, design simplicity resulting ease and speed of construction, sustainability, reliability and predictability of the structural steel, economy and so on.

More accurate, reliable analysis results and detailed shop drawings are obtained with combined use of building information modelling, structural analysis programs and computer-aided design software. However, in the modelling stage of the steel buildings, some assumptions are made about connections. The behavior of connections has considerable influence on the analysis of structures. Connections are designed by using the assumption of a fully rigid or ideally pinned connection behavior for simplicity in conventional practice. A fully rigid connection prevents rotation between the connected members, and completely transfers the end moment of one member to the other one. On the other hand, an ideally pinned connection allows rotation between the connected members, and moment transfer is negligible. Even though the popularity of these idealized models is based on their simplicity and being easy to implement in the design and analysis of steel framing systems, this simplification may lead to an incor-

rect estimation of frame behavior. In reality, the behavior of any connection is between these two idealized extreme conditions. These connections, which are called semi-rigid connections, also possess some rotational stiffness. It is important to include the real behavior of the semi-rigid connections in the structural modelling and analysis stage.

The magnitude 6.7 Northridge Earthquake in 1994 caused beam-to-column fractures in more than 150 buildings with steel moment resisting frames [9, 21]. Even though the buildings were in different state damage ranging from minor cracking to completely damaged columns, the most common damage that the earthquake caused was observed in the weld of the girder bottom flange to the column flange [11, 27], and brittle failures were occurred in these rigid beam-to-column connections [18]. No structural collapse was reported after the Northridge Earthquake, but the damage costs more than $7 billion [18]. Common practice in selection of structural framing to carry seismic loads before the earthquake was welded steel moment resisting frame (MRF). These connections have great moment capacities, but failed in brittle manner after reaching their capacities and caused severe damage to buildings in Northridge Earthquake. Having great moment capacities is not the only criteria for a beam-to-column connection to be earthquake resistant. Besides having sufficient moment capacity, connections should have sufficient ductility and energy dissipation characteristics, as well.

As result of these observations, it was clear that moment resisting framed buildings compliant to design and construction procedures failed to provide the intended performance level. The SAC Joint Venture (SAC), which is funded by the Federal Emergency Management Agency (FEMA), was formed by the Structural Engineers Association of California (SEAOC), the Applied Technology Council (ATC) and the California Universities for Research in Earthquake Engineering (CUREE) in mid-1994 so as to investigate the damage to welded steel moment frame buildings in the 1994 Northridge Earthquake and develop repair techniques and new design approaches to minimize damage to steel moment frame buildings in future earthquakes [24]. The SAC Steel Project consisted of two phases. The first phase concerned mainly with the problem of existing damaged buildings and concentrated on developing interim guidelines related to inspec-

tion, evaluation, repair and construction of steel moment buildings. The second phase focused on the development of performance based guidelines for the seismic evaluation and design of steel moment frame structures. Results were published in FEMA 267 [36, 37].

As part of Phase 2, research on performance prediction and evaluation for three classes of steel MRF buildings was conducted in the report no. SAC/BD-00/25 in 2000 [24]. First, post-Northridge buildings were designed in accordance with 1997 NEHRP (FEMA 1997a) and 1997 AISC provisions. Second, pre-Northridge buildings were designed in accordance with past UBC provisions and with pre-Northridge fully welded connections. Third, performance prediction and evaluation on damaged buildings following an earthquake was conducted.

It is very important to analyze and investigate the real behavior of special moment resisting steel framed structures since they are used in regions of high seismicity. A thorough assessment of the nonlinear response of these structures requires accurate modelling of member and connection behaviors during the modelling and analysis stages. It is known that nonlinear time history analysis provides the most accurate analysis approach to get this assessment, but this mostly comes at a cost in solution time. In this thesis, such a demanding task has been undertaken in order to study the influence of stiffness, strength, ductility and energy dissipation characteristics of a connection on the overall response of low-rise special steel moment resisting frames.

Next, description on steel connections and literature survey on studies investigating nonlinear behavior of semi-rigid connections on framed structures will be presented.

1.2 Structural Steel Connections

There are two types of connections in AISC 360-10; simple connections and moment connections [6]. In a simple connection, a negligible moment is transferred and unrestrained relative rotation is allowed between the connected members. In a moment connection, transferred moment cannot be neglected. There are

two types of moment connections; fully restrained (FR) and partially restrained (PR) moment connections. In an FR connection, moment is transferred with negligible rotation between the connected members. There must be sufficient strength and stiffness to retain the angle between the connected members at the strength limit states in an FR connection [6]. In a PR connection, moment is transferred with non-negligible rotation between the connected members. There must be sufficient strength, stiffness and deformation capacity in the component elements of a PR connection at the strength limit states [6].

1.2.1 Semi-Rigid Connections

In the analysis and design stages of steel framed structures, connection behavior is generally modelled as two idealized extreme cases, such as a fully rigid behavior or ideally pinned behavior. These two connection behavior idealizations bring simplicity to the analysis and design, but the real response of the structure does not match with the predicted response of the idealized structure. The main reason is that connections do not behave in two idealized extreme cases, but they show semi-rigid connection behavior that can significantly affect internal force distribution and structural displacements in the structural members. It is obvious that analysis and design of a steel framed structure based on idealized connection behavior rather than realistic connection behavior may lead to unrealistic response of steel structures. Hence, semi-rigid connection behavior should be implemented in the analysis and design instead of idealized connection behaviors.

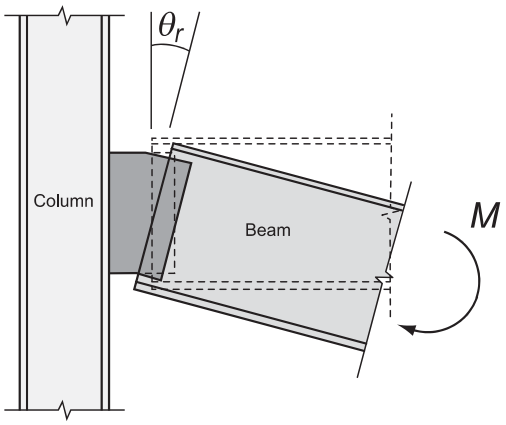

Figure 1.1: Rotational deformation of a connection [13]

1.2.2 Connection Classification

Although an axial force, a shear force and a bending moment are applied on a beam-to column connection, the deformation caused by bending moment is much greater than the deformation by the other two actions when they are compared. Rotational deformation of a connection is shown in Figure 1.1. Thus; it makes more sense to represent a connection behavior with moment-rotation (M-θ) curves, shown in Figure 1.2.

There have been proposals in order to classify the connections in the literature. Bjorhovde et al. [8] classified connections by stiffness and strength of connections. Connection classification in Eurocode 3 is based on rotational stiffness and strength [17]. Furthermore, AISC 360-10 proposes that connections are classified according to connection stiffness, connection strength and connection ductility [6]. Hence, past research and design codes classify the connections by stiffness, strength and ductility of a connection.

1.2.2.1 Stiffness

Most of the connections demonstrate nonlinear behavior right from the beginning at very low moment-rotation values. As seen in Figure 1.3, the very first tangent at zero moment-rotation point mostly gives rise to a unrealistically high initial stiffness description under service level loads. Thus, secant stiffness is taken

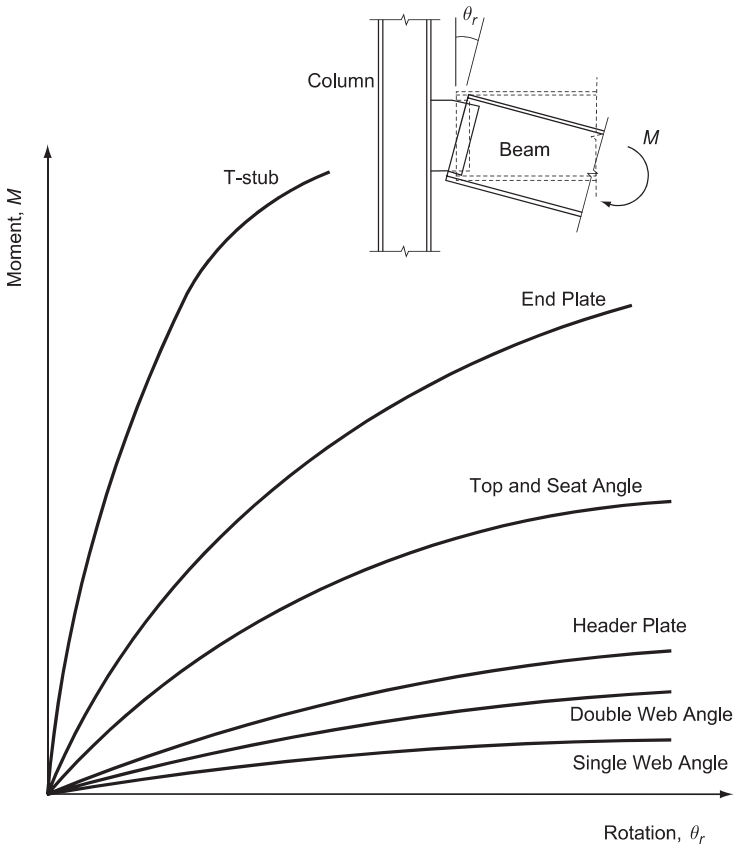

Figure 1.2: Moment-Rotation behavior of a connection [13]

as an index to define the initial stiffness of connections. The secant stiffness at service loads is defined as $K_s = M_s/\theta_s$, where M_s and θ_s are moment and rotation at service loads, respectively. The rigidity of the connection is classified in Table 1.1, where λ is the ratio of connection's secant stiffness to beam's flexural rigidity, $\lambda = K_s/(EI/L)_{beam}$, L is the length of the beam, and EI is the flexural rigidity of the beam.

Table 1.1: Connection classification by stiffness

Connection	**Stiffness**
Simple	$\lambda \leq 2$
Semi-rigid, (or PR)	$2 < \lambda < 20$
FR	$\lambda \geq 20$

A value of λ on the scale from 2 to 20 indicates stiffness level of a connec-

tion. When getting closer to 2, the connection becomes more flexible. Similarly, when getting closer to 20, the connection becomes stiffer. A representation of moment-rotation responses for simple, PR and FR connections are illustrated in Figure 1.4.

1.2.2.2 Strength

The maximum moment that a connection is able to carry, M_n, is called the maximum strength of a connection, which is demonstrated in Figure 1.3. If the connection strength is exceeded by the beam strength, the ductility of the connection becomes important [12]. The strength of a connection can be determined in two ways; an ultimate limit-state model of the connection, or a physical test. If M-θ response of a connection does not exhibit a peak load, the moment at a rotation of 0.02 rad is then taken as the strength of a connection. The strength of a connection is classified in Table 1.2, where M_p^{beam} is the plastic moment capacity of the beam and M is the strength of the connection.

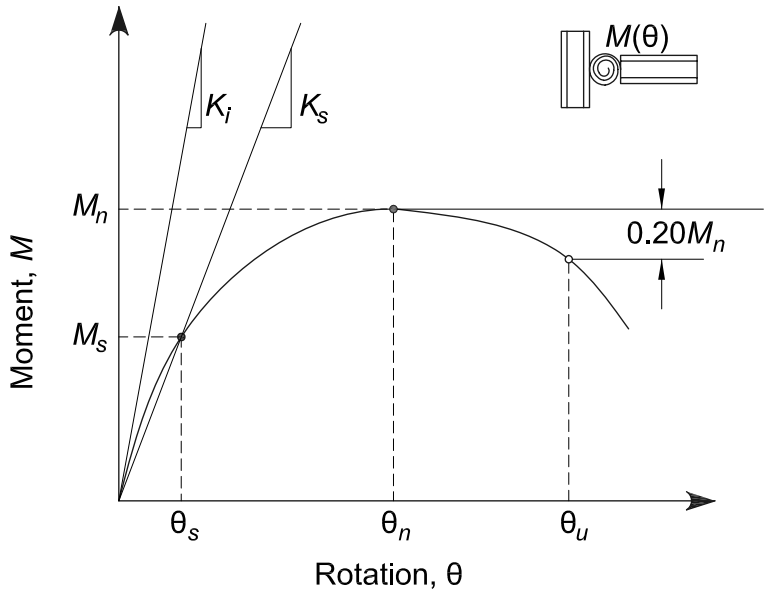

Figure 1.3: Definition of stiffness, strength and ductility characteristics of the moment-rotation response of a partially restrained connection [6]

In Figure 1.4, the points marked as M_n, θ_s and θ_u are the maximum strength states, the service load states and the maximum rotation states of a connection,

Table 1.2: Connection classification by strength

Connection	**Strength**
Full Strength (FS)	$M_n \geq M_p^{beam}$
Partial Strength (PS)	$M_n \leq M_p^{beam}$
No flexural strength	$M \leq 0.2M_p^{beam}$ at $\theta = 0.02rad$

respectively. It is possible that strength of an FR connection is less than the strength of the beam and strength of a PR connection is greater than the strength of the connecting beam. The moment demands in a connection must be met by the strength of the connection.

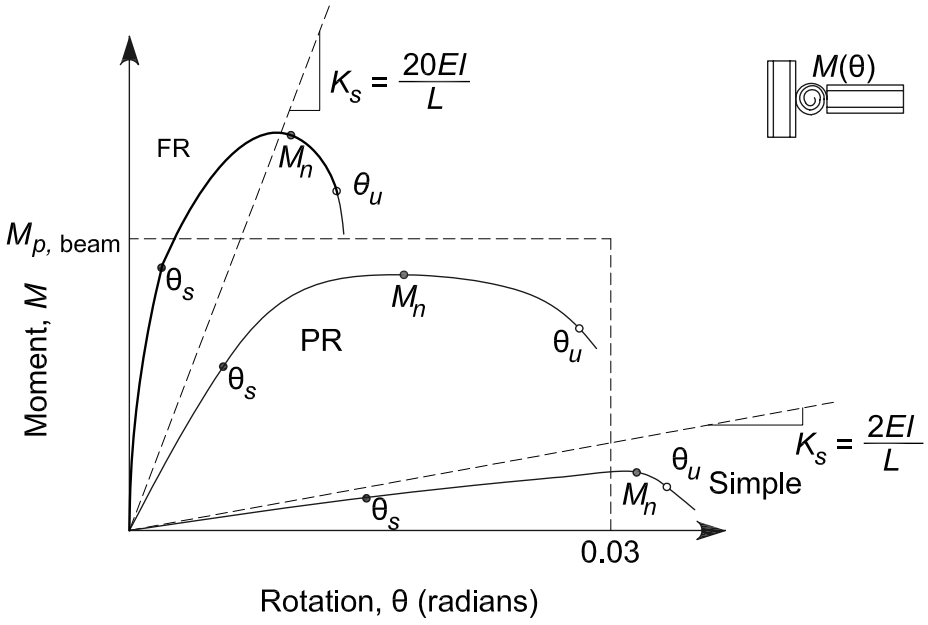

Figure 1.4: Classification of moment-rotation response of fully restrained (FR), partially restrained (PR) and simple connections. [6]

1.2.2.3 Ductility

Ductility of a connection is another important parameter, especially when deformations are concentrated in a PS connection. If the strength of a connection is much greater than the fully plastic moment of the beam, then the beam controls the ductility of the structural system and the connection is considered as elastic connection. If the strength of a connection is slightly greater than the fully plastic moment of the beam, inelastic deformation in the connection might occur before the beam reaches its full strength. If the strength of the beam is greater than the strength of a connection, then deformations can concentrate in the connection. The required ductility of a connection depends on the particular application.

The rotation capacity (θ_u) in Figure 1.3 represents the value of the connection rotation at the point where either the resisting strength of the connection has dropped to 80% of its maximum value or the connection has deformed beyond 0.03 rad [6]. Moreover, it is required that a beam-to-column connection used in the seismic force resisting system (SFRS) must accommodate a story drift angle of at least 0.04 rad in Seismic Provisions for Structural Steel Buildings (AISC 341-10) for Special Moment Frames (SMF) [5]. For Intermediate Moment Frames (IMF), it is required that a beam-to-column connection must accommodate a story drift angle of at least 0.02 rad in AISC 341-10 [5].

1.3 Types of Semi-Rigid Connections

The representative M-θ responses of some of commonly used types of semi-rigid connections are shown in Figure 1.2. Single web-angle connections perform with the lowest stiffness and strength, whereas T-stub connection perform with the highest stiffness and strength.

1.3.1 Single Web-Angle and Single Plate Connections

An angle connects the column flange to the beam web with either weld or bolts in single web-angle connections, as shown in Figure 1.5. A plate connects the members with either weld or bolts in single plate connections, as shown in Figure 1.6. Because one side of the plate is fully welded with the column flange, it is considered that the moment rigidity of the single plate connections is equal to or greater than the single web-angle connections [13].

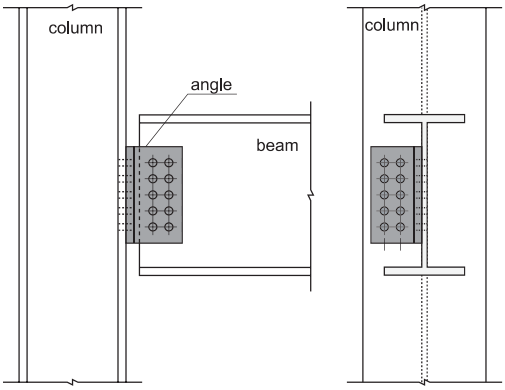

Figure 1.5: Single web-angle connection [13].

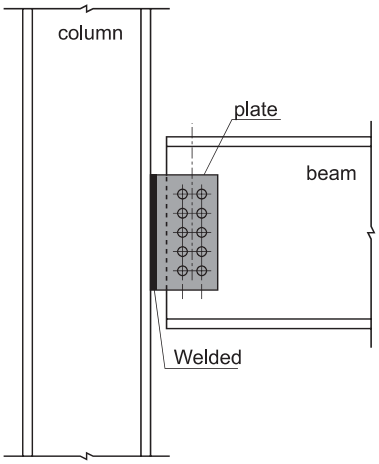

Figure 1.6: Single plate connection [13].

1.3.2 Double Web-Angle Connections

Two angles connect the column flange to the beam web with either bolts or rivets in double web-angle connections, as shown in Figure 1.7. It is considered

that the moment rigidity of the double web-angle connections almost doubles the moment rigidity of the single web-angle connections [13].

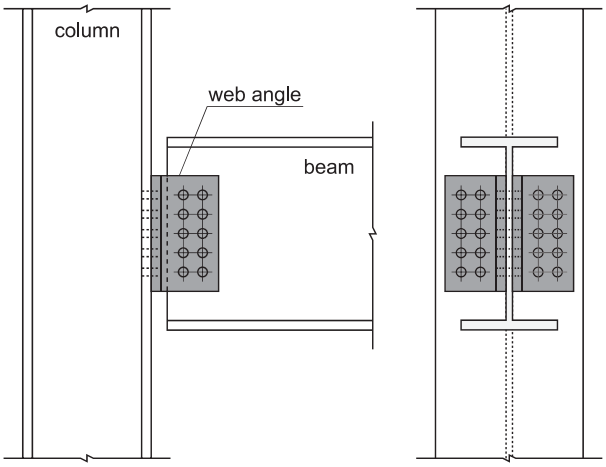

Figure 1.7: Double web-angle connection [13].

1.3.3 Top- and Seat-Angle Connection

Two angles connect the column flange to the beam's top and bottom flanges in top- and seat-angle connection, as shown in Figure 1.8. The top-angle provides lateral support for the compression flange of the beam. The seat-angle, on the other hand, transfers only vertical shear forces coming from the beam to the column, and should not apply a significant restraining moment to the end of the beam [13].

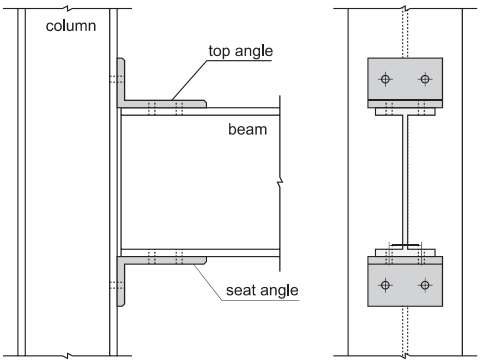

Figure 1.8: Top- and seat-angle connection [13].

1.3.4 Top- and Seat-Angle with Double Web-Angle Connections

A combination of four angles connects the beam and column in top- and seat-angle connection with a double web-angle. A set of two angles connects the column flange to the beam's top and bottom flanges and the other set connects the column flange to the beam web, as shown in Figure 1.9. Comparing to top- and seat-angle connection, top- and seat-angle connection with a double web-angle is more rigid than top- and seat-angle connection [13].

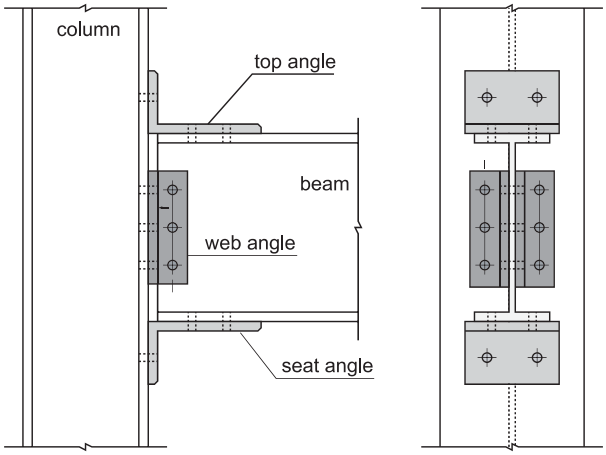

Figure 1.9: Top- and seat-angle connection with a double web-angle [13].

1.3.5 Extended End-Plate Connections and Flush End-Plate Connections

End plates of the connections are welded to the flanges and web of the beam in fabrication stage and end-plated beam is bolted to the column on site. There can be several types of extended end-plate connections depending on the need such as end-plate extended on the tension side only or end-plate extended on both the tension and compression sides as shown in Figure 1.10 and Figure 1.11. A flush end-plate connection can be seen in Figure 1.12. The flush end-plate connection is weaker than the extended end-plate connection. Flexural deformations are minimized by adding stiffeners to the column and this affects the behavior of the end-plate connection [13].

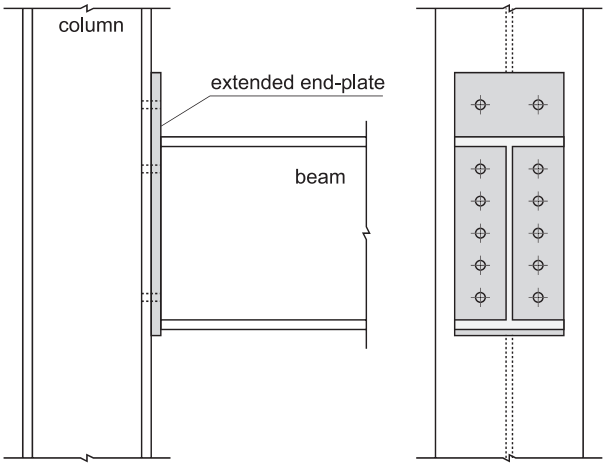

Figure 1.10: Extended end-plate connection only on tension side [13].

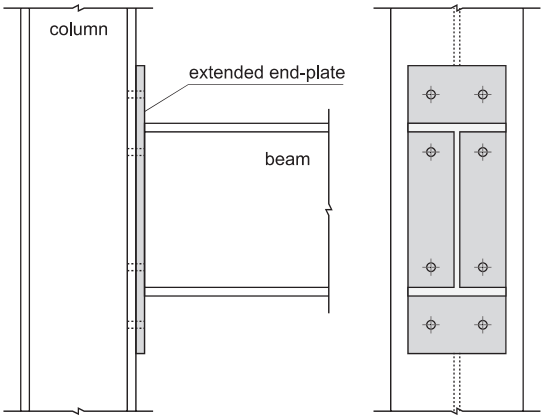

Figure 1.11: Extended end-plate connection on both tension and compression sides [13].

1.3.6 Header Plate Connections

An end plate whose length is less than the depth of the beam connects the column flange to the beam web, as shown in Figure 1.13. Similar to the construction method in extended end-plate connections, end plates of header plate connections are welded to the flanges and web of the beam in fabrication stage and end-plated beam is bolted to the column on site.

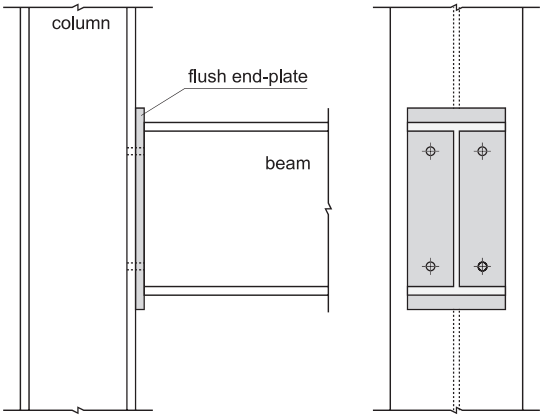

Figure 1.12: Flush end-plate connection [13].

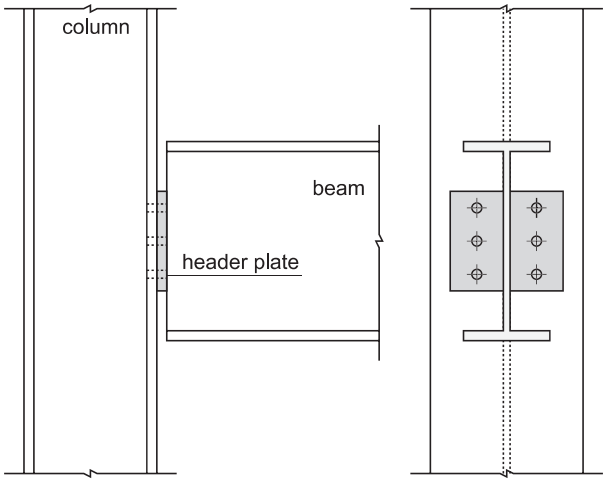

Figure 1.13: Header plate connection [13].

1.3.7 T-stub Connections

Two angles connect the column flange to the beam web with either bolts or rivets. Flanges of two tees are also connected to column flange, and their web are connected to beam's flanges from top and bottom in T-stub connections, as shown in Figure 1.14.

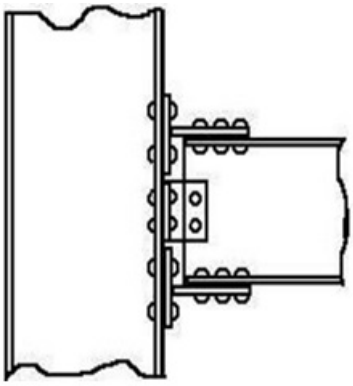

Figure 1.14: T-stub Connection

1.4 Literature Survey

1.4.1 Study of Lui and Chen (1986)

One of the earliest studies on the nonlinear behavior of steel frames having flexible connections was conducted by Lui and Chen [26]. The study was mainly based on element formulation of the beam-column element and the connection element. Numerical examples were also provided. The formulation of the beam-column element was based on an updated Lagrangian approach. The nonlinear moment-rotation behavior of the connection was utilized by an exponential function. It was reported that connection behavior affected the overall stability and ultimate strength behavior of steel frames, and that fully rigid and ideally pinned connections did not existed in reality.

1.4.2 Study of Lui and Chen (1987)

A similar study was also performed by Lui and Chen on steel frame analysis with flexible joints for sway and non-sway frames [25]. Several mathematical models to represent moment-rotation behavior of the connections were discussed, but it was concluded that there was not the best one, and each had its own advantages and disadvantages. It was revealed that connection behavior did not have an influence on frame's maximum load carrying capacity, but frames with flexible connections were observed to have more deformations. In non-sway frames, the

drifts were significantly reduced, and the nonlinear behavior of the connections was not achieved. Thus, a linear elastic frame analysis was expressed to be sufficient for flexibly connected frames loaded in the service load range.

1.4.3 Study of Elnashai and Elghazouli (1994)

A detailed study was carried out by Elnashai and Elghazouli about design and seismic behavior of semi-rigid steel frames [16]. A half of 2-story single-bay frame with rigid and semi-rigid beam-to-column connections was tested. The results from monotonic, cyclic and pseudo-dynamic tests were compared with the results from an analytical model. By using an advanced nonlinear structural analysis program ADAPTIC [22], a component-based cyclic model was developed for beam-to-column connections in analytic model. It was pointed out with both experimental and analytical studies that frames with semi-rigid connections demonstrated adequate earthquake resistance, so they had a ductile and a stable hysteretic behavior.

1.4.4 Study of Gupta and Krawinkler (1999)

A detailed study by Gupta and Krawinkler was conducted on seismic behavior of steel moment resisting frames (SMRF) [19]. All three SAC buildings (3-, 9- and 20-story buildings) were considered for three seismic zones (Los Angeles, Seattle and Boston). It was aimed to contribute to progress in the development of performance-based seismic design and to deeply understand seismic behavior of SMRF structures in this study. Both pushover and nonlinear time history analyses were conducted on DRAIN-2DX nonlinear structural analysis software [4] and seismic demand was estimated for the frames. For the time history analysis, seven sets of 20 ground motion records (3 sets for Los Angeles, 2 sets for Seattle and 2 sets for Boston) were used. It was reported that the bare steel moment resisting frames are very flexible, P-Δ effect might have great influence on the response of the structures. It was also stated that global and story drift angle demands for the post-Northridge structures are similar to those for the pre-Northridge structures.

1.4.5 Study of Maison and Kasai (2000)

A study by Maison and Kasai was carried out on seismic performance of two SAC buildings with semi-rigid connections in SAC report SAC/BD-99-16 [29]. 3-story building for Los Angeles, California and 9-story building for Seattle, Washington were considered in the study. Frames with semi-rigid connections were compared with original frames having fully restrained (FR) connections. Both pushover and time history analyses were performed on PC-ANSR nonlinear structural analysis software [28]. For the dynamic analysis, three sets of 20 ground motion records scaled to match a 10% probability of exceedance, a 2% probability of exceedance and a 50% probability of exceedance in 50 years were used. It was observed that the buildings with semi-rigid connections showed similar ductile performance with the buildings with FR connections and had more redundancy. Also, even though rotation demands in semi-rigid connections were significant, the median demands were attainable with well-designed connection details.

1.4.6 Study of Maison, Kasai and Mayangarum (2000)

Another parametric study by Maison, Kasai and Mayangarum was performed on effects of semi-rigid connection stiffness and strength on seismic performance in SAC report SAC/BD-99-17 [30]. All three SAC buildings (3-, 9- and 20-story buildings) for three seismic zones (Los Angeles, Seattle and Boston) were considered with three different connection's rotational stiffness parameters ($K_c = 5(EI/L)_{beam}$, $K_c = 10(EI/L)_{beam}$ and $K_c = 30(EI/L)_{beam}$), three different connection's yield moment parameters ($M_{cy} = 0.33M_p^{beam}$, $M_{cy} = 0.66M_p^{beam}$ and $M_{cy} = M_p^{beam}$) and two different post-yielding stiffness parameters ($M_{ch} = 1.1M_{cy}$ and $M_{ch} = 1.4M_{cy}$ at 0.03 rad. rotation). K_c, L, EI, M_{cy}, M_p^{beam} and M_{ch} are connection's stiffness, the length of the beam, the flexural rigidity of the beam, connection's yield moment, plastic moment capacity of the beam and connection's hardening moment, respectively. By using PC-ANSR nonlinear structural analysis software [28], pushover and dynamic analyses were performed. Two sets of 20 ground motion records scaled to match a 10% probability of exceedance and a 2% probability of exceedance in 50 years were used

in the dynamic analysis.

Firstly, original 3-, 9- and 20-story fully restrained (FR) buildings for three seismic zones were analyzed. Then, partially restrained (PR) beam-to-column connections were created by defining bilinear moment-curvature curve with defined parameter group for a connection. All frames for three seismic zones having PR connections were analyzed. It was reported that PR connections were ductile, stiff and strong, and vibration period of frames with PR connections did not differ much from that of frames with FR connections. Since yield strength and post-yield stiffness of the frames were directly affected by connection's yield moment and hardening moment, it was suggested that $M_{cy} > 0.5M_p^{beam}$ in order to satisfy UBC seismic design base shear specified for the original FR frame. Due to large drift and P-Δ effect, collapse of the frames was affected much by M_{cy}, M_{ch} and height of the building. For shorter building, it was observed that story drift angles and connection rotation were larger.

1.4.7 Study of Aksoylar, Elnashai and Mahmoud (2011)

A detailed parametric study by Aksoylar, Elnashai and Mahmoud was performed on seismic performance of low-rise long-span moment resisting steel frames with semi-rigid connections [2]. A 3-story 3-bay symmetric building was considered with two different span lengths (7 m and 9 m), four different connection capacities (50%, 60%, 70% and rigid case), two different moment hardening ratios (1.1 and 1.4), two different hysteretic behavior models (no pinching and pinching). First, pushover analysis was performed on Zeus-NL nonlinear analysis software [15]. Then, time history analysis with 25 real strong ground motion records was performed on 26 frames generated with these parameters on Zeus-NL. All frames met the acceptance criteria and showed reliable performance under nonlinear static and dynamic analyses, so the overdesign problem in low-rise long-span moment resisting steel frames is eliminated to some extent without using perimeter frame approach.

1.4.8 Study of Metin (2013) and Study of Metin and Sarıtaş (2014)

A detailed parametric study was carried out by Metin about the influence of semi-rigid connection nonlinearity on steel special moment frames in pushover analysis[32, 33]. Three 3-bay buildings (3-, 9- and 15-story buildings) which were assumed to be located in a high seismic area in Turkey were considered with two different bay length parameter (L = 6 m and L = 10 m), two different connection's rotational stiffness parameters ($K_c = 7(EI/L)_{beam}$ and $K_c = 15(EI/L)_{beam}$), only one connection's yield moment parameter ($M_{cy} = 0.66M_p^{beam}$) and two different connection's peak moment capacity parameters ($M_{cp} = 0.75M_p^{beam}$ and $M_{cp} = 1.5M_p^{beam}$ at 0.032 rad. rotation). K_c, L, EI, M_{cy}, M_p^{beam} and M_{cp} are connection's stiffness, the length of the beam, the flexural rigidity of the beam, connection's yield moment, plastic moment capacity of the beam and connection's peak moment capacity, respectively.

SAP2000 [41], a structural analysis program, was used for all pushover analyses in this study. Also, Overstrength Reduction Factor (R_o) and Ductility Reduction Factor (R_μ) of rigid and semi-rigid steel special moment frames were calculated and explained by using the pushover curves. It was concluded that special moment frames with semi-rigid connections could eliminate overdesign problem. Rigid frames were more ductile than frames with semi-rigid connections since plastic hinges in the semi-rigid connections formed earlier than plastic hinges in beams. It was also reported that stiffness of semi-rigid connections had no significant effect on the post-yield slope of the load-deformation curve. When connection had Full Strength (FS) (the maximum moment that a connection is able to carry is greater than the plastic moment capacity of the beam), independent of height of the building, the response of the semi-rigid frame was almost the same with rigid frame.

1.4.9 Study of Pirmoz and Liu (2017)

A study by Pirmoz and Liu was performed on a displacement-based method for seismic design of semi-rigid steel frame structures [35]. It was claimed that semi-

rigid steel frames had been designed using the traditional force-based method which was meant for fully rigid steel frame design, and that this led to a difficulty in design stage. In this study, a facile displacement-based method was proposed in order to eliminate the problems that the sizing of structural members was firstly performed per strength requirements of codes and revised iteratively to meet stiffness criteria for individual members and the overall frame. With the new method, it was proposed that the target displacement and deformation to the appropriate sizing of various structural members in terms of their strength, stiffness, and ductility were directly and explicitly obtained. It was assumed that the structural plastic deformation was mainly concentrated within the semi-rigid connections and beams and columns mostly remain elastic. The procedure for this method and numerical examples were given in the study. The proposed method and traditional one were compared.

1.5 Objectives and Scope

In this thesis, the effect of several parameters to nonlinear behavior of semi-rigid connections on general response of low-rise steel special moment resisting frames is studied. For this purpose, influence of connection flexibility, strength, ductility and energy dissipation characteristics to the overall system response is parametrically investigated.

Firstly, preliminary comparison studies on vibration characteristics of a portal frame and post-Northridge 3-story SAC building are conducted. Then, the parameters to give desired hysteretic moment-rotation behaviors of semi-rigid connections are determined. After selecting the parameter group used to observe different behaviors on low-rise steel special moment resisting frame, modal analysis, nonlinear static analysis and nonlinear time history analysis are carried out.

In order to achieve most accurate nonlinear analysis results, accurate modelling of member and connection behaviors is the first step in this study. However, performing nonlinear time history analysis is time consuming. Since this is a

parametric study, parameters in each group should be well diversified to capture overall response on low-rise special steel moment resisting frames with semi-rigid connections. With this study, it is aimed to conclude if low-rise special steel moment resisting frames perform at a level of safety when they are designed with semi-rigid connections.

1.6 Organization of the Thesis

The presentation of this thesis has been divided into six chapters including this chapter.

In Chapter 2, firstly, a general discussion on modelling of frame elements and specifically fiber formulation is made. Capabilities to model beam-column elements in OpenSees are explained, and the application of fiber formulation (force-based beam-column element) in OpenSees is clarified. Secondly, information on hysteretic material models for semi-rigid connections is given. Finally, analysis types are discussed.

In Chapter 3, a detailed information about the building layout, material properties, loading conditions and steel sections is given.

In Chapter 4, preliminary studies on comparison of vibration characteristics of a portal frame and post-Northridge 3-story SAC building are performed. Also, modelling cyclic behavior of semi-rigid connection is studied, and the parameters for desired behaviors are obtained with a preliminary study.

In Chapter 5, the sets of ground motions and the parameter groups are introduced. Then, the results of modal, pushover and nonlinear time history analyses are presented in figures.

In Chapter 6, summary and conclusion of thesis are presented. Recommendations on future research are given.

CHAPTER 2

MODELLING OF FRAME MEMBERS AND SEMI-RIGID CONNECTIONS

There are widely available structural analysis and finite element analysis programs to model and analyze the structures such as SAP 2000 [41], ANSYS [7] and Abaqus [20]. In this thesis, research oriented OpenSees [31] is used for modelling and analysis purposes. Due to its vast library of material models, element models and solution algorithms developed specifically for the response of structural systems under seismic forces. Especially, there are powerful element models that gives more realistic nonlinear behavior with single element discretization per span. In addition to OpenSees, SAP 2000 is also used for linear-elastic verification purposes for modal analysis, as well.

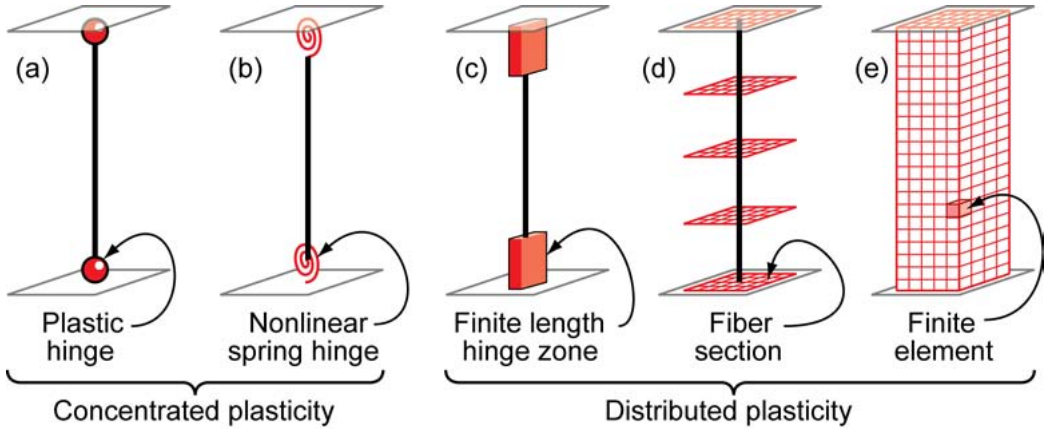

Figure 2.1: Idealized models of beam-column elements [14]

2.1 Modelling of Frame Members

OpenSees offers many frame element models ranging from elastic beam-column element (elasticBeamColumn) to force-based beam-column element (forceBeam-Column). In Table 2.1, beam-column elements and their behaviors are presented.

Inelastic response of a beam-column member can be idealized in the models represented in Figure 2.1. Models (a) and (b) are the simplest ones as they concentrate the inelastic deformations at the end of the elements through plastic hinge in model (a) and nonlinear spring with hysteretic behavior in model (b). Model (c) distributes plasticity with specified hinge zones at the end of the elements. The behavior in the inelastic hinge zones are identified through either nonlinear moment-curvature relationship or explicit fiber-section integrations that are compliant to the assumption that plane sections remain plane. Model (c) is more realistic than models (a) and (b) due to integration of deformation along the hinge length. In model (d), plasticity is distributed with numerical integrations along the member length and through the member cross section. Uniaxial material models are defined through element, and the nonlinear hysteretic stress-strain characteristics in the cross sections along the member are obtained. At fiber locations along the element, the plane-sections-remain-plane assumption is enforced, and axial force, moment, incremental moment-curvature and axial force-strain relations are obtained over the cross section. Model (e) is considered as the most complicated model since the member is discretized along its length and through the cross section into solid (3d) finite elements. Nonlinear hysteretic constitutive properties are defined with many input parameters. Whereas finite element model is more challenging than the other models in calibrating model parameters and computational resources, it is more versatile than them and time wise demanding, as well. Models (a), (b) and (c) may consider the axial force-moment (P-M) interactions through yield surfaces, but (P-M) response is obtained directly in models (d) and (e).

In this study, fiber formulation (model (d) in Figure 2.1) is used with uniaxial bilinear steel material model. In OpenSees, force-based beam-column element (forceBeamColumn) is used for this purpose. It captures spread of plasticity

Table 2.1: Beam-column elements, scripts in OpenSees and their behaviors [31]

Element Name and Script in OpenSees	**Behavior**
Elastic Beam Column Element (elasticBeamColumn)	Creates an elastic beam-column element.
Elastic Beam Column Element with Stiffness Modifiers (ModElasticBeam2d)	Creates a structural element with an equivalent combination of one elastic element with stiffness-proportional damping, and two springs at its two ends with no stiffness proportional damping to represent a prismatic section.
Elastic Timoshenko Beam Column Element (ElasticTimoshenkoBeam)	Creates an elastic beam-column element that accounts for shear deformations.
Beam with Hinges Element (beamWithHinges)	Creates a structural element, which is based on the non-iterative (or iterative) flexibility formulation. The locations and weights of the element integration points are based on so-called plastic hinge integration, which allows the user to specify plastic hinge lengths at the element ends.
Displacement-Based Beam-Column Element (dispBeamColumn)	Creates a structural element, which is based on the displacement formulation, and considers the spread of plasticity along the element.
Force-Based Beam-Column Element (forceBeamColumn)	Creates a structural element, which is based on the iterative force-based formulation. A variety of numerical integration options can be used in the element state determination and encompass both distributed plasticity and plastic hinge integration.

along element length and section depth. An optimum number of 5 Gauss-Legendre integration points are taken along the element length for both beams and columns, as done by Saritas et al. [39]. The force-deformation response at each integration point is defined by the section which is introduced as fibers. For all W-shapes (I sections) used in any of the models in this study, there are 10

fibers along web depth (d_w) and flange width (b_f), and 5 fibers along web thickness (t_w) and flange thickness (t_f). As it is stated in the previous paragraph, only P-M response is obtained in this model. In order to include shear effect and get axial force-moment-shear force (P-M-V) response, section aggregator in OpenSees is used. For this reason, Charney's formulation [10] is considered as done by Ozel et al. [34]. Shear area (A_v) is calculated from the following formula where A and d are area of W-shape and depth of the section, respectively;

$$A_v = \frac{A}{\kappa} \quad \text{and} \quad \kappa = 0.85 + 1.16\frac{2b_f t_f}{dt_w}$$

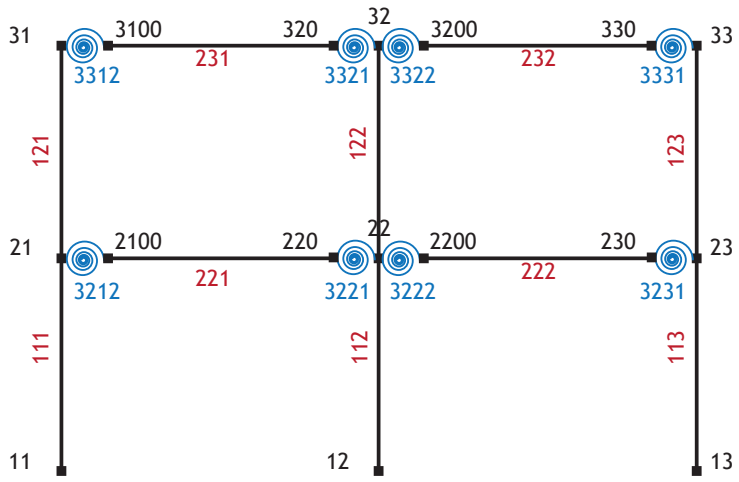

Figure 2.2: Representation of nodes, members, semi-rigid connections, and node and element numbering in a 2-bay 2-story frame

2.2 Modelling of Semi-Rigid Connections

In this study, beam-to-column connections are modelled as semi-rigid connections. In order to do that in OpenSees, zero length rotational spring elements are defined between the nodes that are at the same location, and connect beams to the columns. A representation of nodes, members, semi-rigid connections, and node and element numbering in a 2-bay 2-story frame is presented for demonstration purposes in Figure 2.2. The nodes at the same location are constrained in degrees-of-freedom of 1 and 2 (X and Y direction) and released in rotational degrees-of-freedom of 6 (around Z direction) in 3D coordinate system with

OpenSees command "equalDOF". A material property is needed to be defined for the zero length elements. In this case, the material property is moment-rotation relationship of semi-rigid connection. The material property can be either linear elastic or nonlinear. Linear elastic moment rotation behavior can be defined with initial stiffness. OpenSees has variety of nonlinear material models, such as Hysteretic Material (Hysteretic), Modified Ibarra-Medina-Krawinkler Deterioration Model with Bilinear Hysteretic Response (Bilin), Modified Ibarra-Medina-Krawinkler Deterioration Model with Peak-Oriented Hysteretic Response (ModIMKPeakOriented) and Modified Ibarra-Medina-Krawinkler Deterioration Model with Pinched Hysteretic Response (ModIMKPinching). Since Modified Ibarra-Medina-Krawinkler Deterioration Models needs lots of parameters and Hysteretic Material Model is simpler, Hysteretic Material Model is used to define material property of zero length rotational springs.

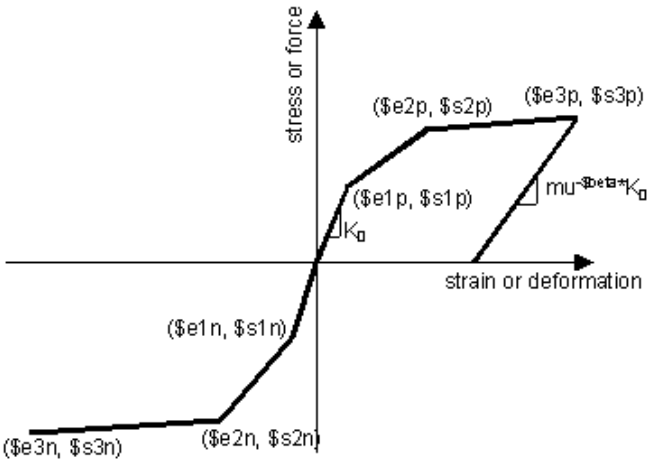

Figure 2.3: Hysteretic Material Model in OpenSees [31]

Hysteretic Material Model needs certain parameters like the values of yield stress-strain (force-deformation), ultimate stress-strain (force-deformation), some other parameters to control pinching of force and deformation, and damage due to ductility and energy. The required script in OpenSees to define Hysteretic Material Model is as follows;

```
uniaxialMaterial Hysteretic $matTag $s1p $e1p $s2p $e2p
<$s3p $e3p> $s1n $e1n $s2n $e2n <$s3n $e3n> $pinchX
$pinchY $damage1 $damage2 <$beta>
```

In this script, $matTag is the unique material tag. As it can be seen from Figure 2.3, $s1p and $e1p are stress and strain (or force & deformation) at first point of the envelope in the positive direction. $s2p and $e2p are stress and strain (or force & deformation) at second point of the envelope in the positive direction. Note that in OpenSees a term in angle brackets <> is optional. $s3p and $e3p are stress and strain (or force & deformation) at third point of the envelope in the positive direction (optional). $s1n and $e1n are stress and strain (or force & deformation) at first point of the envelope in the negative direction. $s2n and $e2n are stress and strain (or force & deformation) at second point of the envelope in the negative direction. $s3n and $e3n stress and strain (or force & deformation) at third point of the envelope in the negative direction (optional). $pinchx is pinching factor for strain (or deformation) during reloading. $pinchy is pinching factor for stress (or force) during reloading. $damage1 and $damage2 are damage parameters due to ductility and energy, respectively. $beta is power used to determine the degraded unloading stiffness based on ductility (optional, default=0.0) [31].

2.3 Analysis Types

In this study, the following analysis types are performed; modal analysis, nonlinear static (pushover) analysis and nonlinear time history analysis.

2.3.1 Modal Analysis

In modal analysis, the natural vibration periods at is achieved using the overall mass of the structure and its stiffness. The periods and frequencies of the building and modal shapes can be obtained by performing modal analysis on OpenSees. A preliminary study on comparing periods of a bare frame and a low-rise SMRF is conducted and presented in Chapter 4.

2.3.2 Nonlinear Static (Pushover) Analysis

A pattern of monotonically increasing lateral forces is applied to a structure, which is subjected to gravity loading and having nonlinear behavior, through elastic and inelastic behavior until an ultimate condition is reached or until a target displacement is exceeded. This pattern is a representation of inertia forces in an earthquake. The target displacement should represent the maximum displacement which is probably obtained in a design earthquake. In this study, loading pattern is considered as the fundamental modes of the structures as FEMA 356 suggests [1].

2.3.3 Nonlinear Time History Analysis

More accurate structural response under strong ground motions is obtained with nonlinear time history analysis because inelastic and cyclic behaviors of the members and connections are included in the analysis and it explicitly simulates hysteretic energy dissipation in the nonlinear range [14]. The analysis should be done with multiple ground motion data due to their inherent variability. In this way, statistically robust response of the structure is achieved for a given ground motion intensity or earthquake scenario. Linear time history analysis, of course, can be performed, but it is not in the scope of this study. The aim in this thesis is to consider nonlinear behavior.

As well as the mass (inertial mass) of the structure, gravity loads must be included in the model. There are two ways of defining the mass in a structural model. Either lumped mass matrix or consistent mass matrix can be defined in the model. A preliminary study on the ways of defining mass is conducted and presented in Chapter 4. Determining the period of the structure is vital as it affects the vibration characteristics of the structure. How the mass is distributed on a floor is important for the vibration characteristics. To examine this, a preliminary study on the ways of mass distribution on a floor is conducted and presented in Chapter 4. Vibration characteristics of a building influences the earthquake loads acting/acted on buildings. For that reason, the same building

(post-Northridge three-story SAC Building) with two different periods designed within upper and lower bound limits is considered in this study. In other words, a flexible (higher period) and a rigid (lower period) structures with semi-rigid connections are taken into account. In the next chapter, a detailed information about the building layout, material properties, loading conditions, steel sections and other properties is given.

CHAPTER 3

POST-NORTHRIDGE SAC BUILDINGS

This chapter gives detailed information about the selected steel moment frame, which is used throughout the parametric studies.

3.1 Description of the Building

Before the second phase of SAC Steel Project started, three prototype buildings, compliant to the 1994 Uniform Building Code, were designed for Los Angeles, Seattle and Boston sites. The pre-Northridge prototypes consist of 3, 9 and 20-story buildings. As a part of the second phase of SAC Steel Project, post-Northridge buildings were designed for a Los Angeles site and a Seattle site. The frame configurations of post-Northridge buildings were the same as those of pre-Northridge buildings, but they were redesigned in accordance with 1997 NEHRP (FEMA 1997a) and 1997 AISC provisions. As a requirement of 1997 NEHRP provision, an additional moment bay in each direction is added in 3-story buildings to satisfy the redundancy criteria [24].

In this study, 3-story post-Northridge SMRF building of SAC Steel Project is used with semi-rigid connections. In Figure 3.1, plan view and elevation of the building are given. The building has span length of 9.14 m (30 ft.) in both direction and story height of 3.96 m (13 ft.) The column bases are considered as fixed at the base. Perimeter moment frames were designed to carry all of the seismic loads [24]. The triangle symbol at the ends of the girders in the perimeter frames indicates moment connections.

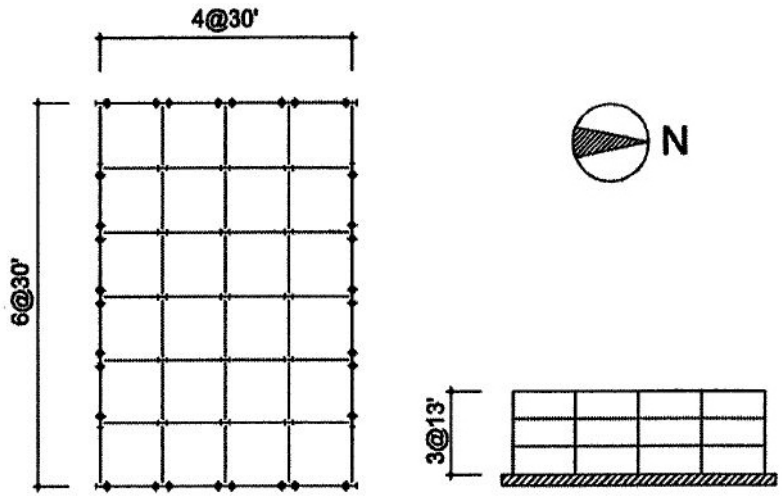

Figure 3.1: Plan and elevation view of 3-story post-Northridge building [24]

The structural steel used in the building is A572 Grade 50 steel. It has a yield strength of 345 MPa (50 ksi), a modulus of elasticity of 200 GPa (29,000 ksi), a shear modulus of 77 GPa (11,154 ksi) and a Poisson's ratio of 0.3. A strain hardening ratio of 0.03 is used for all beams and columns.

In SAC Steel Project, the same loading conditions and design assumptions were used to be consistent and comparable [24]. The loading conditions used in design of prototype buildings are indicated in SAC/BD-00/25 report and as follows;

- Steel framing configuration - as designed by design firms
- Floor and roof – use 7.62 cm (3 in.) metal decking with 6.35 cm (2.5 in.) of normal weight concrete fill
- Roofing - assume 0.335 kPa (7 psf) average
- Ceiling/Flooring - assume 0.144 kPa (3 psf) average
- Mechanical/Electrical - assume 0.335 kPa (7 psf) for all floors, 1.915 kPa (40 psf) will be added for penthouse area
- Partitions - use code requirements (0.479 kPa (10 psf) for seismic dead load, 0.958 kPa (20 psf) for gravity design)
- Exterior wall - assume 1.197 kPa (25 psf) of wall surface area, including any penthouse

- Live load - use typical code values for office occupancy, with area reduction
- Wind load - use typical code design procedures for frame analysis, assuming congested area (exposure B per UBC definition)

The seismic mass of the building was obtained from these loads and presented in SAC/BD-00/25 report [24]. For the 3-story building, seismic masses of 955.9 t (65.5 $kips\text{-}sec^2/ft$) for the first and second floors and 1034.7 t (70.9 $kips\text{-}sec^2/ft$) for the roof are specified. Also, it was reported in the SAC report that a Rayleigh damping of 4.3% was specified for 3-story structure [24].

In order to determine maximum and minimum expected performance levels of SAC buildings, two design categories were used; upper bound (UB) design and lower bound (LB) design. The upper bound design was made by using an empirical period which is specified in the code for the drift check. This caused a conservative design due to the large seismic base shear. The lower bound design was made by applying the calculated period to get the base shear for the drift check as allowed by the 1997 NEHRP. Compared to the lower bound design, the upper bound design is more conservative in terms of strength and stiffness. The minimum strength and stiffness that the seismic codes allow is used in the lower bound design.

There were four different frame configurations depending its column sections (W14, W24, W30 and W36) in post-Northridge buildings. In this study, in order to investigate the vibration characteristics, the frame configurations with the most flexible and most rigid ones are taken, namely W14 lower bound (LB) design and W36 upper bound (UB) design. The fundamental periods given are 0.96 sec for LB design and 0.78 sec for UB design. Note that these periods are obtained without including shear effects. That is why the analysis program (Drain-2DX [4]) used in SAC report [24] is not capable of including shear effects. In Table 3.1 and Table 3.2, the member properties of these two frame configurations are given. The section properties of these sections are given in Table 3.3.

Table 3.1: Member properties of W14 lower bound design

Story/Floor	**Columns**		**Girder**
	Exterior	**Interior**	
1/2	W14x257	W14x283	W30x99
2/3	W14x257	W14x283	W33x118
3/Roof	W14x257	W14x283	W21x68

Table 3.2: Member properties of W36 upper bound design

Story/Floor	**Columns**		**Girder**
	Exterior	**Interior**	
1/2	W36x135	W36x135	W30x108
2/3	W36x135	W36x135	W33x130
3/Roof	W36x135	W36x135	W24x76

Table 3.3: Section properties

W Shape	A	I_z	I_y	$W_{p,z}$	d	b_f	t_w	t_f
	(in^2)	(in^4)	(in^4)	(in^3)	(in)	(in)	(in)	(in)
W14x257	75.6	3400	1290	487	16.4	16.0	1.18	1.89
W14x283	83.3	3840	1440	542	16.7	16.1	1.29	2.07
W21x68	20.0	1480	64.7	160	21.1	8.27	0.430	0.685
W24x76	22.4	2100	82.5	200	23.9	8.99	0.440	0.680
W30x108	31.7	4470	146	346	29.8	10.5	0.545	0.760
W30x99	29.0	3990	128	312	29.7	10.5	0.520	0.670
W33x118	34.7	5900	187	415	32.9	11.5	0.550	0.740
W33x130	38.3	6710	218	467	33.1	11.5	0.580	0.855
W36x135	39.9	7800	225	509	35.6	12.0	0.600	0.790

CHAPTER 4

ASSESSMENT OF UTILIZED MODELS

In this chapter, preliminary comparison studies on vibration characteristics of a basic portal frame and post-Northridge 3-story SAC building are conducted. Also, the parameters to get desired cyclic behavior of semi-rigid connections to be used in the parametric studies are determined with a preliminary study in this chapter.

4.1 Comparison Study on Vibration Characteristics of a Portal Frame

In order to test and compare OpenSees element models, a preliminary study on a portal steel frame, which is introduced in the paper by Al-Aasam et al.[3], is conducted. Modal analysis is done with different OpenSees elements using different parameters of the elements for only rigid case. Even though the purpose in the paper was to assess the effect of the flexibility of the connections, FR connections is taken into account for beam-to-column connections. UB 254x146x37 section for the beam and UC 203x203x60 section for both columns are used. Section properties are given in Table 4.1. The height of the columns is 3 m and the length of the beam is 2.9 m as represented in Figure 4.1.

The structural steel used in the models is European S355 steel. It has yield strength of 355 MPa, modulus of elasticity of 210,000 MPa, shear modulus of 80,770 MPa and Poisson's ratio of 0.3. Linear transformation is used in all models. As seismic mass of the frame, only member self-weights are considered. In this case, a frame with only its self-weight is called as bare frame. The results

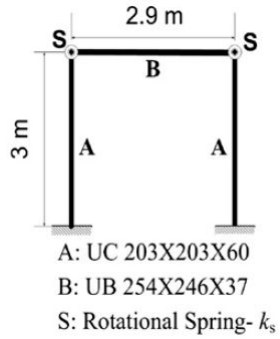

Figure 4.1: Portal frame [3]

Table 4.1: Section properties of the portal frame

Section	A	I_z	d	b_f	t_w	t_f
	(mm^2)	(mm^4)	(mm)	(mm)	(mm)	(mm)
UC 203x203x60	7637	6.125E+07	209.6	205.8	9.4	14.2
UB 254x146x37	4717	5.537E+07	256.0	146.4	6.3	10.9

by different options are given in Table 4.2.

In this comparison study, the effects of different element types presented in Table 2.1, the number of elements used in each span, the approach of defining mass matrix, shear correction on vibration characteristics are investigated. Only three element types are used; elastic beam-column element, elastic Timoshenko beam-column element and force-based beam-column element. For elastic beam-column element, OpenSees' capabilities on how to use lumped and consistent mass matrices are primarily tested. Note that the results from OpenSees models are compared with the result from SAP 2000 where each member of the frames is divided into 32 elements in SAP 2000 to get converged results. In Model 1, for example, lumped mass matrix is used by defining nodal masses on beam-column connection. However, in Model 2, lumped mass matrix is imposed by defining mass density along the members in mass per length, and the element itself creates lumped mass matrix. Elastic beam-column element and elastic Timoshenko beam-column element has an option (cMass) to impose consistent mass matrix. To activate cMass, mass density along the members has to be defined. Model 3 uses consistent mass matrix, and the error in period decreases to 5.2 % from 8.5 % when compared with Models 1 and 2. By increasing the

Table 4.2: Comparison study on vibration charateristics of the portal frame

Model	OpenSees Element Type	Uniaxial Material Type	# of Elements of Each Member	massDens	cMass	Mass Matrix	Shear Area	Section Aggregator	Period (sec)	Frequency (1/sec)	Difference in Period by SAP 2000 (%)
1	elasticBeamColumn	-	1	No	No	Lumped	N/A	No	0.0381298	26.2262	8.519
2	elasticBeamColumn	-	1	Yes	No	Lumped	N/A	No	0.0380798	26.2606	8.377
3	elasticBeamColumn	-	1	Yes	Yes	Consistent	N/A	No	0.0333088	30.0221	5.202
4	elasticBeamColumn	-	4	No	No	Lumped	N/A	No	0.0335736	29.7853	4.448
5	elasticBeamColumn	-	4	Yes	No	Lumped	N/A	No	0.0335832	29.7768	4.421
6	elasticBeamColumn	-	4	Yes	Yes	Consistent	N/A	No	0.0334203	29.9220	4.884
7	elasticBeamColumn	-	16	Yes	No	Lumped	N/A	No	0.0334312	29.9121	4.853
8	elasticBeamColumn	-	32	Yes	No	Lumped	N/A	No	0.0334238	29.9188	4.874
9	elasticBeamColumn	-	16	Yes	Yes	Consistent	N/A	No	0.0334213	29.9210	4.881
10	elasticBeamColumn	-	32	Yes	Yes	Consistent	N/A	No	0.0334213	29.9210	4.881
11	ElasticTimoshenkoBeam	-	1	No	No	Lumped	Web area	No	0.0401074	24.9331	14.148
12	ElasticTimoshenkoBeam	-	1	No	No	Lumped	Charney	No	0.0402938	24.8177	14.678
13	ElasticTimoshenkoBeam	-	1	Yes	No	Lumped	Web area	No	0.0400547	24.9659	13.998
14	ElasticTimoshenkoBeam	-	1	Yes	No	Lumped	Charney	No	0.0402408	24.8504	14.527
15	ElasticTimoshenkoBeam	-	1	Yes	Yes	Consistent	Web area	No	0.0349846	28.5840	0.432
16	ElasticTimoshenkoBeam	-	1	Yes	Yes	Consistent	Charney	No	0.0351429	28.4552	0.018
17	ElasticTimoshenkoBeam	-	4	No	No	Lumped	Web area	No	0.0353034	28.3259	0.475
18	ElasticTimoshenkoBeam	-	4	No	No	Lumped	Charney	No	0.0354697	28.1931	0.948
19	ElasticTimoshenkoBeam	-	4	Yes	No	Lumped	Web area	No	0.0353113	28.3195	0.498
20	ElasticTimoshenkoBeam	-	4	Yes	No	Lumped	Charney	No	0.0354775	28.1869	0.971
21	ElasticTimoshenkoBeam	-	4	Yes	Yes	Consistent	Web area	No	0.0351458	28.4529	0.027
22	ElasticTimoshenkoBeam	-	4	Yes	Yes	Consistent	Charney	No	0.0353093	28.3211	0.492
23	forceBeamColumn	steel01	1	Yes	No	Lumped	N/A	No	0.0383107	26.1024	9.034
24	forceBeamColumn	steel01	4	Yes	No	Lumped	N/A	No	0.0337863	29.5978	3.843
25	forceBeamColumn	steel01	16	Yes	No	Lumped	N/A	No	0.0336334	29.7324	4.278
26	forceBeamColumn	steel01	32	Yes	No	Lumped	N/A	No	0.0336259	29.7390	4.299
27	forceBeamColumn	steel01	64	Yes	No	Lumped	N/A	No	0.0336240	29.7406	4.304
28	forceBeamColumn	steel01	1	Yes	No	Lumped	Charney	Yes	0.0404594	24.7161	15.150
29	forceBeamColumn	steel01	2	Yes	No	Lumped	Charney	Yes	0.0362942	27.5526	3.295
30	forceBeamColumn	steel01	4	Yes	No	Lumped	Charney	Yes	0.0356698	28.0349	1.518
31	forceBeamColumn	steel01	8	Yes	No	Lumped	Charney	Yes	0.0355286	28.1463	1.116
32	forceBeamColumn	steel01	16	Yes	No	Lumped	Charney	Yes	0.0354941	28.1737	1.018
33	forceBeamColumn	steel01	32	Yes	No	Lumped	Charney	Yes	0.0354855	28.1806	0.993
34	forceBeamColumn	steel01	64	Yes	No	Lumped	Charney	Yes	0.0354833	28.1823	0.987
35	forceBeamColumn	steel01	100	Yes	No	Lumped	Charney	Yes	0.0354829	28.1826	0.986
36	SAP 2000		32			Lumped	Web area		0.0351364	28.4605	0.000

number of elements along a member from 1 to 4, the error in period decreases to the level of 4.4 % in Models 4, 5 and 6. Since two way of defining lumped mass matrix gives the pretty same results, only the approach with mass density is used in the next models with lumped matrix, not the one with nodal masses. In Models 7 to 10, element number is increased first to 16 then to 32 with lumped and consistent mass matrices, but the error even goes slightly up to 4.8 %.

When element type is changed to elastic Timoshenko beam-column element, shear area must be defined. There are two ways of defining shear area. Firstly, shear area along web area can be taken; i.e. $A_v = dt_w$. Secondly, Charney's formulation [10] can be used to get shear area as mentioned in Section 2.1. Models 11 to 14 are created with 1 element, lumped mass matrix and two different shear correction ways, and the error in period is around 14 %. When it is changed to consistent mass matrix in Model 15 and 16, the period is obtained with an error of less than 0.5 % even with 1 element. For the sake of completeness, it is remodeled with 4 elements in Models 17 to 22. The error in period is decreased as expected to less than 1 % in the models with lumped matrix. The models with consistent mass matrix keep their good accuracy level.

The models with force-based beam-column element are more important since the main aim in this study is to carry on nonlinear analysis, where force-based beam-column elements are used for that purpose. Uniaxial bilinear steel material model (steel01) is used with a strain hardening ratio of 0.001. There are five integration points along the element length for all members. The force-deformation response at each integration point is defined by the section which is introduced as fibers. There are 16 fibers along web depth (d_w) and flange width (b_f), and 4 fibers along web thickness (t_w) and flange thickness (t_f). First, models with no shear correction and increasing number of elements along a member are built. As it can be seen, the error in period is not less than 4 % even with 64 elements along a member. When shear effect is included with Charney's formulation via section aggregator in OpenSees, the error in period is decreased from 15.1 % to 1.5 % as the number of elements increased from 1 to 4. If it is increased beyond 4 elements, the error in period fall below 1 %.

Briefly, for the study of vibration characteristics, elastic beam-column element, elastic Timoshenko beam-column element and force-based beam-column element on a bare frame are tested with first the number of elements to be used to discretize a member, second the approach of defining mass matrix (lumped or consistent), lastly the use of shear correction. The models with elastic elements and elastic Timoshenko beam-column elements demonstrate the importance of the effect of lumped/consistent mass matrix and shear correction on vibration characteristics in OpenSees. Among the elastic elements, the best approximation in period is achieved with 1 element elastic Timoshenko beam-column elements modelled with consistent mass matrix and shear correction. It is worth to add that elastic elements in OpenSees can not be used for the capture of spread of inelasticity, but force-based beam-column elements offer such an option. It is seen that at least 4 elements should be used in force-based beam-column elements with Charney's shear correction for bare frames.

4.2 Comparison Study on Vibration Characteristics of Post-Northridge SAC Buildings

Post-Northridge 3-story SAC building has special moment resisting frames (SMRF) in the exterior perimeter to resist against earthquake forces and interior gravity frames to carry gravity loads. As previously mentioned, force-based beam-column elements are going to be used in order to include nonlinear behavior of the structure. The only way to define masses in force-based beam-column elements is to define lumped mass matrix by either creating nodal masses or using the mass density along a member. Since vibration characteristics of a structure directly affects the earthquake loads acted on a building, it should be modelled correctly to get real behavior of the structure. Perimeter frames are the only frames to carry seismic forces. In this thesis, only a perimeter frame is going to be investigated in 2D, so real vibration characteristics should be obtained by lumping the masses in correct positions.

In Figure 4.2, plan view of the post-Northridge 3-story SAC building is given. Since the structure is symmetric, only one perimeter frame is modelled and

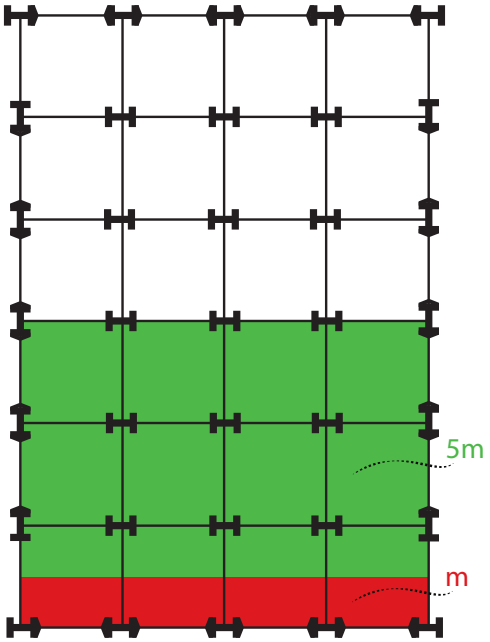

Figure 4.2: Mass distribution on plan view

analyzed in the following models and the model that is used in main analysis. The mass shown in the figure represents the half of a floor mass in the structure. Mass distribution in the following models is given by assuming that the half of a floor mass is equal to $6m$. Story mass highlighted with red area (m) is carried by the perimeter frame, but how the story mass highlighted with green area ($5m$) is carried is complicated. For this reason, a preliminary comparison study on vibration characteristics of post-Northridge 3-story SAC building is conducted. Several models of W14 lower bound design with FR connections are created and their periods are compared with the periods presented in SAC/BD-00/25 report. In each model, the number of elements along a member is increased to investigate their effect on the accuracy of the period.

As previously specified in Chapter 3, the structural steel used in the structure is A572 Grade 50 steel. It has yield strength of 50 ksi, modulus of elasticity of 29,000 ksi, shear modulus of 11,154 ksi and Poisson's ratio of 0.3. A strain hardening ratio of 0.03 is used for all beams and columns. Linear coordinate transformation is used for the beams in all models. Corotational coordinate transformation for the columns is used in all models except the models with elastic Timoshenko beam-column elements because the element does not support

corotational transformation. Thus, P-Delta coordinate transformation is used in the models with elastic Timoshenko beam-column elements.

4.2.1 Model 1

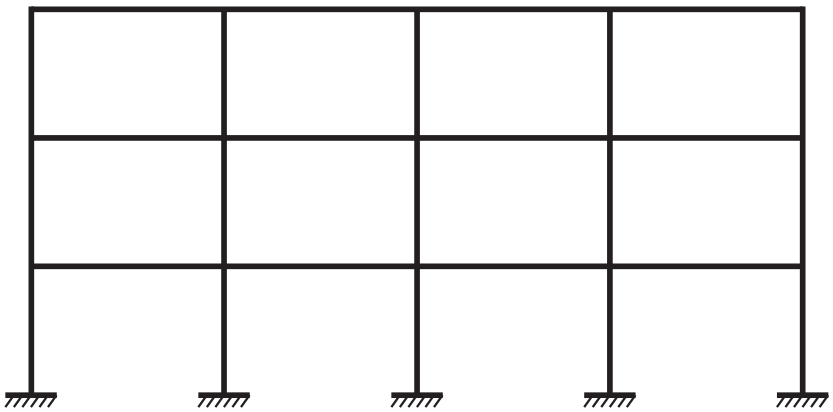

Figure 4.3: Mass distribution in Model 1

Since in Section 4.1, a comparison study on vibration characteristics of a bare portal frame is conducted, before performing a modal analysis on 4-bay 3-story SMRF with all floor masses, it makes sense to perform a modal analysis with a bare frame in order to compare both. To put it differently, in this model, only member self-weights are considered as seismic mass of the frame. Density of the steel is taken as $\rho_{steel} = 0.0152\ kips\text{-}sec^2/ft^4$. Lumped mass matrix is used by defining mass density along the members in mass per length, and force-based beam-column elements create lumped mass matrix. There are 5 Gauss-Legendre integration points along the element length for all members. The force-deformation response at each integration point is defined by the section which is introduced as fibers. There are 10 fibers along web depth (d_w) and flange width (b_f), and 5 fibers along web thickness (t_w) and flange thickness (t_f). Shear correction is also applied with Charney's formulation by using section aggregator in OpenSees. The comparison results are given in Table 4.3.

Table 4.3: Model 1 results

# of Elements Along a Member	OpenSees Element Type	Mass Matrix	Shear Correction	Period (sec)
1	elasticBeamColumn	Consistent	No	0.1318807
1	ElasticTimoshenkoBeam	Consistent	Charney	0.1409165
1	ElasticTimoshenkoBeam	Lumped	Charney	0.1424655
1	forceBeamColumn	Lumped	Charney	0.1431694
2	forceBeamColumn	Lumped	Charney	0.1419035
4	forceBeamColumn	Lumped	Charney	0.1417496
8	forceBeamColumn	Lumped	Charney	0.1417035

4.2.2 Model 2

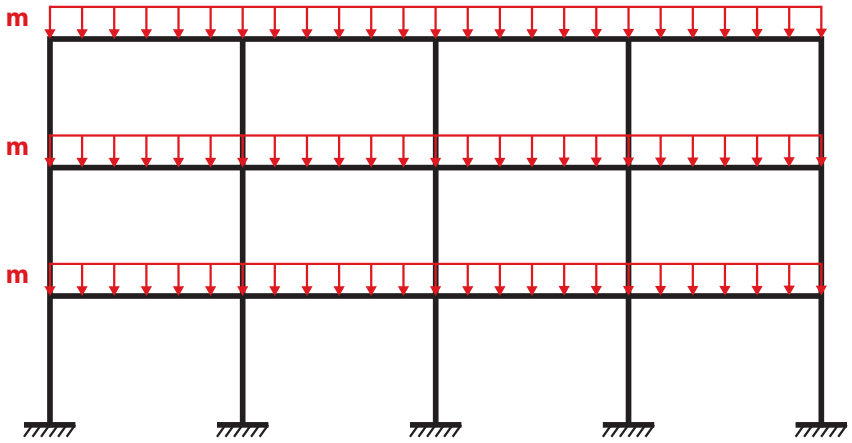

Figure 4.4: Mass distribution in Model 2

In this model, the floor masses presented in Section 3.1 are used as seismic masses applied to the structure. Since they already include steel member's self-weight, density of the steel is taken as zero. Only the floor mass highlighted with the red area in Figure 4.2 is considered for all stories in Model 2. The mass is distributed along the beams and converted to mass per length through the beams as shown in Figure 4.4. Force-based beam-column elements create lumped mass matrix at the ends of each element. Gauss-Legendre integration points of 5 along the element length for all members are considered with fibers on the section to get force-deformation response at each integration point. There are 10 fibers along web depth (d_w) and flange width (b_f), and 5 fibers along web thickness (t_w) and

flange thickness (t_f). Shear correction is also applied with Charney's formulation by using section aggregator in OpenSees. The comparison results are given in Table 4.4.

Table 4.4: Model 2 results

# of Elements Along a Member	OpenSees Element Type	Mass Matrix	Shear Correction	Period (sec)
1	elasticBeamColumn	Consistent	No	0.3826069
1	ElasticTimoshenkoBeam	Consistent	Charney	0.4079732
1	ElasticTimoshenkoBeam	Lumped	Charney	0.4074776
1	forceBeamColumn	Lumped	Charney	0.4095446
2	forceBeamColumn	Lumped	Charney	0.4097559
4	forceBeamColumn	Lumped	Charney	0.4102432
8	forceBeamColumn	Lumped	Charney	0.4102865

4.2.3 Model 3

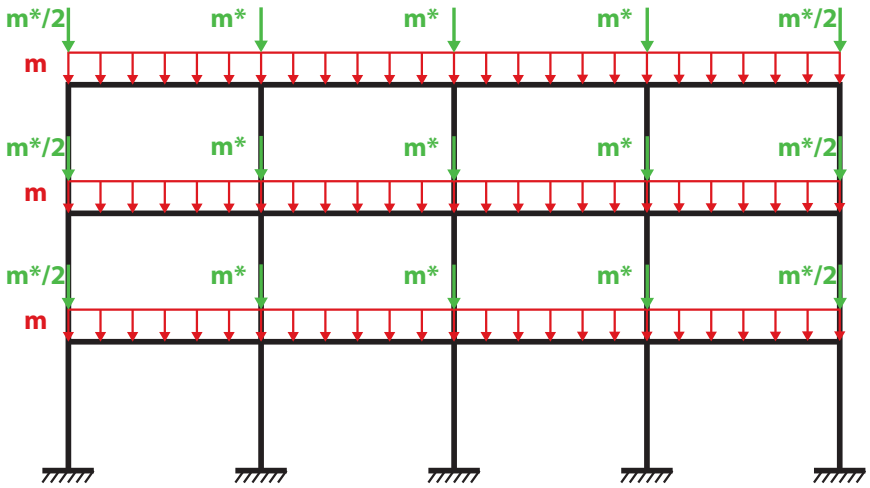

Figure 4.5: Mass distribution in Model 3

In this model, the seismic mass coming from red area on each floor is applied in the same way like in Model 2. The mass coming from green area is lumped at the connections of out-of-plane frames. Mass distribution of red (m) and green ($5m$) areas on the perimeter frame is shown in Figure 4.5. Assume each member on a floor of the perimeter frame has green area mass of m^* and that would be a total

of $4m^*$ on each floor, so the mass of the green area is $5m = 4m^*$ and $m^* = 1.25m$. There should be a mass of $m^*/2$ at each node. Thus, a mass of $m^*/2$ should be on exterior columns of the perimeter frame and a mass of m^* should be on interior columns of the perimeter frame. Gauss-Legendre integration points of 5 along the element length for all members are considered with fibers on the section to get force-deformation response at each integration point. There are 10 fibers along web depth (d_w) and flange width (b_f), and 5 fibers along web thickness (t_w) and flange thickness (t_f). Shear correction is also applied with Charney's formulation by using section aggregator in OpenSees. The comparison results are given in Table 4.5.

Table 4.5: Model 3 results

# of Elements Along a Member	**OpenSees Element Type**	**Mass Matrix**	**Shear Correction**	**Period (sec)**
1	elasticBeamColumn	Consistent	No	0.9450778
1	ElasticTimoshenkoBeam	Consistent	Charney	1.0080198
1	ElasticTimoshenkoBeam	Lumped	Charney	0.9981121
1	forceBeamColumn	Lumped	Charney	1.0031752
2	forceBeamColumn	Lumped	Charney	1.0031947
4	forceBeamColumn	Lumped	Charney	1.0033758
8	forceBeamColumn	Lumped	Charney	1.0033893

4.2.4 Model 4

In order to include P-Δ effect which is mainly caused by interior gravity frames, an additional bay is included with the same bay length. The elements of (lean-on) column of the additional bay are rigid links and simply connected at the ends. For the lean-on column, linear elastic material is used with a very large section area ($1 * 10^6\ in^2$) and moment of inertia close to zero ($1 * 10^{-6}\ in^4$). Instead of having rigid links simply connected at the ends as beams, the nodes connect the exterior perimeter frame and the additional column are constrained with equalDOF feature of OpenSees. In this way, the effects of the additional bay on the stiffness and strength of the existing frame are eliminated. The additional

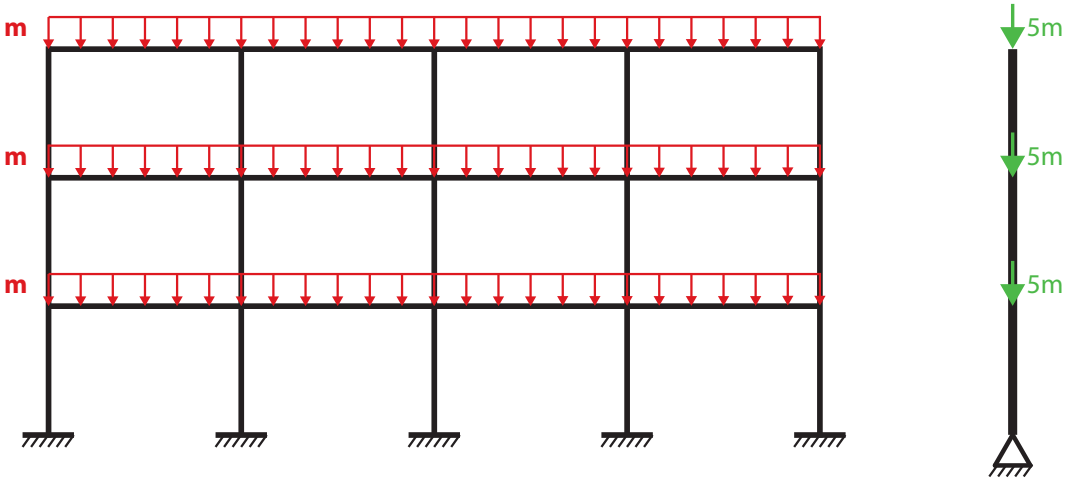

Figure 4.6: Mass distribution in Model 4

bay does not contribute to horizontal carrying capacity of whole frame, but the lean-on column carries the axial loads on it. The seismic mass highlighted with red area on each floor is applied in the same way like in Models 2 and 3. The mass is distributed along the beams and converted to mass per length through the beams. Force-based beam-column elements create lumped mass matrix at the ends of each element. The seismic mass which is coming from interior gravity frames and highlighted with green area on each floor is lumped at the nodes on the lean-on column, as shown in Figure 4.6. By doing this, P-Δ effect of interior gravity frames is included. Gauss-Legendre integration points of 5 along the element length for all members are considered with fibers on the section to get force-deformation response at each integration point. There are 10 fibers along web depth (d_w) and flange width (b_f), and 5 fibers along web thickness (t_w) and flange thickness (t_f). Shear correction is also applied with Charney's formulation by using section aggregator in OpenSees. The comparison results are given in Table 4.6.

Table 4.6: Model 4 results

# of Elements Along a Member	OpenSees Element Type	Mass Matrix	Shear Correction	Period (sec)
1	elasticBeamColumn	Consistent	No	0.9642226
1	ElasticTimoshenkoBeam	Consistent	Charney	1.0246951
1	ElasticTimoshenkoBeam	Lumped	Charney	1.0245156
1	forceBeamColumn	Lumped	Charney	1.0296325
2	forceBeamColumn	Lumped	Charney	1.0296446
4	forceBeamColumn	Lumped	Charney	1.0298109
8	forceBeamColumn	Lumped	Charney	1.0298230

4.2.5 Model 5

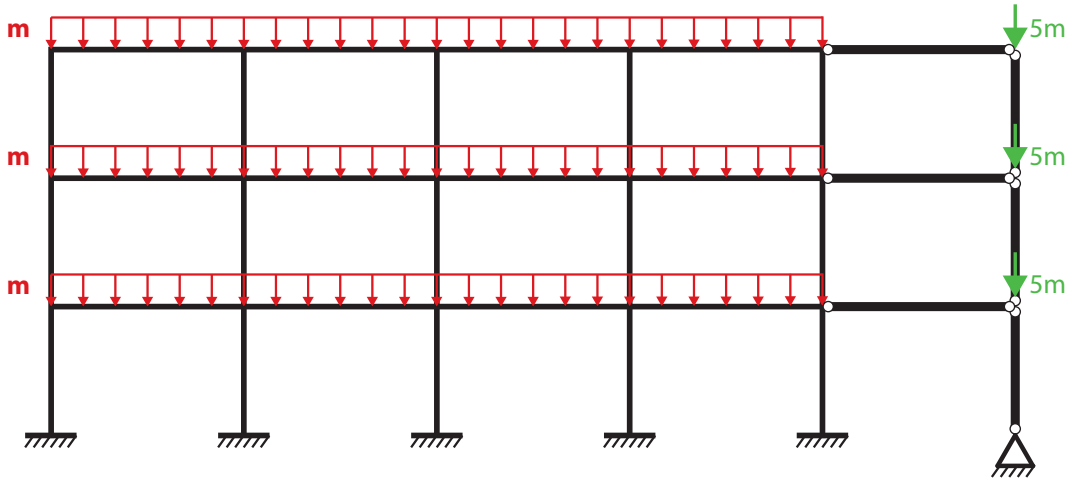

Figure 4.7: Mass distribution in Model 5

In this model, a similar approach with Model 4 is used. An additional bay is included to the exterior perimeter frame to include P-Δ effect caused by interior gravity frames. As a part of the additional bay, a lean-on column is modelled with similar approach in Model 4 and different modelling elements. In order to make the column elements simply connected at the ends, zero length elastic rotational springs are defined at the ends of elements with a stiffness close to zero ($1*10^{-9}$ $kips\text{-}in/rad$). The lean-on column elements have very large section area of ($1*10^{6}$ in^2) and moment of inertia close to zero ($1*10^{-6}$ in^4). In this way, they are modelled as rigid frame element with hinges at the end and the moment

is not transferred. Rigid truss element are used as beams of the additional bay with very large section area of $(1 * 10^6\ in^2)$. The additional bay does not affect stiffness and strength of the exterior perimeter frame, but helps including P-Δ effect. The mass distribution is the same as the one in Model 4. The mass in red area is distributed along the beam elements and converted to mass per length through the beams. Then, lumped mass matrix is created with the help of mass density feature in force-based beam-column elements in OpenSees. The seismic mass which is coming from interior gravity frames and highlighted with green area on each floor is lumped at the nodes on the lean-on column. The frame configuration and mass distribution are shown in Figure 4.7. There are 5 Gauss-Legendre integration points along the element length for all members with fibers on the section to obtain force-deformation response at each integration point. There are 10 fibers along web depth (d_w) and flange width (b_f), and 5 fibers along web thickness (t_w) and flange thickness (t_f). Charney's formulation to catch shear effects is used with the help of section aggregator in OpenSees. In this model, the whole frame is only analyzed with 1 element along a member because it is known from previous trials that the results are satisfying with 1 element. The result is shown in Table 4.7.

Table 4.7: Model 5 results

# of Elements Along a Member	**OpenSees Element Type**	**Mass Matrix**	**Shear Correction**	**Period (sec)**
1	forceBeamColumn	Lumped	Charney	1.0296331

4.2.6 Discussion of Results

First, in order to have a notion for vibration characteristics of post-Northridge 3-story bare SAC frame, Model 1 is created. For force-based beam-column elements, it is seen that 1 element along a member is adequate in terms of the estimating the fundamental period. The reason why the results for a bare frame in this section differ from the results for another bare frame in the previous Section 4.1 might be because of having more than one story and one bay in this

section.

From Model 2 to Model 4, different approaches of defining mass are tried to approximate the fundamental period (0.96 sec for LB design) defined in SAC report. It is observed that in Model 2 and periods are far from the real case because the mass from gravity frames (highlighted with green) is not given to the frame. In other words, P-Δ effect is not taken into consideration. In Model 3, the mass from gravity frames is lumped at nodes as explained previously. In this way, all floor masses are given to the frame. Since gravity loads are also needed to be assigned to the same way, this might cause misleading internal reactions in the frame members and misleading drift demands. In Model 4, an additional bay with a lean-on column is added to apply the masses from gravity frames. In this fashion, P-Δ effect of gravity frames is included. Increasing the number of elements does not significantly change the period for force-based beam-column elements, so only 1 element is enough. It is observed that only the case for elastic beam-column element with no shear correction approximates the period in SAC report, but not the cases for elastic Timoshenko and force-based beam-column elements. The reason is that the analysis program used in SAC project (Drain-2DX [4]) is not capable of including shear, so the period in SAC report is for no shear correction case. In order to get most accurate nonlinear analysis results, force-based beam-column elements with Charney's shear correction are used in this thesis.

Parametric studies in Chapter 5 are first performed by applying the approach in Model 4, but convergence problems are faced in nonlinear time-history analysis. Hence, a new model, Model 5, is created with similar mass defining approach only for force-based beam-column elements with 1 element along a member and Charney's shear correction. This model does not lead to convergence problems in nonlinear time-history analysis, so parametric studies in Chapter 5 are carried out with the approach presented in Model 5.

4.3 Cyclic Behavior of Semi-Rigid Connection

Beam-to-column connections are identified as semi-rigid connections in this study. As previously mentioned in Section 2.2, semi-rigid connections are modelled as zero length rotational spring elements, and their material property to define its behavior is needed. Even though the cyclic response of these connections are affected by the type of the connection, geometry and failure limit states, a semi-rigid connection typically show a pinched hysteretic behavior. Cyclic loads cause bolts to slip and cause permanent deformations in holes or bolts. Contact and separation movements of the connected elements lead to local plastic deformations. This behavior on hysteretic response is called pinching effect. A semi-rigid connection can show mild pinching behavior or severe pinching behavior, as demonstrated by Saritas et al [38]. At the same time, it can have strength loss or no strength loss. For this purpose, a preliminary study to determine parameters of hysteretic material for these specific circumstances is performed.

A cantilever column with a semi-rigid base connection is modelled. The horizontal loading is applied to the top of the linear elastic column to get nonlinear hysteretic response of the semi-rigid connection. The cyclic load pattern applied on the top of the columns is shown in time series in Figure 4.8.

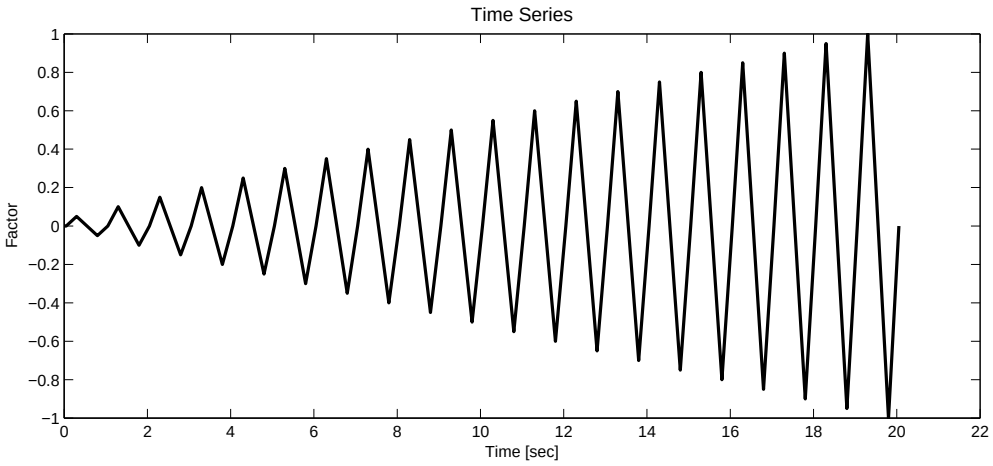

Figure 4.8: Time series

Hysteretic Material Model in OpenSees is used to define hysteretic moment-

rotation behavior of a semi-rigid connection. Its script and required parameters are as follows;

```
uniaxialMaterial Hysteretic $matTag $s1p $e1p $s2p $e2p
<$s3p $e3p> $s1n $e1n $s2n $e2n <$s3n $e3n> $pinchX
$pinchY $damage1 $damage2 <$beta>
```

Four cases are investigated to determine models with mild pinching and strength loss, mild pinching and no strength loss, severe pinching and strength loss, and severe pinching and no strength loss. In all cases, λ, which is the ratio of initial connection stiffness to EI/L of connecting beam, is taken as 11, and connection's peak moment capacity (M_{cp}) is taken as 75% of the beam's plastic moment capacity (M_p^{beam}). In Figure 4.9, M_1 is equal to connection's yield moment M_{cy}. The requirement for ductility in SMRF in AISC 341-10 implies that at least 80% of the nominal flexural strength of the connection should be present at a drift angle of 0.04 rad [5]. A simple way of expressing this is also provided by Chen, and it is suggested that rotation capacity of a connection $\theta_u \geq 0.04\ rad$ [12]. It is simpler because it directly places its ultimate rotation value as totally present in the connection excluding the other flexure behavior of stories, columns and beams. So, it is assumed that rotation capacity of a connection θ_u is equal to 0.04 rad for SMRF.

The rotation value θ_2 at connection's peak moment ($M_2 = M_{cp}$) is equal to $0.8 \times \theta_u = 0.032\ rad$. Using similarity transformation in strength loss case, θ_3 is found as 0.072. Hysteretic behavior models for a semi-rigid connection with and without strength loss are given in Figure 4.9. There are some other parameters to define pinching behavior on a hysteretic model. Pinching factor for deformation during reloading ($pinchX) and pinching factor for force during reloading ($pinchY) are determined by trial and error for mild and severe pinching cases, where these values were also reported by Saritas et al. [38]. The parameters are presented in Table 4.8, and hysteretic response of the models are given in Figures 4.10.

The parameters of these four models are going to be used in the main analysis.

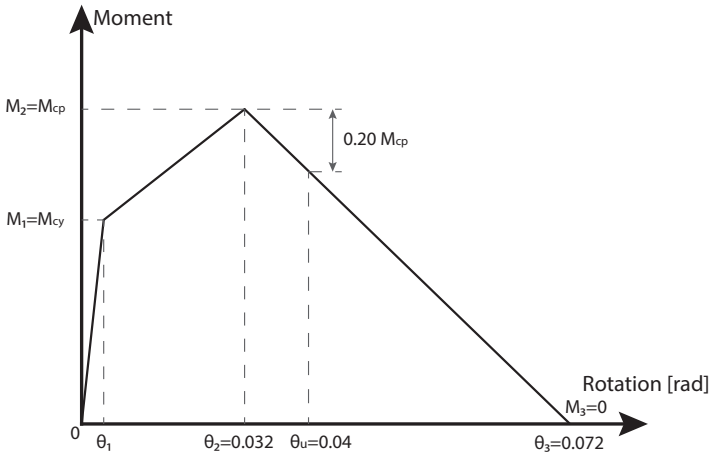

(a) With strength loss

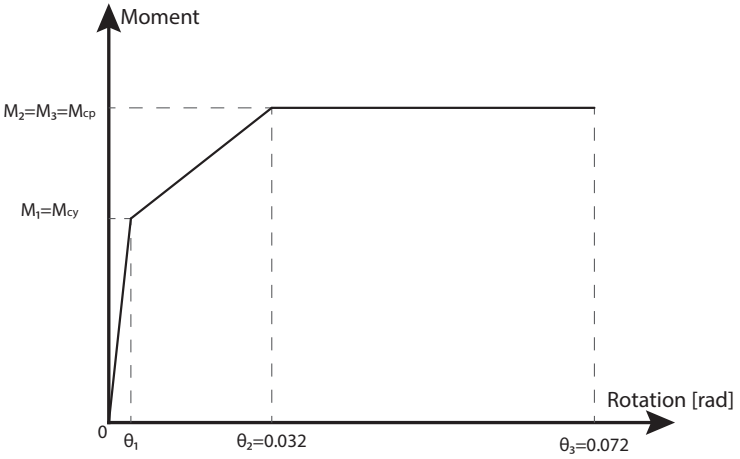

(b) With no strength loss

Figure 4.9: Hysteretic behavior model for semi-rigid connection

Table 4.8: Parameters required for cyclic behavior of semi-rigid connection

Model	**Pinching**	**Strength Loss**	**$s1p**	**$e1p**	**$s2p**	**$e2p**	**$s3p**	**$e3p**	**$pinchX**	**$pinchY**
			M_1	θ_1	M_2	θ_2	M_3	θ_3		
1	**Mild**	**Yes**	M_{cy}	M_{cy}/k_r	M_{cp}	0.032	0	0.072	0.4	0.4
2	**Mild**	**No**	M_{cy}	M_{cy}/k_r	M_{cp}	0.032	M_{cp}	0.072	0.4	0.4
3	**Severe**	**Yes**	M_{cy}	M_{cy}/k_r	M_{cp}	0.032	0	0.072	0.8	0.2
4	**Severe**	**No**	M_{cy}	M_{cy}/k_r	M_{cp}	0.032	M_{cp}	0.072	0.8	0.2

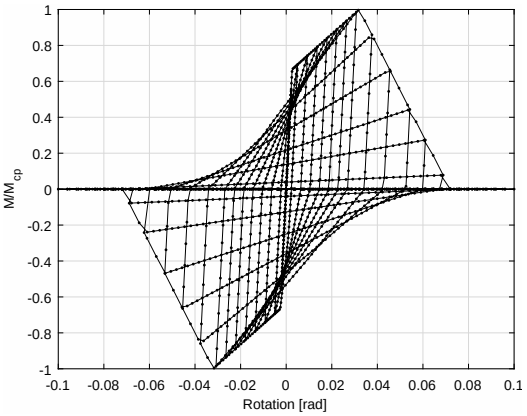

(a) Model 1: Mild pinching - strength loss

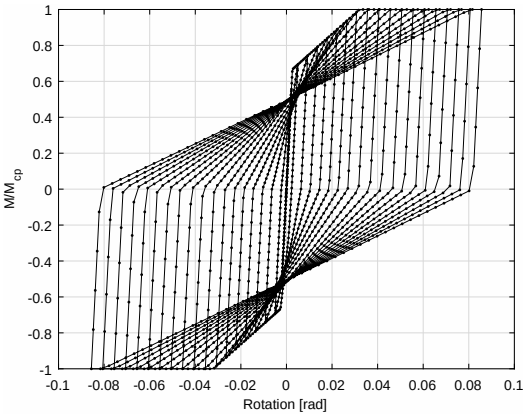

(b) Model 2: Mild pinching - no strength loss

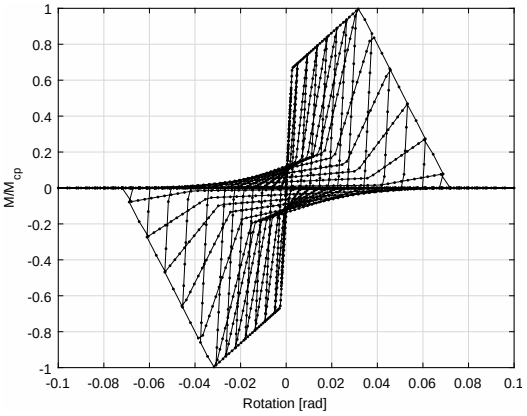

(c) Model 3: Severe pinching - strength loss

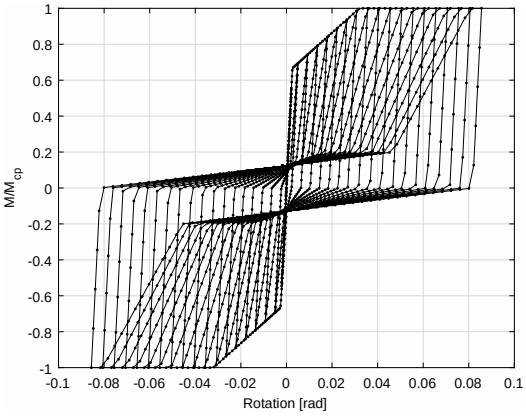

(d) Model 4: Severe pinching - no strength loss

Figure 4.10: Cyclic behavior of the models with determined parameters

CHAPTER 5

PARAMETRIC STUDIES

In this chapter, influence of stiffness, strength, ductility and energy dissipation characteristics of connections on the global behavior of low-rise special steel moment resisting structures are parametrically studied. To this end, the sets of ground motions that are used in the main analysis are introduced. Also, the parameters that are used to observe different behaviors are explained and listed. Modal analysis, pushover analysis and nonlinear time history analysis are performed, and their results are compared.

5.1 Ground Motions

In the report SAC/BD-97/04, Somerville et al. provided several sets of ground motions based on location, soil type and hazard level [40]. They are prepared for three locations in United States of America; Boston, Seattle and Los Angeles. In order to perform nonlinear time history analysis in this thesis, two sets of ground motion records for Los Angeles (LA) are used namely Contingency Level Earthquake (CLE) and Maximum Considered Earthquake (MCE). CLE has 10% probability of exceedance in 50 years (2.10×10^{-3} annual probability of exceedance: 475 years return period). MCE has 2% probability of exceedance in 50 years (4.04×10^{-4} annual probability of exceedance: 2,475 years return period). In the event of CLE, controlled inelastic structural behavior can result during an earthquake. This may cause temporary loss of use of a structure, which shall be restored within an acceptable period of time. In the event of MCE, building performance exhibits significant inelasticity, but where collapse

of the building is prevented so as to allow for safety and escape of occupants, rather than complete structural survival of the building.

There are 20 time histories in each set of ground motions. The information about the ground motions are given in Table 5.1 and Table 5.2, and the 4.3% damped response spectra is given for the two sets of ground motion records in Figure 5.1 and Figure 5.2. In Figure 5.1, the peak response accelerations are observed between the period values of 0.1 sec and 0.5 sec, and change between $2g$ to $4g$ in general. In Figure 5.2, the peak response accelerations are observed between the period values of 0.2 sec and 1.0 sec, and change between $2.5g$ to $5g$ in general. Some ground motion records are even imposing response acceleration close to $2g$ even at about 1.7 sec.

Table 5.1: Los Angeles (LA) ground motions for the 10% in 50 years hazard level

EQ Code	Record	Earthquake Magnitude	Distance (km)	Scale Factor	Number of Points	Time Step (sec)	Duration (sec)	PGA (cm/sec^2)	PGA (g's)
LA01	Imperial Valley, 1940, El Centro	6.9	10	2.01	2674	0.02	53.46	452.03	0.46
LA02	Imperial Valley, 1940, El Centro	6.9	10	2.01	2674	0.02	53.46	662.88	0.68
LA03	Imperial Valley, 1979, Array #05	6.5	4.1	1.01	3939	0.01	39.38	386.04	0.39
LA04	Imperial Valley, 1979, Array #05	6.5	4.1	1.01	3939	0.01	39.38	478.65	0.49
LA05	Imperial Valley, 1979, Array #06	6.5	1.2	0.84	3909	0.01	39.08	295.69	0.3
LA06	Imperial Valley, 1979, Array #06	6.5	1.2	0.84	3909	0.01	39.08	230.08	0.23
LA07	Landers, 1992, Barstow	7.3	36	3.2	4000	0.02	79.98	412.98	0.42
LA08	Landers, 1992, Barstow	7.3	36	3.2	4000	0.02	79.98	417.49	0.43
LA09	Landers, 1992, Yermo	7.3	25	2.17	4000	0.02	79.98	509.70	0.52
LA10	Landers, 1992, Yermo	7.3	25	2.17	4000	0.02	79.98	353.35	0.36
LA11	Loma Prieta, 1989, Gilroy	7.0	12	1.79	2000	0.02	39.98	652.49	0.67
LA12	Loma Prieta, 1989, Gilroy	7.0	12	1.79	2000	0.02	39.98	950.93	0.97
LA13	Northridge, 1994, Newhall	6.7	6.7	1.03	3000	0.02	59.98	664.93	0.68
LA14	Northridge, 1994, Newhall	6.7	6.7	1.03	3000	0.02	59.98	644.49	0.66
LA15	Northridge, 1994, Rinaldi RS	6.7	7.5	0.79	2990	0.005	14.945	523.30	0.53
LA16	Northridge, 1994, Rinaldi RS	6.7	7.5	0.79	2990	0.005	14.945	568.58	0.58
LA17	Northridge, 1994, Sylmar	6.7	6.4	0.99	3000	0.02	59.98	558.43	0.57
LA18	Northridge, 1994, Sylmar	6.7	6.4	0.99	3000	0.02	59.98	801.44	0.82
LA19	North Palm Springs, 1986	6.0	6.7	2.97	3000	0.02	59.98	999.43	1.02
LA20	North Palm Springs, 1986	6.0	6.7	2.97	3000	0.02	59.98	967.61	0.99

Table 5.2: Los Angeles (LA) ground motions for the 2% in 50 years hazard level

EQ Code	Record	Earthquake Magnitude	Distance (km)	Scale Factor	Number of Points	Time Step (sec)	Duration (sec)	PGA (cm/sec^2)	PGA (g's)
LA21	1995 Kobe	6.9	3.4	1.15	3000	0.02	59.98	1258.00	1.28
LA22	1995 Kobe	6.9	3.4	1.15	3000	0.02	59.98	902.75	0.92
LA23	1989 Loma Prieta	7.0	3.5	0.82	2500	0.01	24.99	409.95	0.42
LA24	1989 Loma Prieta	7.0	3.5	0.82	2500	0.01	24.99	463.76	0.47
LA25	1994 Northridge	6.7	7.5	1.29	2990	0.005	14.945	851.62	0.87
LA26	1994 Northridge	6.7	7.5	1.29	2990	0.005	14.945	925.29	0.94
LA27	1994 Northridge	6.7	6.4	1.61	3000	0.02	59.98	908.70	0.93
LA28	1994 Northridge	6.7	6.4	1.61	3000	0.02	59.98	1304.10	1.33
LA29	1974 Tabas	7.4	1.2	1.08	2500	0.02	49.98	793.45	0.81
LA30	1974 Tabas	7.4	1.2	1.08	2500	0.02	49.98	972.58	0.99
LA31	Elysian Park (simulated)	7.1	17.5	1.43	3000	0.01	29.99	1271.20	1.3
LA32	Elysian Park (simulated)	7.1	17.5	1.43	3000	0.01	29.99	1163.50	1.19
LA33	Elysian Park (simulated)	7.1	10.7	0.97	3000	0.01	29.99	767.26	0.78
LA34	Elysian Park (simulated)	7.1	10.7	0.97	3000	0.01	29.99	667.59	0.68
LA35	Elysian Park (simulated)	7.1	11.2	1.1	3000	0.01	29.99	973.16	0.99
LA36	Elysian Park (simulated)	7.1	11.2	1.1	3000	0.01	29.99	1079.30	1.1
LA37	Palos Verdes (simulated)	7.1	1.5	0.9	3000	0.02	59.98	697.84	0.71
LA38	Palos Verdes (simulated)	7.1	1.5	0.9	3000	0.02	59.98	761.31	0.78
LA39	Palos Verdes (simulated)	7.1	1.5	0.88	3000	0.02	59.98	490.58	0.5
LA40	Palos Verdes (simulated)	7.1	1.5	0.88	3000	0.02	59.98	613.28	0.63

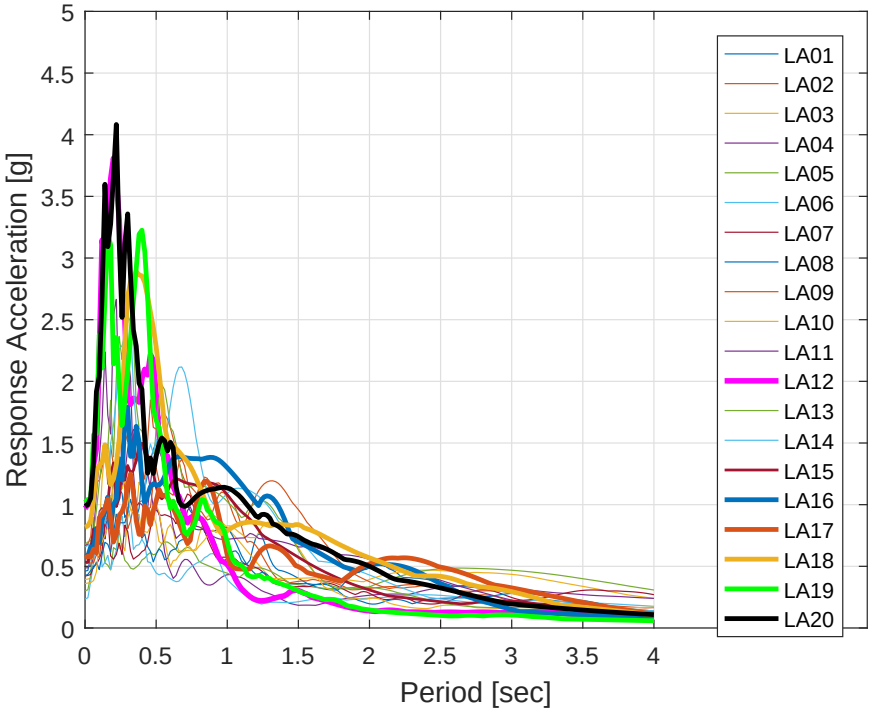

Figure 5.1: Response Spectra for Los Angeles (LA) Ground Motions for the 10% in 50 Years Hazard Level

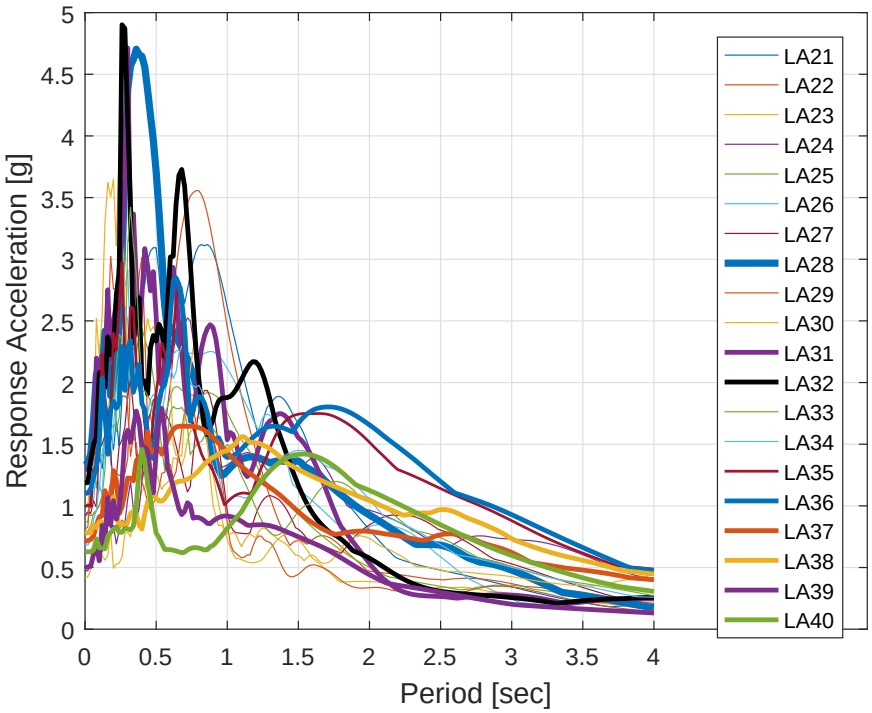

Figure 5.2: Response Spectra for Los Angeles (LA) Ground Motions for the 2% in 50 Years Hazard Level

5.2 Parameter Group

In this parametric study, mainly 6 different parameter groups are used in post-Northridge 3-story SAC building. The required information about the building is given in Section 3.1. For modelling of the structures, the modelling approach in Section 4.2.5 is used in this analysis with semi-rigid connections. For modelling of semi-rigid connection response, the modelling approach in Section 4.3 is used with the determined parameters in Table 4.8. In this scope, the following parameters are used;

- Two different connection rotational stiffness parameters as $\lambda = 7$ and $\lambda = 15$ where $K_s = \lambda \times (EI/L)_{beam}$
- One connection yield moment parameter as $M_{cy} = 2/3M_p^{beam}$
- Three different connection peak moment capacity parameters as $\beta = 0.75$, $\beta = 1.1$ and $\beta = 1.45$ where $M_{cp} = \beta M_p^{beam}$
- Two different conditions of presence of connection strength loss as strength loss and no strength loss
- Two different conditions of pinching effect on connection as mild pinching and severe pinching
- Two different frame configurations as flexible frame (W14 lower bound structure) and rigid frame (W36 upper bound structure)

The models prepared with combination of these parameters are presented in Table 5.3.

Table 5.3: Paramaters by model number

W14 LB					W36 UB				
Model #	λ	β	Strength Loss	Pinching	Model #	λ	β	Strength Loss	Pinching
1	7	0.75	Yes	Mild	**25**	7	0.75	Yes	Mild
2	7	0.75	Yes	Severe	**26**	7	0.75	Yes	Severe
3	7	0.75	No	Mild	**27**	7	0.75	No	Mild
4	7	0.75	No	Severe	**28**	7	0.75	No	Severe
5	7	1.1	Yes	Mild	**29**	7	1.1	Yes	Mild
6	7	1.1	Yes	Severe	**30**	7	1.1	Yes	Severe
7	7	1.1	No	Mild	**31**	7	1.1	No	Mild
8	7	1.1	No	Severe	**32**	7	1.1	No	Severe
9	7	1.45	Yes	Mild	**33**	7	1.45	Yes	Mild
10	7	1.45	Yes	Severe	**34**	7	1.45	Yes	Severe
11	7	1.45	No	Mild	**35**	7	1.45	No	Mild
12	7	1.45	No	Severe	**36**	7	1.45	No	Severe
13	15	0.75	Yes	Mild	**37**	15	0.75	Yes	Mild
14	15	0.75	Yes	Severe	**38**	15	0.75	Yes	Severe
15	15	0.75	No	Mild	**39**	15	0.75	No	Mild
16	15	0.75	No	Severe	**40**	15	0.75	No	Severe
17	15	1.1	Yes	Mild	**41**	15	1.1	Yes	Mild
18	15	1.1	Yes	Severe	**42**	15	1.1	Yes	Severe
19	15	1.1	No	Mild	**43**	15	1.1	No	Mild
20	15	1.1	No	Severe	**44**	15	1.1	No	Severe
21	15	1.45	Yes	Mild	**45**	15	1.45	Yes	Mild
22	15	1.45	Yes	Severe	**46**	15	1.45	Yes	Severe
23	15	1.45	No	Mild	**47**	15	1.45	No	Mild
24	15	1.45	No	Severe	**48**	15	1.45	No	Severe
49	W14 Rigid Case				**50**	W36 Rigid Case			

5.3 Effect of Vibration Characteristics

In this section, modal analysis is performed in order to investigate vibration characteristics of post-Northridge 3-story SAC building with semi-rigid connection. The periods of the models and their differences by rigid case are presented in Table 5.4. Also, it is visualized in Figure 5.3.

The rise in periods of semi-rigid frames shows that semi-rigid frames are more flexible than the rigid frames. The results show that only the parameter λ, the ratio of connection's initial stiffness to beam's flexural rigidity, has an influence on a period of a structure. The other parameters do not affect the vibration characteristics. Furthermore, it is observed that the influence of connection stiffness

ratio, λ, has the same level of period change for both frame configurations, i.e. LB and UB frames.

Table 5.4: Periods and Differences by Rigid Case of the Models

W14 LB			W36 UB		
Model #	**Period (sec)**	**Difference by Rigid Case (%)**	**Model #**	**Period (sec)**	**Difference by Rigid Case (%)**
1	1.1976485	16.32	**25**	1.0094828	16.71
2	1.1976485	16.32	**26**	1.0094828	16.71
3	1.1976485	16.32	**27**	1.0094828	16.71
4	1.1976485	16.32	**28**	1.0094828	16.71
5	1.1976485	16.32	**29**	1.0094828	16.71
6	1.1976485	16.32	**30**	1.0094828	16.71
7	1.1976485	16.32	**31**	1.0094828	16.71
8	1.1976485	16.32	**32**	1.0094828	16.71
9	1.1976485	16.32	**33**	1.0094828	16.71
10	1.1976485	16.32	**34**	1.0094828	16.71
11	1.1976485	16.32	**35**	1.0094828	16.71
12	1.1976485	16.32	**36**	1.0094828	16.71
13	1.1140734	8.20	**37**	0.9383479	8.48
14	1.1140734	8.20	**38**	0.9383479	8.48
15	1.1140734	8.20	**39**	0.9383479	8.48
16	1.1140734	8.20	**40**	0.9383479	8.48
17	1.1140734	8.20	**41**	0.9383479	8.48
18	1.1140734	8.20	**42**	0.9383479	8.48
19	1.1140734	8.20	**43**	0.9383479	8.48
20	1.1140734	8.20	**44**	0.9383479	8.48
21	1.1140734	8.20	**45**	0.9383479	8.48
22	1.1140734	8.20	**46**	0.9383479	8.48
23	1.1140734	8.20	**47**	0.9383479	8.48
24	1.1140734	8.20	**48**	0.9383479	8.48
49	1.0296331	0.00	**50**	0.8649796	0.00

In order to see the difference in period of rigid frames (Models 49 and 50) with the period of the same frames without including the effect of shear area like in SAC report, two rigid frame configurations (LB and UB) are modelled with the approach in Section 4.2.5. Force-based beam-column elements in OpenSees are used without including shear effects using shear aggregator. Periods are presented in Table 5.5. Thus, periods of the models without including shear effects are are close to the ones in SAC report. The difference between these two periods might be reduced by increasing the number of integration points along the members. Also, when shear area is taken into consideration, frames become more flexible. Determining a more accurate period is important because it has

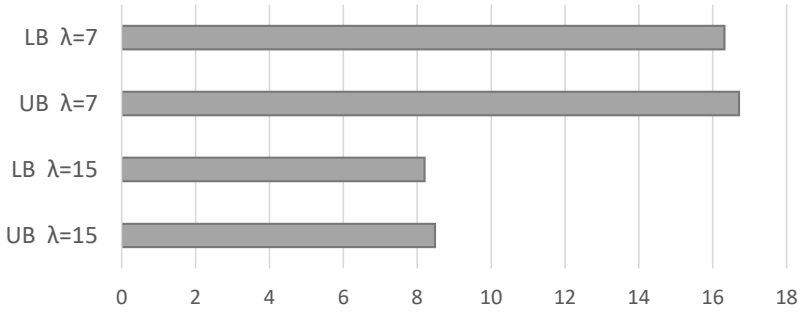

Figure 5.3: Differences in Period (%) by Rigid Case of the Models

a direct effect on the seismic load on the structure, as it is shown on response spectra in Figure 5.1 and Figure 5.2.

Table 5.5: Comparison of Rigid Frames

Model	Shear Area	Period (sec)
LB Rigid (SAC Report)	N/A	0.96
LB Rigid (This study)	N/A	0.9700126
LB Rigid (This study - Model 49)	Charney	1.0296331
UB Rigid (SAC Report)	N/A	0.78
UB Rigid (This study)	N/A	0.8040864
UB Rigid (This study - Model 50)	Charney	0.8649796

5.4 Effect of Pinching Level and Strength Loss by Frame Configurations

In this section, the responses from pushover analysis and time-history analysis are discussed. The responses of the models are presented and compared with each other for all ground motion data. Normalized base shear (absolute maximum of base shear over structure's seismic weight) vs. roof drift ratio (absolute maximum roof displacement over structure height) figure with pushover curve is given for each model on the left hand side of a figure. On the right hand side of a figure, interstory drift profiles are given with mean, median, 84th percentile and 95th percentile values. Percentile is a way to express the value below which a given percentage of observations in a group of observations fall. For example, 84th percentile is the value below which 84% of the observations fall. Similarly, 95th percentile is the value below which 95% of the observations fall. In

FEMA 355C report, how to find median and 84th percentile are explained [23]. Since MATLAB is used to draw these figures, MATLAB's *mean*, *median* and *quantile* commands are used to obtain mean, median, 84th and 95th percentile values. 84th percentile and 95th percentile values provide higher confidence to the obtained set of results and responses than mean and median values. In the literature, 84th percentile is used for higher confidence and median is used for the discussion of average results.

After getting results from pushover analysis and time-history analysis, it is seen that some of ground motions cause convergence problems since their effect is enormous. For that reason, maximum drift ratio is limited to 15%, and unrealistic values coming from outlier data are omitted. Moreover, pushover analysis is carried out up to 10% roof drift ratio for the demonstration of the results between two different analysis approaches.

FEMA 356 defines structural performance levels and ranges [1]. There are four discrete structural performance levels and two intermediate structural performance ranges. The discrete structural performance levels are Intermediate Occupancy (IO) Level (S-1), Life Safety (LS) Level (S-3), Collapse Prevention (CP) Level (S-5) and Not Considered (S-6). The intermediate structural performance ranges are Damage Control Range (S-2) and Limited Safety Range (S-4). Their definitions are as follows;

- In **Immediate Occupancy Level (S-1)**, the structure has very little damage after the earthquake and can retain nearly all of its pre-earthquake design strength and stiffness.
- **Damage Control Range (S-2)** is the continuous range of damage states between Immediate Occupancy Level (S-1) and Life Safety Level (S-3). (S-2) is desired to reduce repair time and operation interruption.
- In **Life Safety Level (S-3)**, some structural elements can have severe damage, but the structure retains a margin against onset of partial or total collapse.
- **Limited Safety Range (S-4)** is the continuous range of damage states

between Life Safety Level (S-3) and Collapse Prevention Level (S-5).

- In **Collapse Prevention Level (S-5)**, structural elements have severe damage, but the structure still carries gravity loads. It retains no margin against collapse. That is, the structure is close to collapse. Since there is substantial damage in the structure, significant degradation in the stiffness and strength, large permanent lateral deformation and degradation in vertical load carrying capacity are expected.

- In **Not Considered (S-6)**, a building rehabilitation does not address the performance of the structure.

For steel moment frames, drift ratios are given in Table 5.6,

Table 5.6: Drift ratios by structural performance level for steel moment frames in FEMA 356 [1]

	Drift Ratio (%)	
Structural Performance Level	**Transient**	**Permanent**
Immediate Occupancy Level (S-1)	0.7	Negligible
Life Safety Level (S-3)	2.5	1.0
Collapse Prevention Level (S-5)	5.0	5.0

Six cases plus rigid case are created in order to see the effect of some parameters easily. Results will be presented in the following cases;

1. Rigid Case
2. Case 1: $\lambda = 7$, $\beta = 0.75$
3. Case 2: $\lambda = 15$, $\beta = 0.75$
4. Case 3: $\lambda = 7$, $\beta = 1.1$
5. Case 4: $\lambda = 15$, $\beta = 1.1$
6. Case 5: $\lambda = 7$, $\beta = 1.45$
7. Case 6: $\lambda = 15$, $\beta = 1.45$

5.4.1 Rigid Case

The rigid cases of both frame configurations must be studied first in order to compare the models created with different parameter groups,. For this reason, pushover and nonlinear time history analyses are carried out on post-Northridge 3-story SAC building (rigid case). The results for rigid cases are presented in Figure 5.4. They show that for LB rigid case, mean, median and 84th percentile interstory drift ratios (IDR) are below CP level of 5%, but 95th percentile IDR slightly passes this limit. For UB rigid case, all of mean, median, 84th and 95th percentile IDR values are below CP level. Thus, rigid cases for LB and UB structures can be considered safe in terms of CP level.

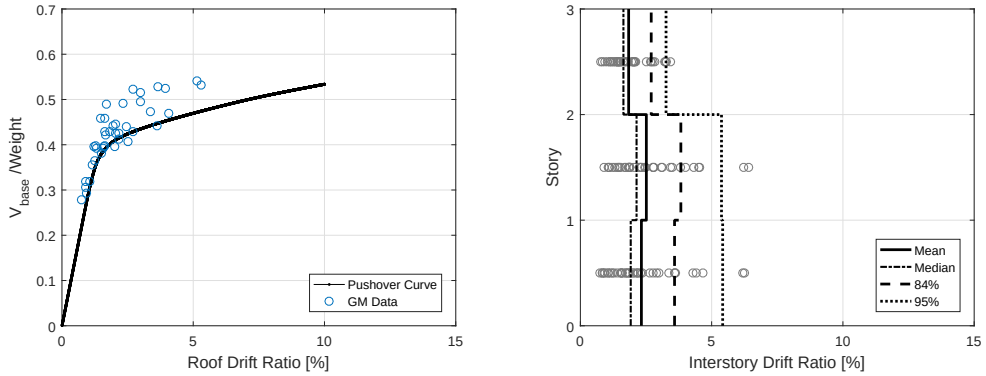

(a) Model 49: LB Rigid Case

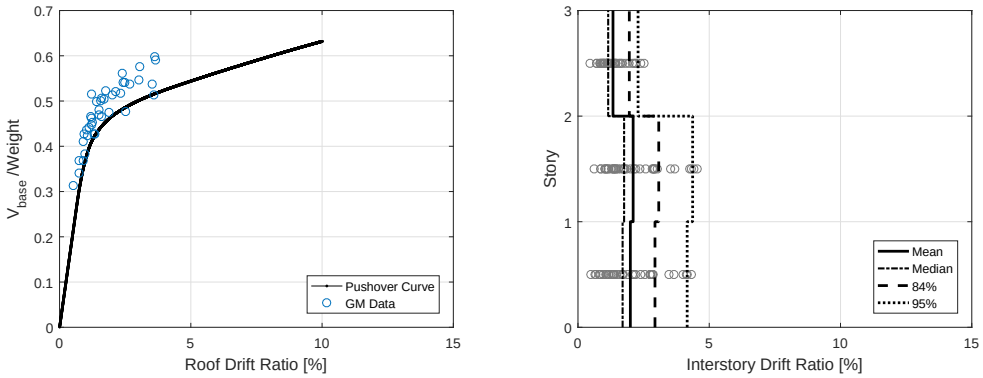

(b) Model 50: UB Rigid Case

Figure 5.4: Models 49 and 50 (Rigid Cases)

Median IDR values of two frame configurations in this study are compared with median IDR values of two frame configurations in SAC report [24]. It is presented in Figure 5.5. Because shear deformations in the models in SAC report are not taken into account, their periods are lower than the models in this study. Thus,

this causes slight differences in interstory drifts.

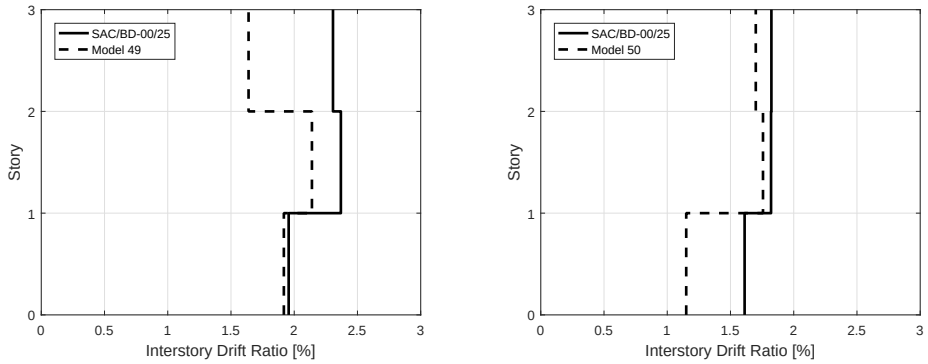

Figure 5.5: Median IDR Profile Comparison of LB (on the left) and UB (on the right) Rigid Cases in SAC Report and This Study

5.4.2 Case 1: $\lambda = 7$, $\beta = 0.75$

The results for this case are presented in Figure 5.6. When there is strength loss for both frame configurations, LB and UB, (Models 1, 2, 25 and 26), 95th percentile interstory drift ratios (IDR) in these four models are much beyond CP level (5%). Mean, median and 84th percentile IDR values are similar between these models. Mean and median IDR values are lower than CP level. When severe and mild pinching conditions are compared, IDR in models with mild pinching is less than IDR in models with severe pinching.

When there is no strength loss and whether pinching is mild or severe for both LB and UB structures (Models 3, 4, 27 and 28), IDR values significantly decrease compared with the model results with strength loss. 95th percentile IDR values in these four models are beyond CP level, but mean, median and 84th percentile IDR values are lower than CP level.

Pushover curve in Model 1 shows clear strength degradation while nonlinear time history analysis shows as if it does not have strength degradation. However, in reality, it does show strength degradation. The reason is that all the ground motion figures (Vbase vs. RDR) belong to the cases are presented in absolute maximum value and that roof drift does not happen at the same time with base shear. To make it more clear, a new figure (Figure 5.12) is created only for the ground motion data (LA40) close to 10% roof drift ratio in Model 1 in Figure 5.6.

Figure 5.12 contains base shear (base shear over structure's seismic weight) vs. roof drift ratio (roof displacement over structure height) figure with pushover curve for Model 1. There is a sudden excitation after some initial cycles, and then the structure is pushed into nonlinear range. There is an unloading, and the structure collapses about 7-10% roof drift ratio.

5.4.3 Case 2: $\lambda = 15$, $\beta = 0.75$

The results are presented in Figure 5.7. When there is strength loss for both frame configurations (Models 13, 14, 37 and 38), similar to Case 1, 95th percentile IDR values in these four models are much beyond CP level (5%). Only in Model 14, 84th percentile IDR value is over CP level. Mean, median and 84th percentile IDR values are below CP level in all four models except for Model 14 - 84th percentile IDR value.

When there is no strength loss and whether pinching is mild or severe for both LB and UB structures (Models 15, 16, 39 and 40), IDR values significantly decreases comparing models with strength loss. 95th percentile IDR values in these four models are beyond CP level except for Model 15. Mean, median and 84th percentile IDR values are in the limits of CP level.

5.4.4 Case 3: $\lambda = 7$, $\beta = 1.1$

The results are presented in Figure 5.8. With the increase of β parameter from 0.75 to 1.1, connection's peak moment capacity is increased comparing previous cases and it is visible from all Case 3 figures. Different than first two cases, second floor drifts are always higher than the first and the top floor in this case for all models.

When there is strength loss for both frame configurations (Models 5, 6, 29 and 30), although 95th percentile IDR values are over CP level (5%), mean, median and 84th percentile IDR values are below CP level. Similarly, when there is no strength loss (Models 7, 8, 31 and 32), 95th percentile IDR value is over CP level, and mean, median and 84th percentile IDR values are less than 5% CP

level.

5.4.5 Case 4: $\lambda = 15$, $\beta = 1.1$

The results are presented in Figure 5.9. It is apparent that connection's peak moment capacity is increased comparing first two cases. Similar to Case 3, second floor drifts are higher than the first and the top floor in this case for all models.

For both frame configurations (Models 17 to 20, 41 to 44), comparing two frame configurations, LB and UB, IDR values in UB structures (Models 41 to 44) are lower than that in LB structures (Models 17 to 22). In these eight models, although 95th percentile IDR values are over CP level (5%), mean, median and 84th percentile IDR values are below CP level.

5.4.6 Case 5: $\lambda = 7$, $\beta = 1.45$

The results are presented in Figure 5.10. As expected, connection's peak moment capacity is increased due to the change of β parameter from 1.1 to 1.45, comparing previous cases and it is visible in all Case 5 figures. It is also remarkable that models with strength loss (Models 9, 10, 33 and 34) shows higher ductility comparing with the models with strength loss in the previous cases.

Similar to previous cases, IDR values in UB structures (Models 33 to 36) are lower than that in LB structures (Models 9 to 12). In these eight models, 95th percentile IDR values are over CP level (5%), and mean, median and 84th percentile IDR values are below CP level.

5.4.7 Case 6: $\lambda = 15$, $\beta = 1.45$

The results are presented in Figure 5.11. It is apparent that connection's peak moment capacity is increased comparing first four cases. Similar to Case 5, second floor drifts are higher than the first and the top floor in this case for all models.

In LB structures (Models 21 to 24), 95th percentile IDR values are over CP level (5%), and mean, median and 84th percentile IDR values are below CP level. In UB structures (Models 45 to 48), on the other hand, mean, median, 84th and 95th percentile IDR values are in the limits of CP level.

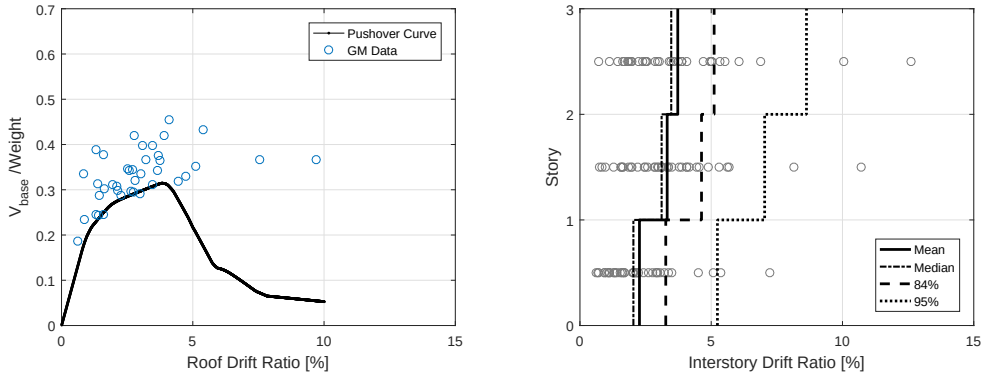

(a) Model 1: LB, Strength Loss, Mild Pinching

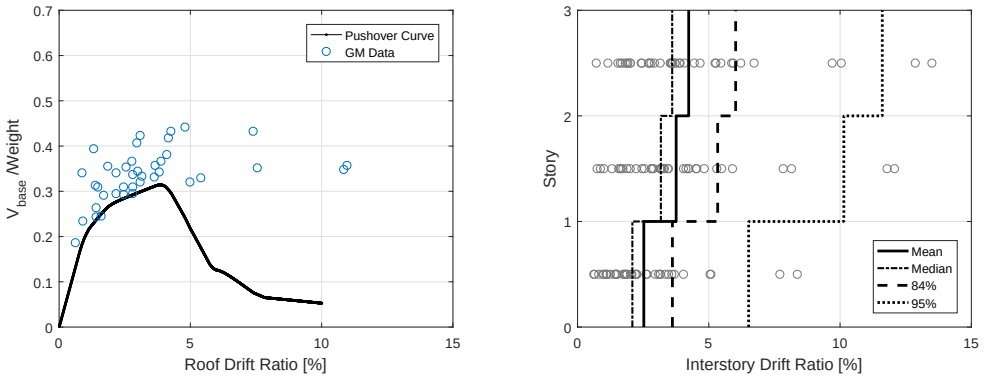

(b) Model 2: LB, Strength Loss, Severe Pinching

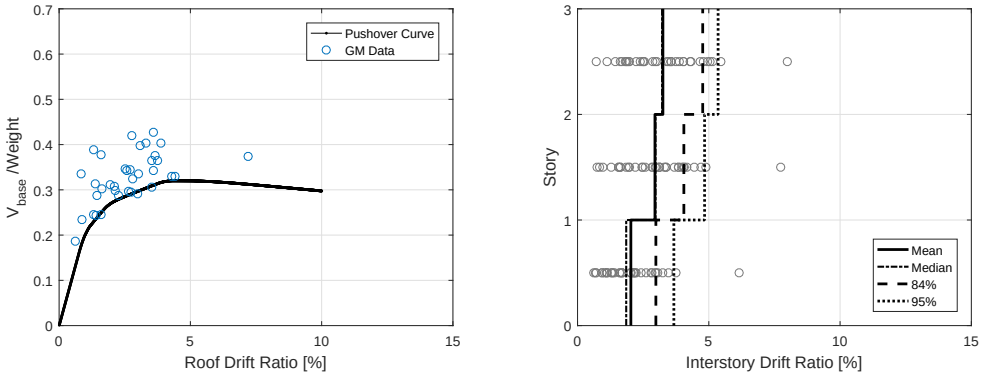

(c) Model 3: LB, No Strength Loss, Mild Pinching

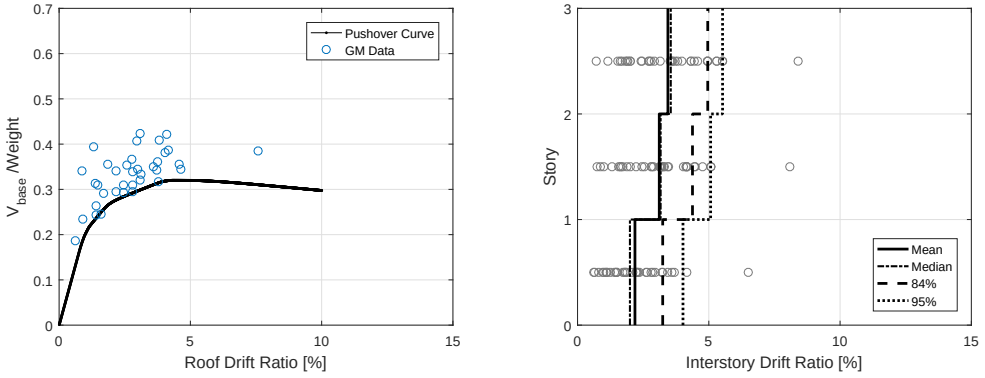

(d) Model 4: LB, No Strength Loss, Severe Pinching

Figure 5.6: Case 1: $\lambda = 7$, $\beta = 0.75$

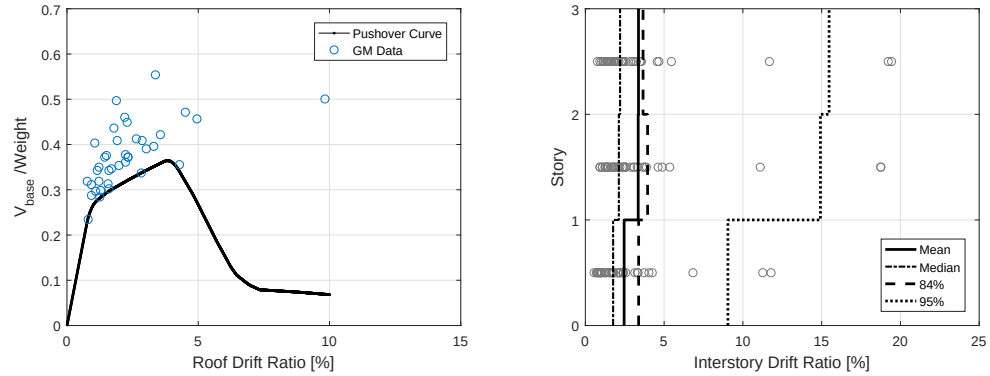

(e) Model 25: UB, Strength Loss, Mild Pinching

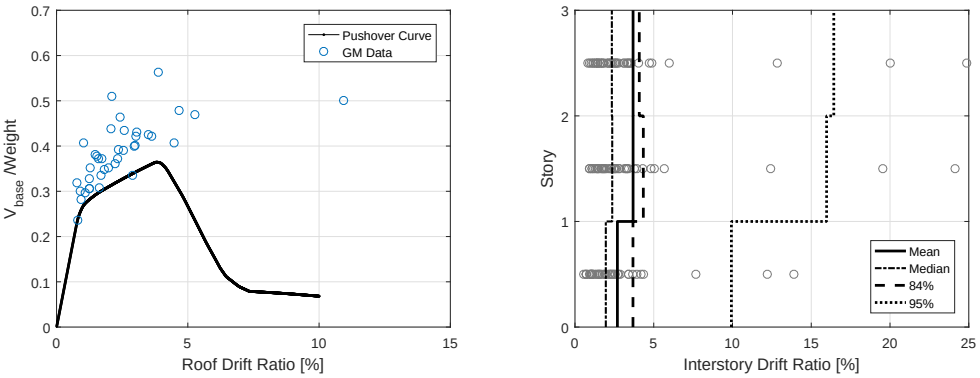

(f) Model 26: UB, Strength Loss, Severe Pinching

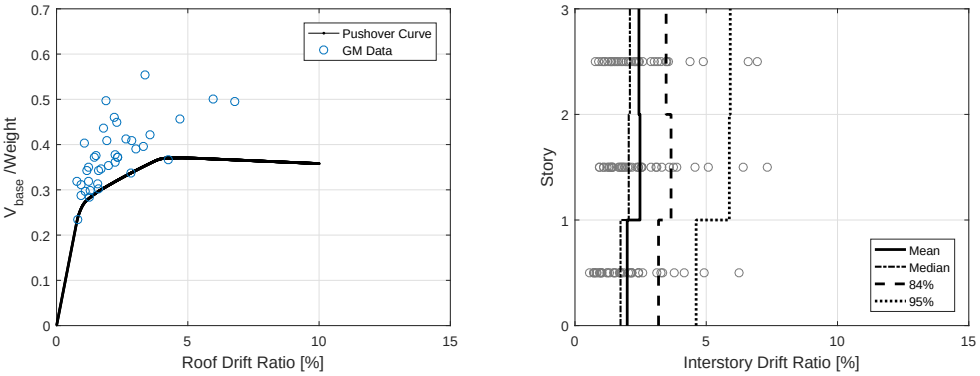

(g) Model 27: UB, No Strength Loss, Mild Pinching

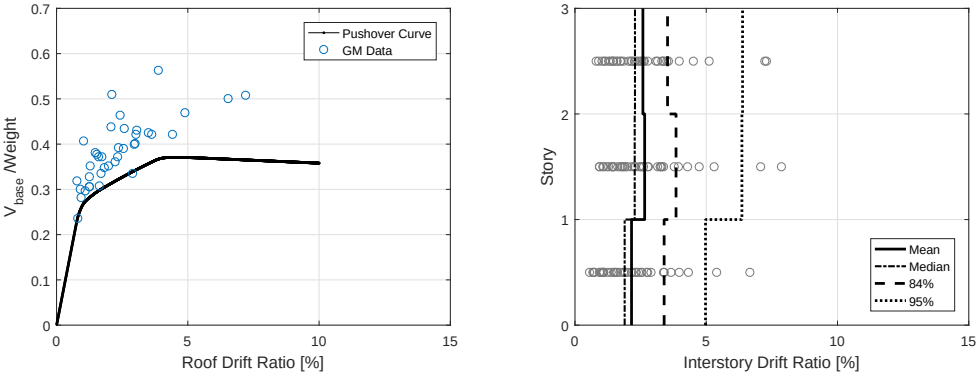

(h) Model 28: UB, No Strength Loss, Severe Pinching

Figure 5.6: Case 1: $\lambda = 7$, $\beta = 0.75$ (cont.)

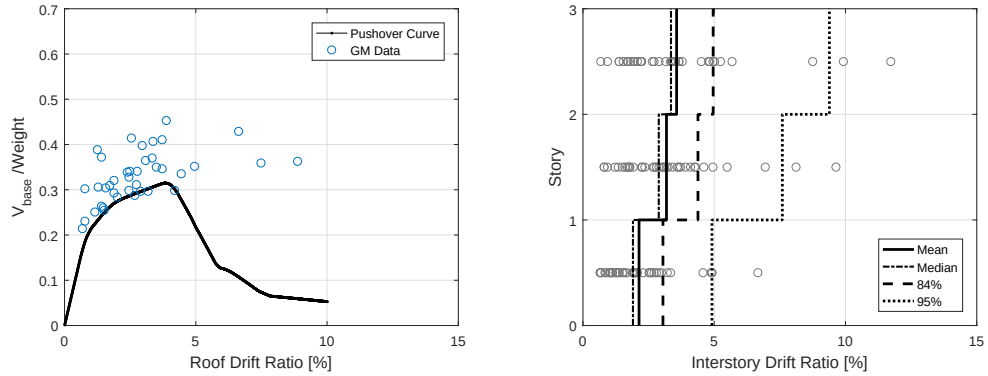

(a) Model 13: LB, Strength Loss, Mild Pinching

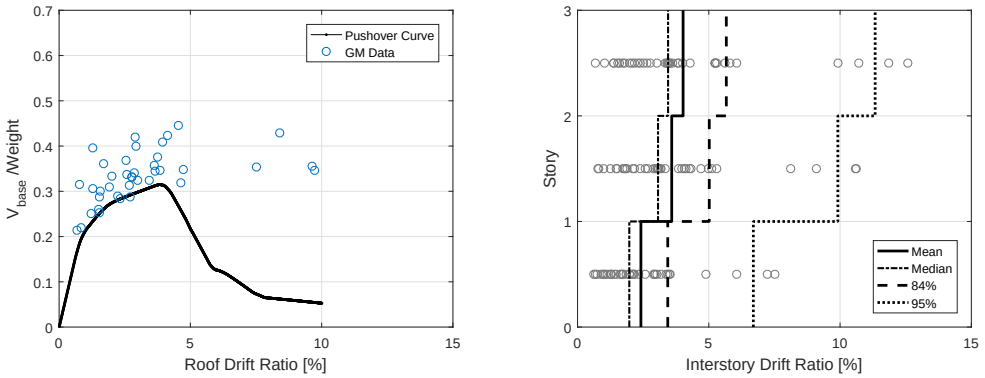

(b) Model 14: LB, Strength Loss, Severe Pinching

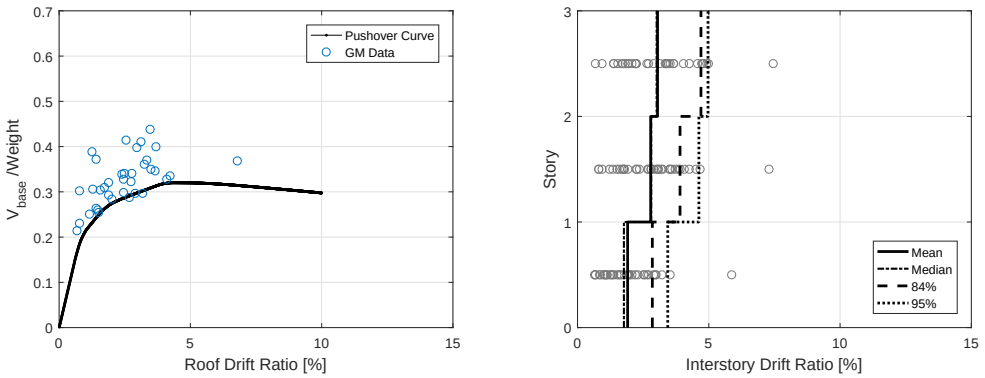

(c) Model 15: LB, No Strength Loss, Mild Pinching

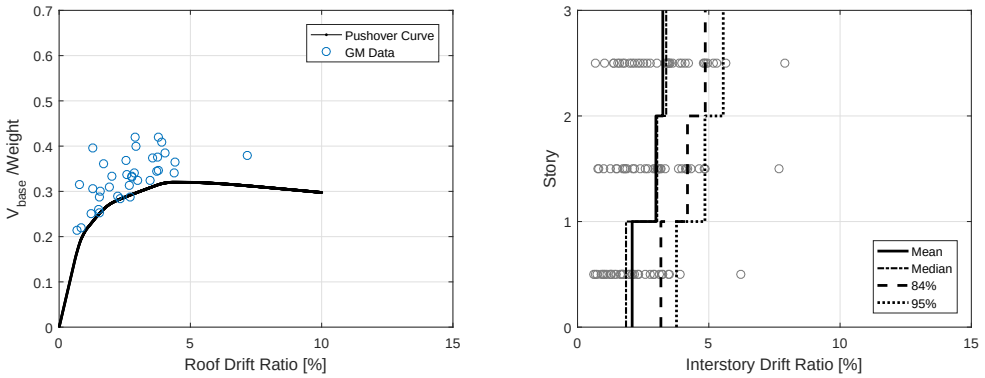

(d) Model 16: LB, No Strength Loss, Severe Pinching

Figure 5.7: Case 2: $\lambda = 15$, $\beta = 0.75$

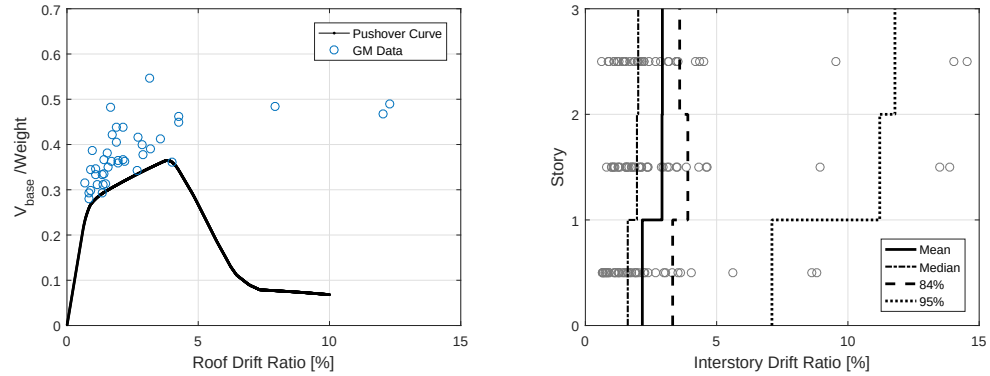

(e) Model 37: UB, Strength Loss, Mild Pinching

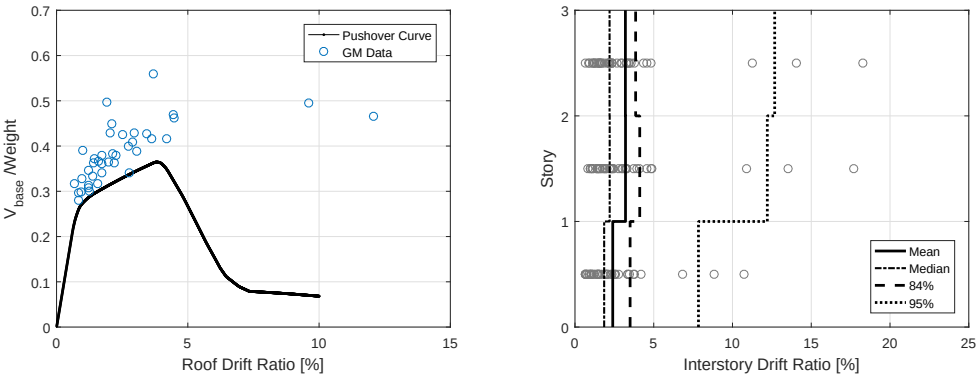

(f) Model 38: UB, Strength Loss, Severe Pinching

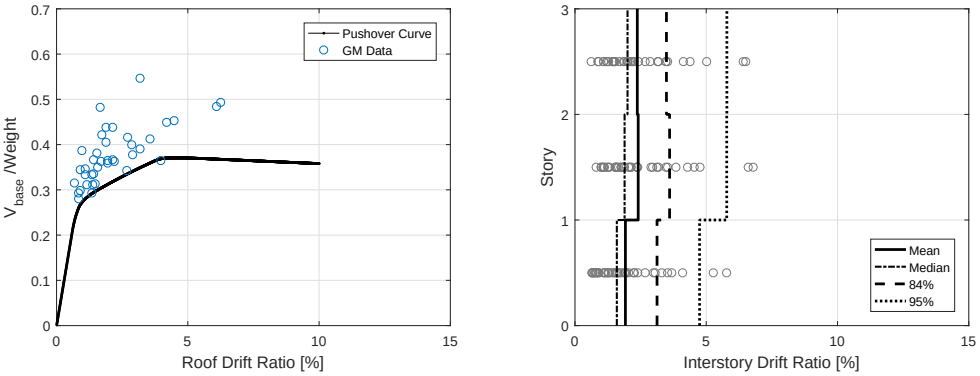

(g) Model 39: UB, No Strength Loss, Mild Pinching

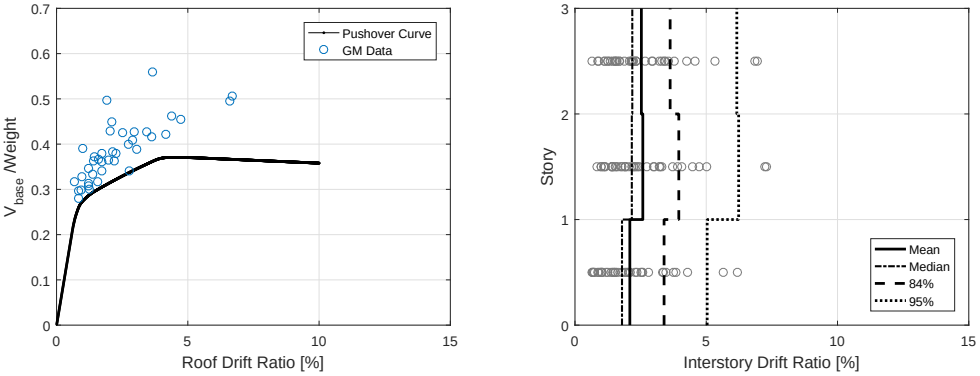

(h) Model 40: UB, No Strength Loss, Severe Pinching

Figure 5.7: Case 2: $\lambda = 15$, $\beta = 0.75$ (cont.)

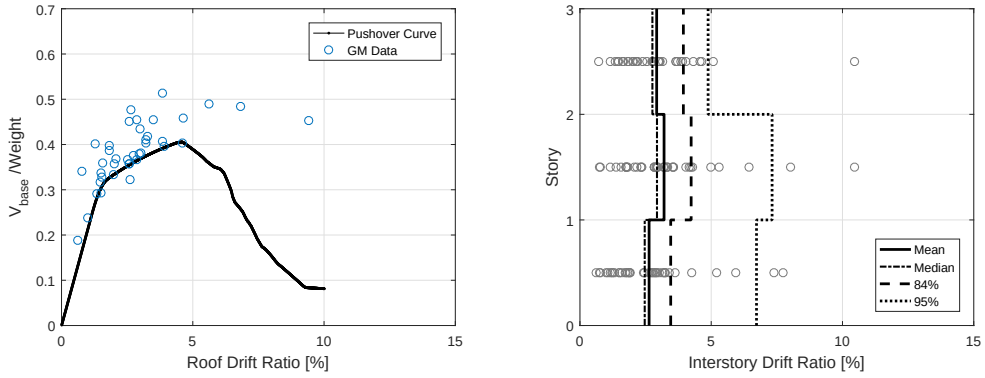

(a) Model 5: LB, Strength Loss, Mild Pinching

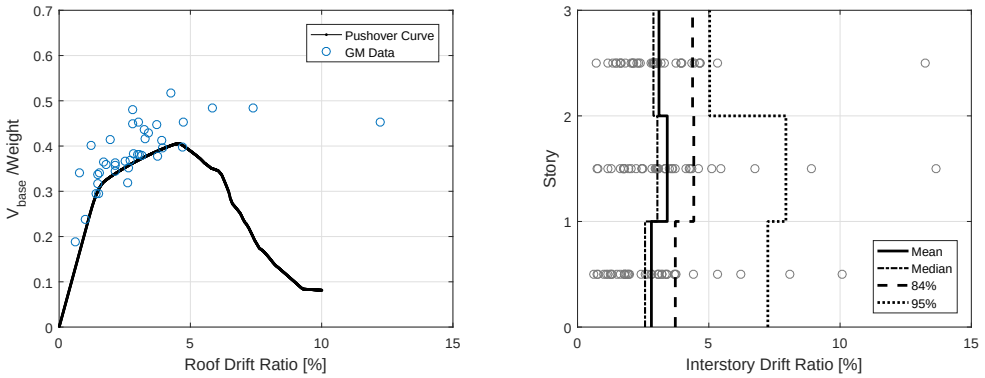

(b) Model 6: LB, Strength Loss, Severe Pinching

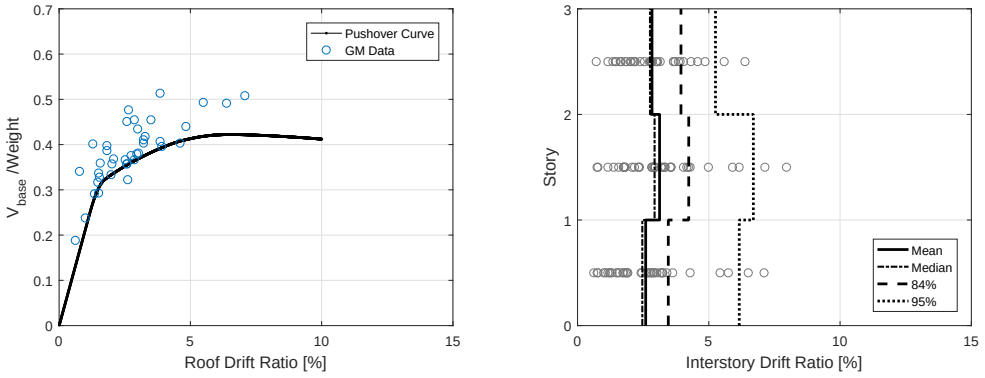

(c) Model 7: LB, No Strength Loss, Mild Pinching

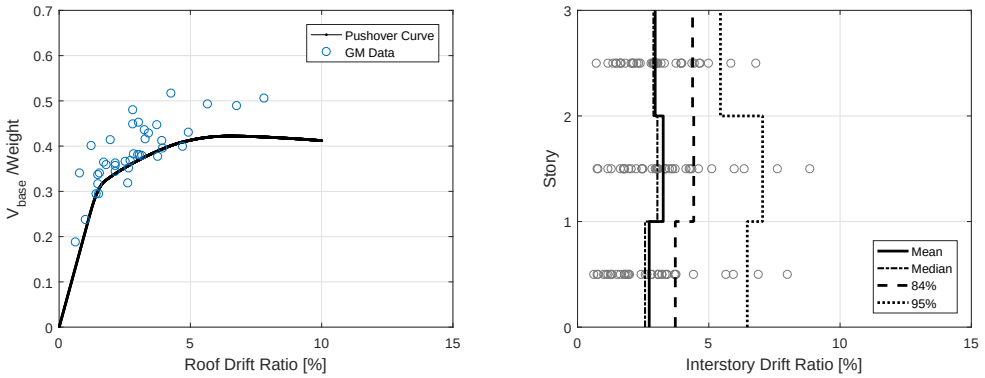

(d) Model 8: LB, No Strength Loss, Severe Pinching

Figure 5.8: Case 3: $\lambda = 7$, $\beta = 1.1$

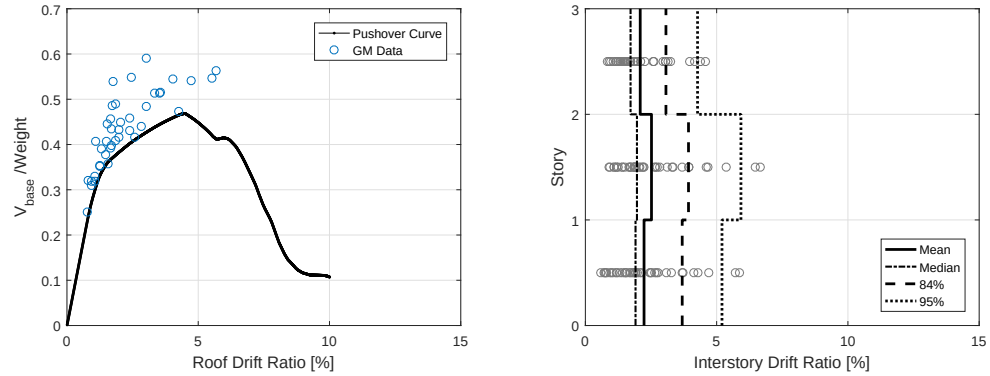

(e) Model 29: UB, Strength Loss, Mild Pinching

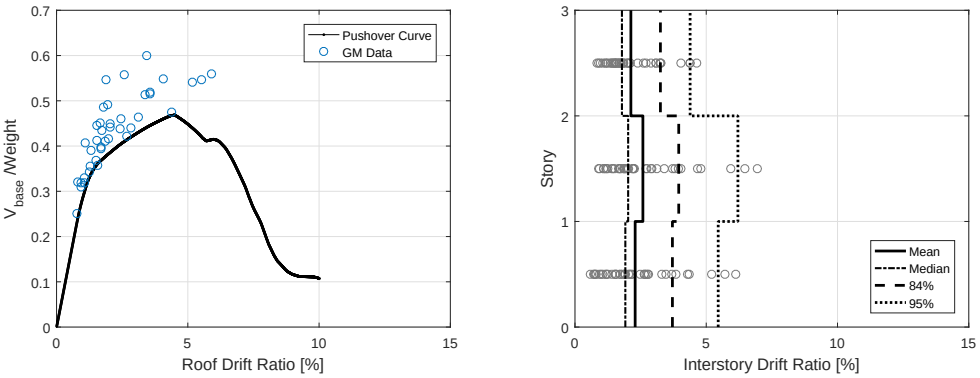

(f) Model 30: UB, Strength Loss, Severe Pinching

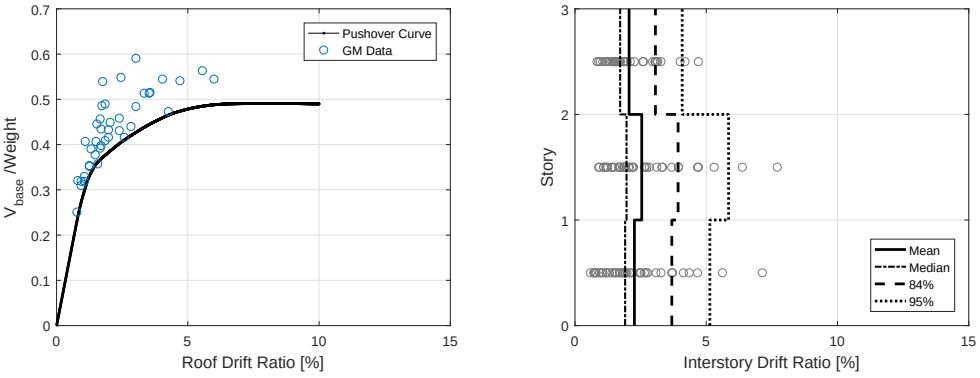

(g) Model 31: UB, No Strength Loss, Mild Pinching

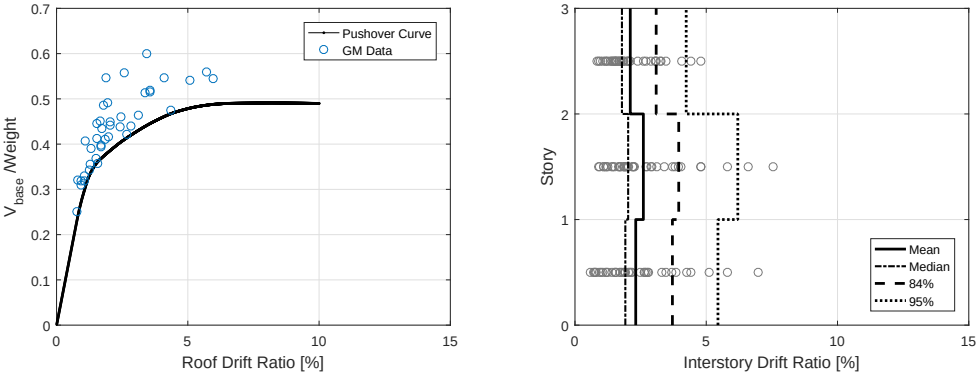

(h) Model 32: UB, No Strength Loss, Severe Pinching

Figure 5.8: Case 3: $\lambda = 7$, $\beta = 1.1$ (cont.)

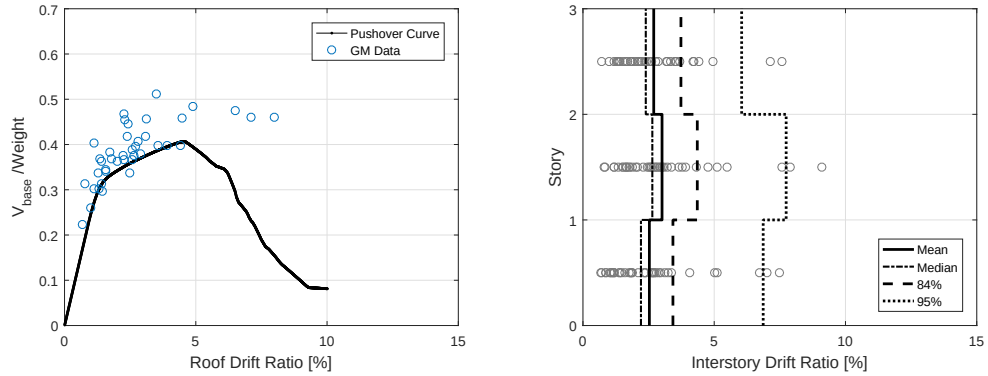

(a) Model 17: LB, Strength Loss, Mild Pinching

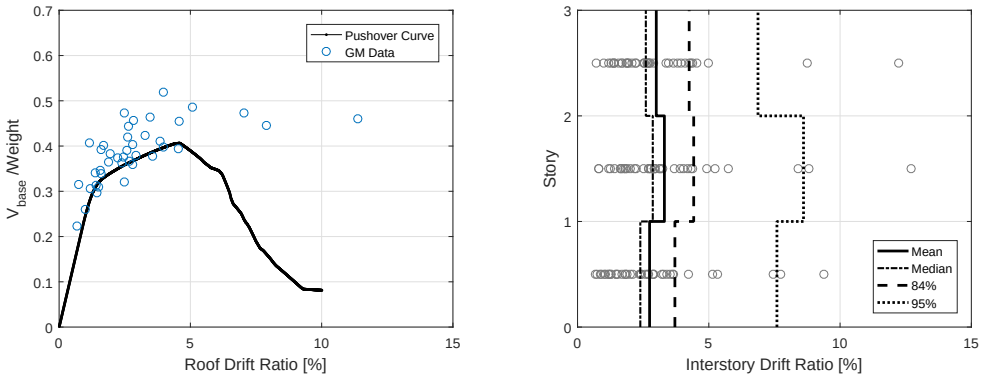

(b) Model 18: LB, Strength Loss, Severe Pinching

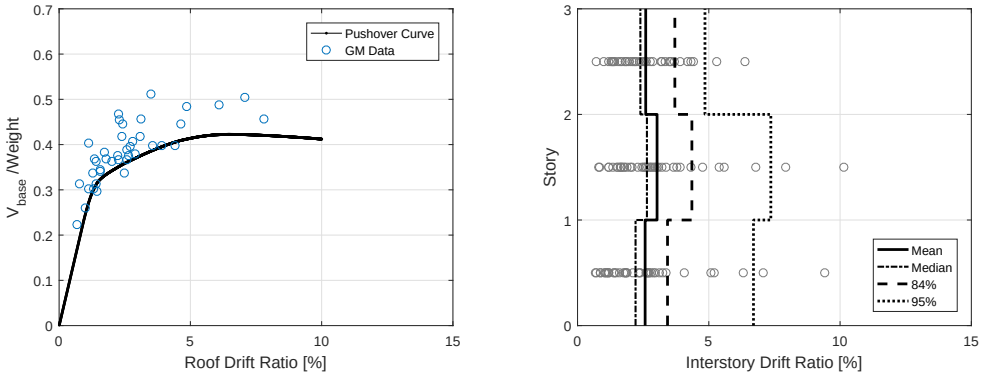

(c) Model 19: LB, No Strength Loss, Mild Pinching

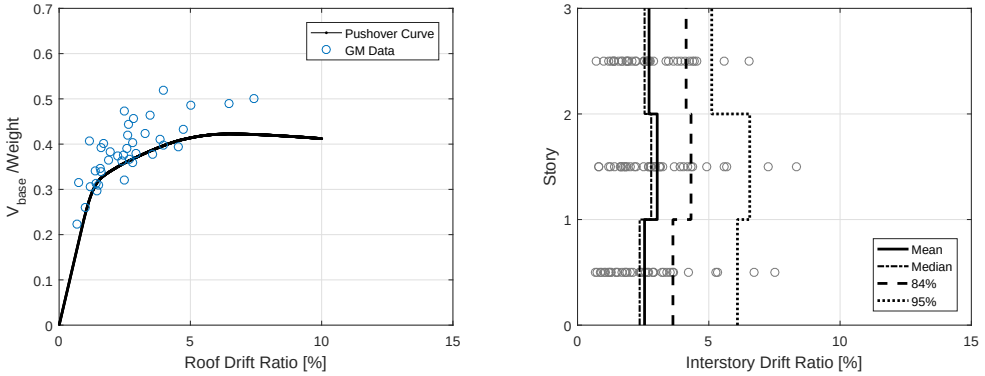

(d) Model 20: LB, No Strength Loss, Severe Pinching

Figure 5.9: Case 4: $\lambda = 15$, $\beta = 1.1$

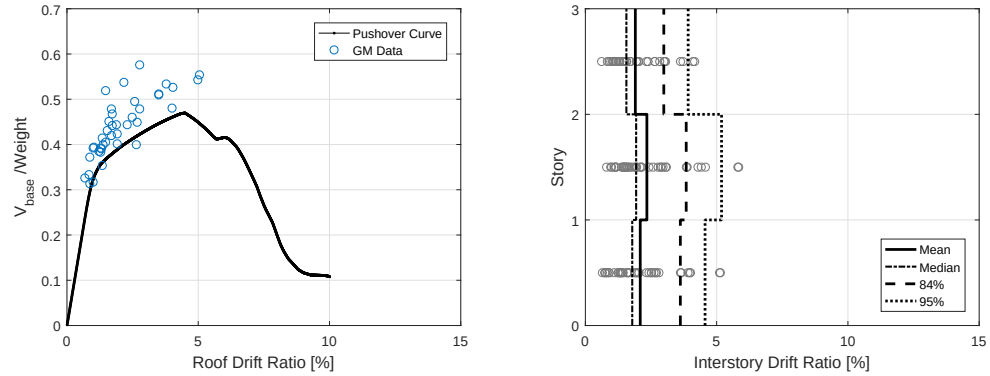

(e) Model 41: UB, Strength Loss, Mild Pinching

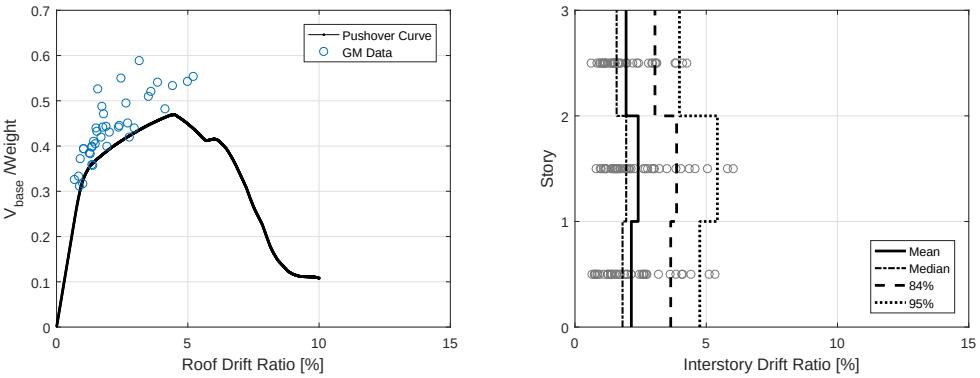

(f) Model 42: UB, Strength Loss, Severe Pinching

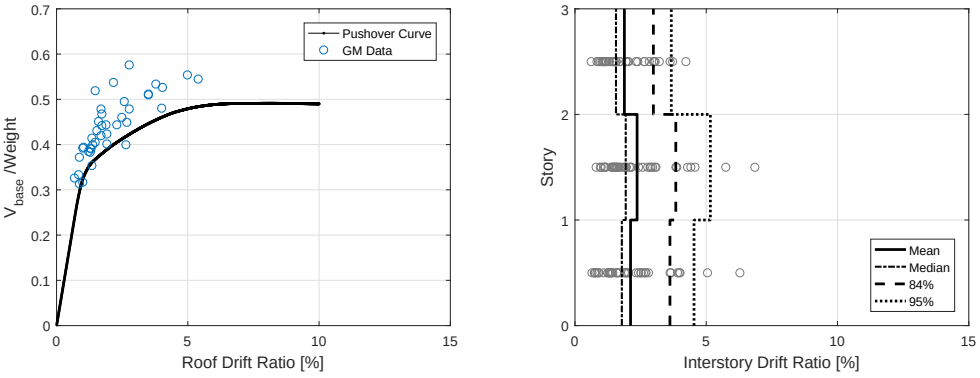

(g) Model 43: UB, No Strength Loss, Mild Pinching

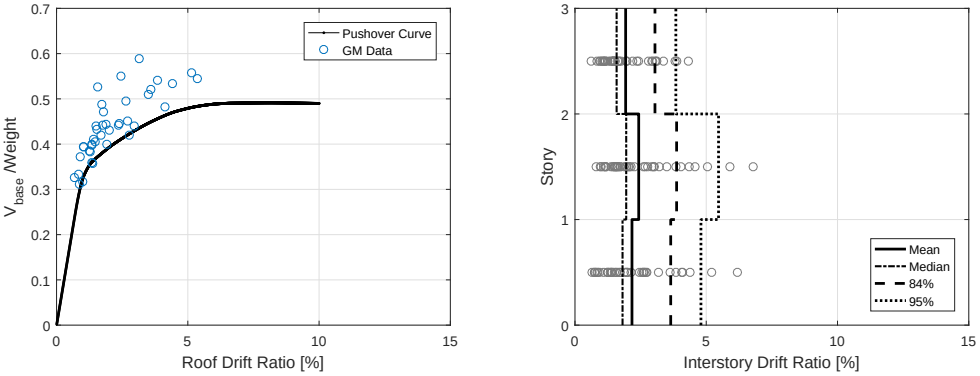

(h) Model 44: UB, No Strength Loss, Severe Pinching

Figure 5.9: Case 4: $\lambda = 15$, $\beta = 1.1$ (cont.)

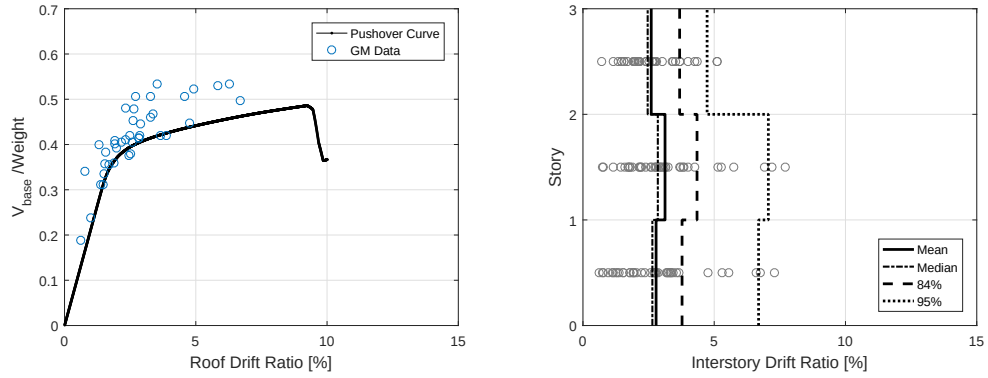

(a) Model 9: LB, Strength Loss, Mild Pinching

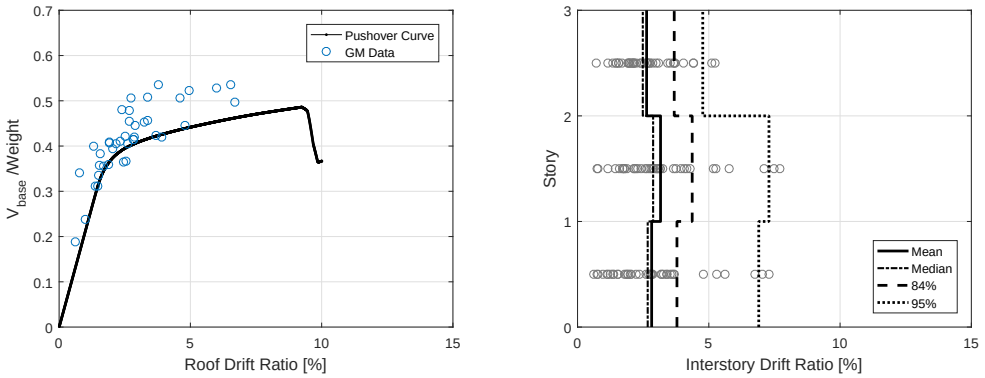

(b) Model 10: LB, Strength Loss, Severe Pinching

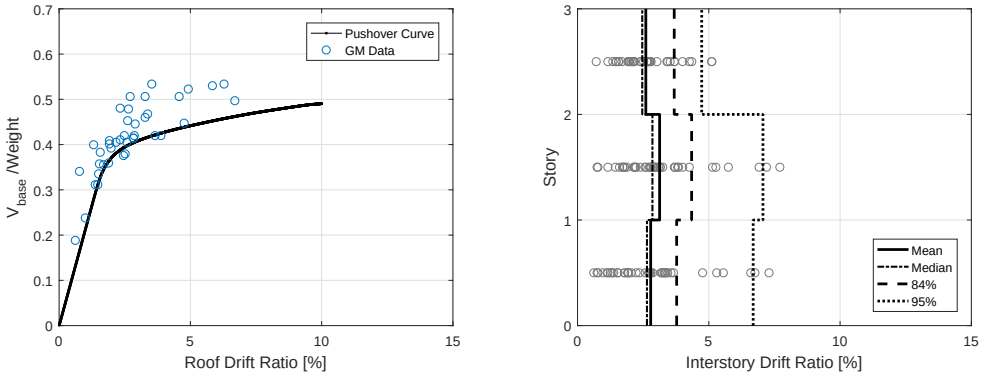

(c) Model 11: LB, No Strength Loss, Mild Pinching

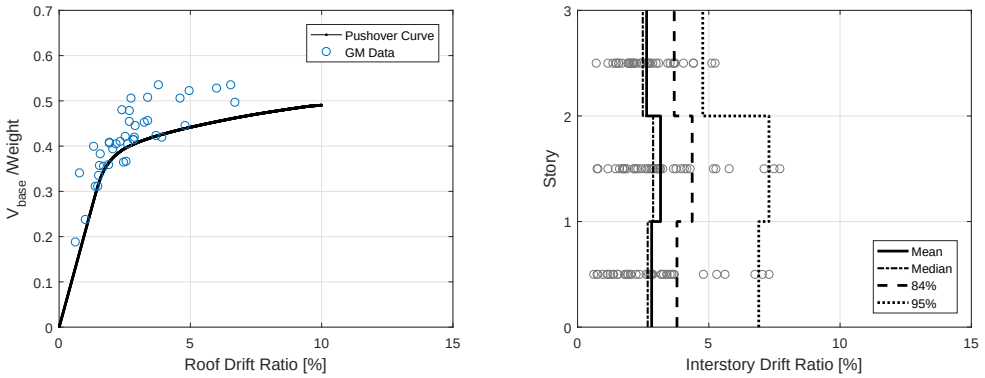

(d) Model 12: LB, No Strength Loss, Severe Pinching

Figure 5.10: Case 5: $\lambda = 7$, $\beta = 1.45$

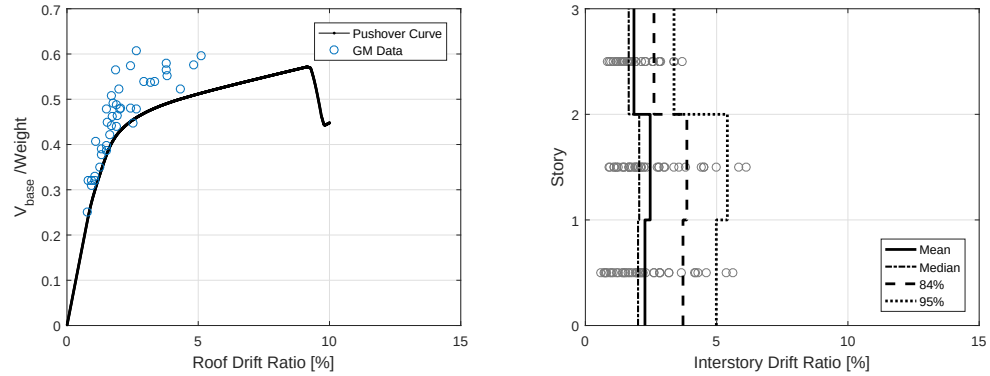

(e) Model 33: UB, Strength Loss, Mild Pinching

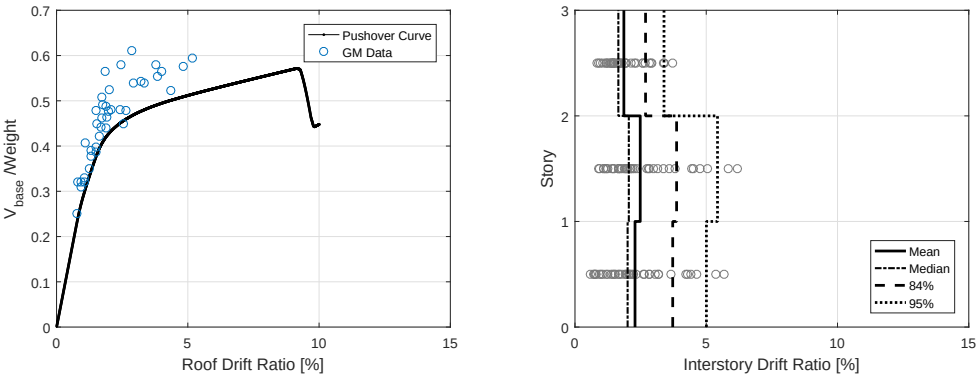

(f) Model 34: UB, Strength Loss, Severe Pinching

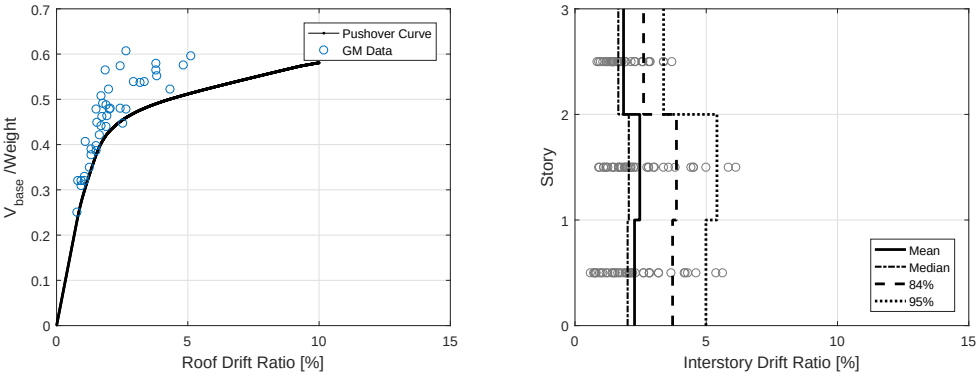

(g) Model 35: UB, No Strength Loss, Mild Pinching

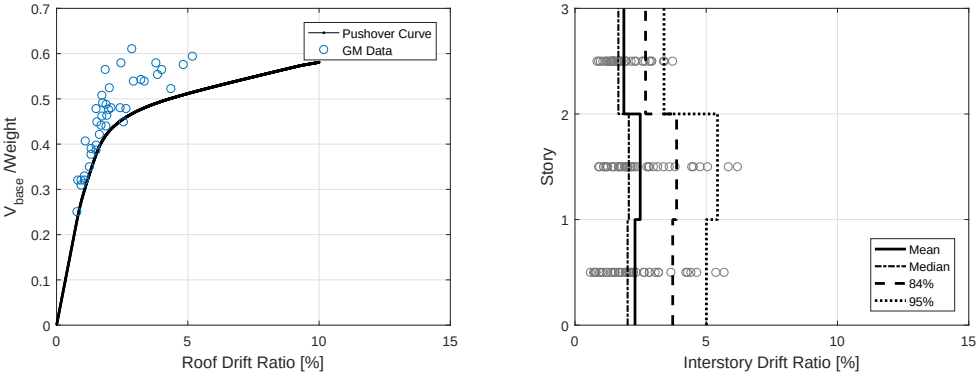

(h) Model 36: UB, No Strength Loss, Severe Pinching

Figure 5.10: Case 5: $\lambda = 7$, $\beta = 1.45$ (cont.)

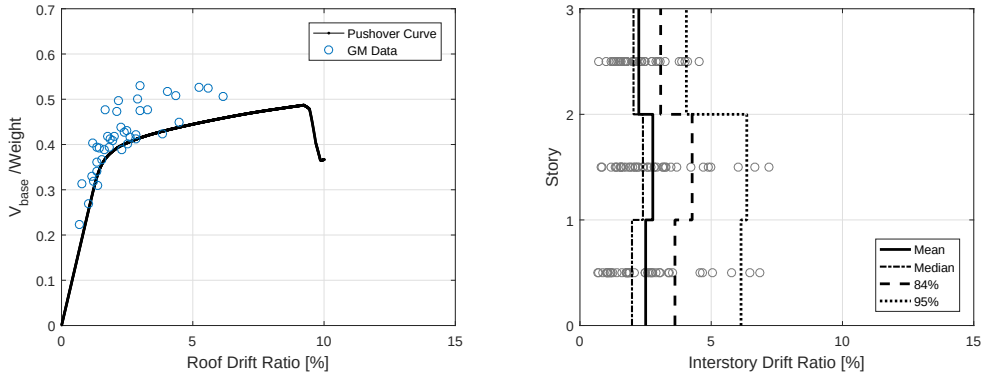

(a) Model 21: LB, Strength Loss, Mild Pinching

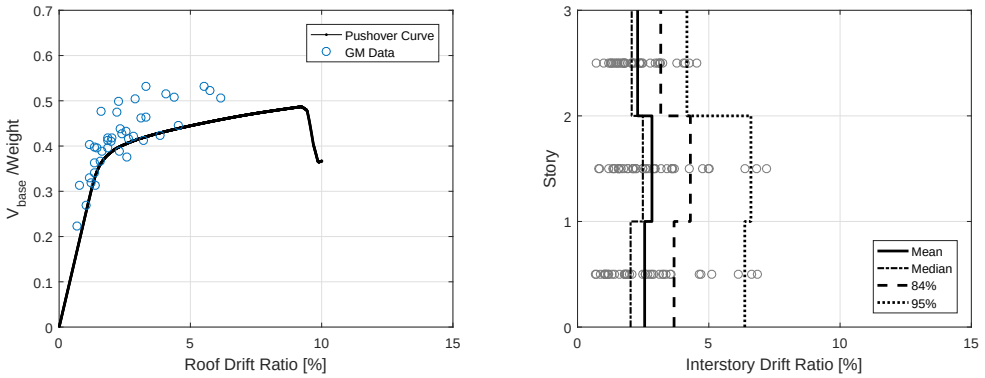

(b) Model 22: LB, Strength Loss, Severe Pinching

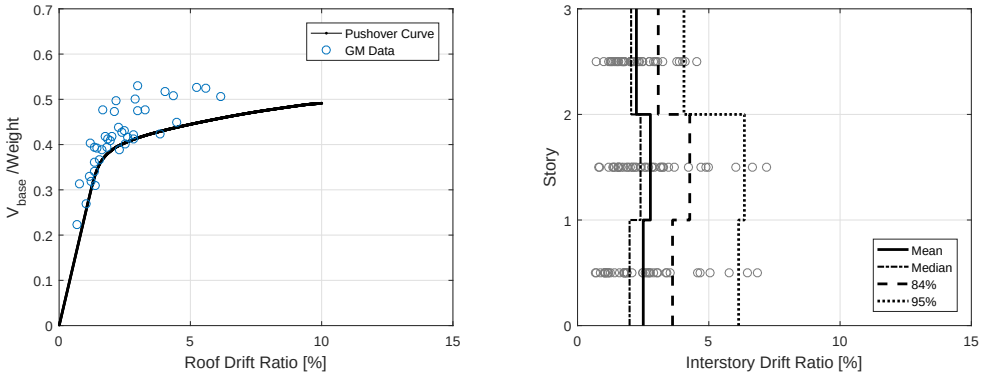

(c) Model 23: LB, No Strength Loss, Mild Pinching

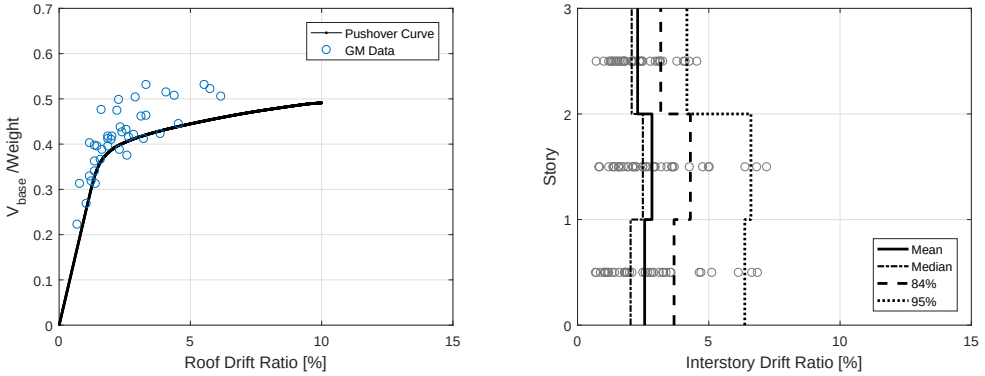

(d) Model 24: LB, No Strength Loss, Severe Pinching

Figure 5.11: Case 6: $\lambda = 15$, $\beta = 1.45$

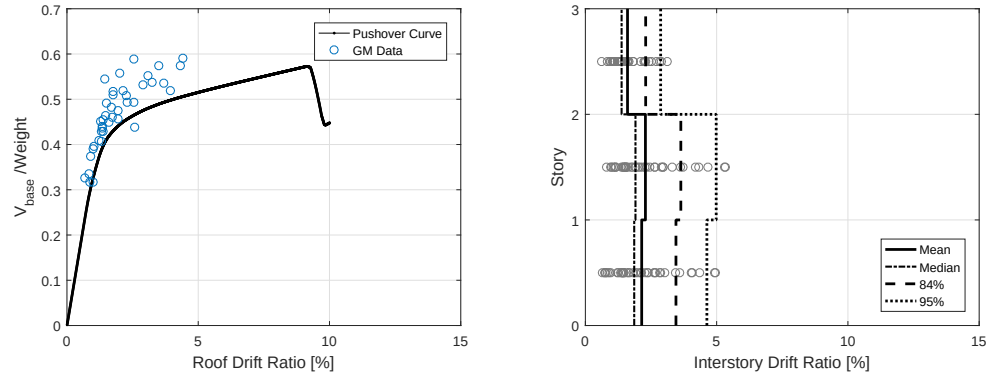

(e) Model 45: UB, Strength Loss, Mild Pinching

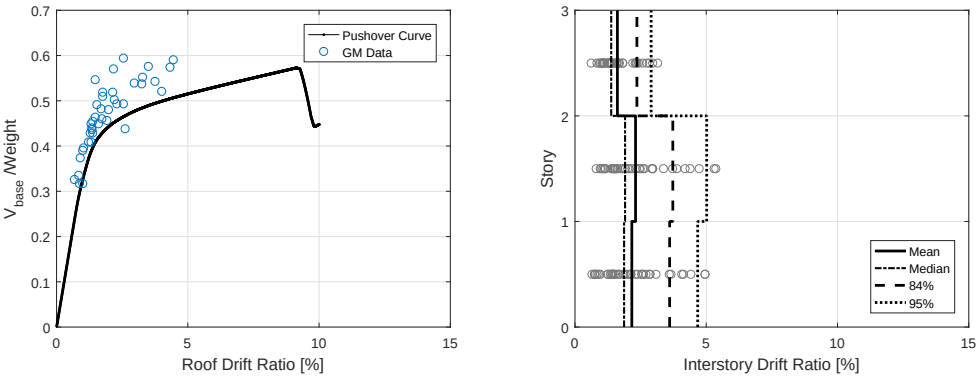

(f) Model 46: UB, Strength Loss, Severe Pinching

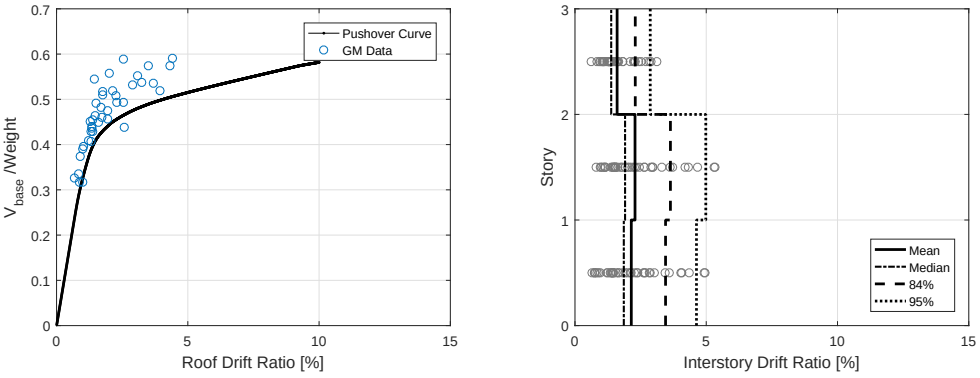

(g) Model 47: UB, No Strength Loss, Mild Pinching

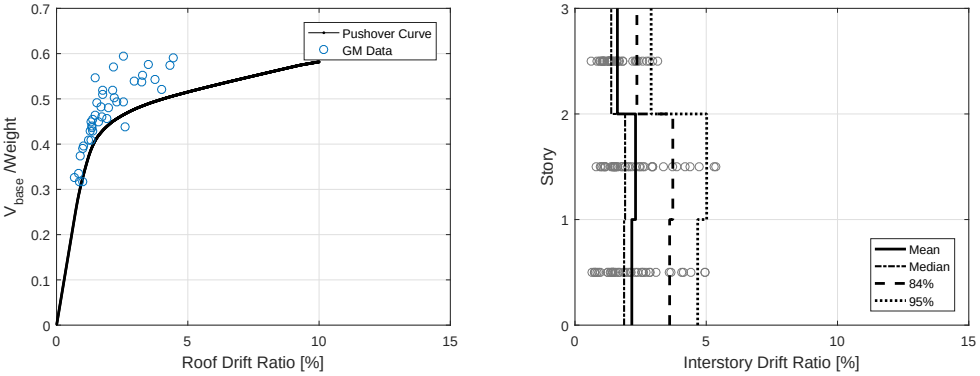

(h) Model 48: UB, No Strength Loss, Severe Pinching

Figure 5.11: Case 6: $\lambda = 15$, $\beta = 1.45$ (cont.)

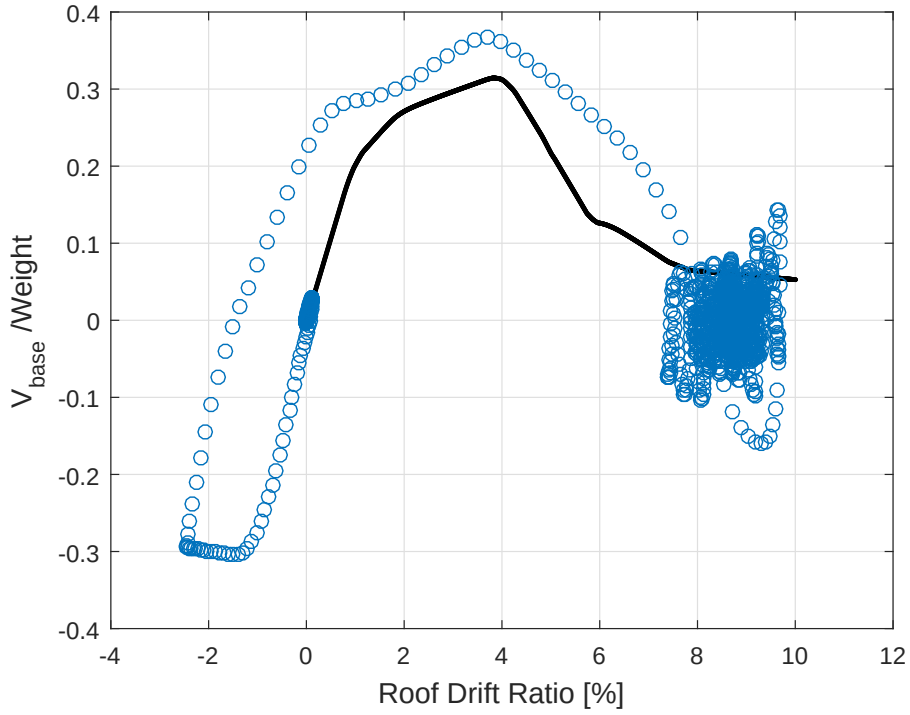

Figure 5.12: V_{base}/W vs. RDR of LA40 Ground Motion and Pushover Curve in Model 1

5.5 Assessment of the Structural Responses from Parametric Study

The maximum absolute value of interstory drift ratio (IDR) for each model of a frame is determined separately for median and 84th percentile and compared with the maximum absolute IDR in rigid frame in order to assess structural responses from parametric studies in previous section. The ratio of the maximum IDR value in a model to the maximum IDR value in rigid case separately for median and 84th percentile according to their frame configuration $\Delta_{IDR\,max}^{Model\,i}/\Delta_{IDR\,max}^{Rigid}$ is calculated. Physical significance of the results that are presented in radar charts is explained in Figure 5.13. On horizontal axis from left to right, a connection goes from partial strength to full strength. Similarly, on vertical axis, from top to bottom, a connection gains stiffness and goes from flexible connection to stiff connection. The results are presented with radar charts for median values in LB and UB structures in Figure 5.14 and Figure 5.15, and for 84th percentile values in LB and UB structures in Figure 5.16 and Figure 5.17.

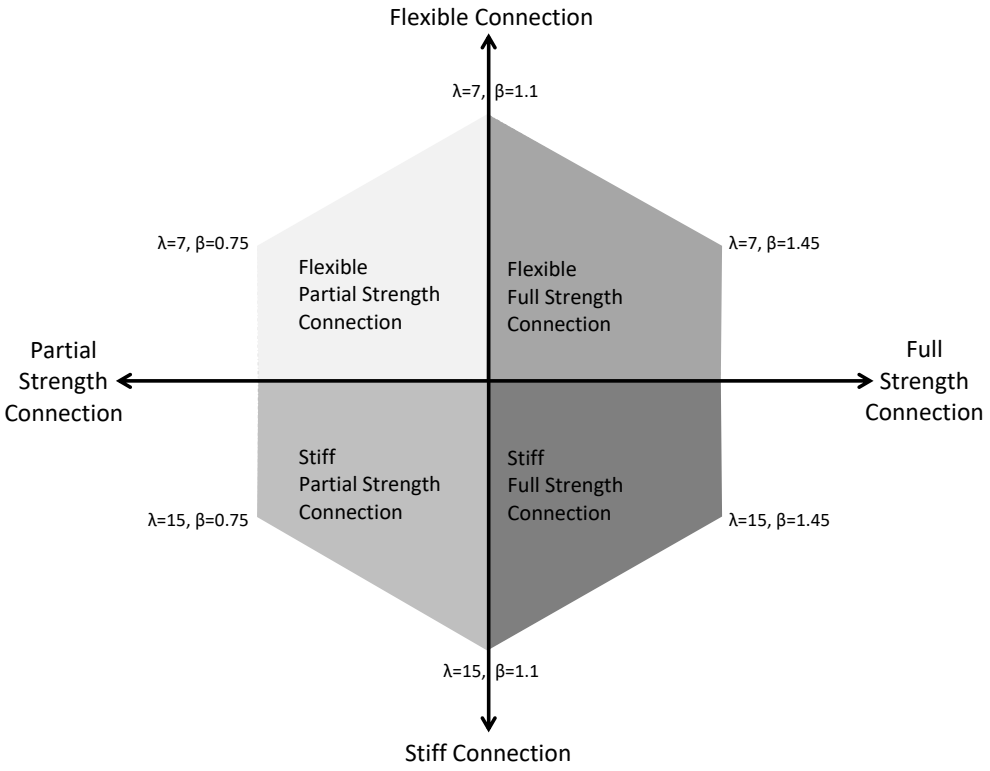

Figure 5.13: Guide for radar charts presented next

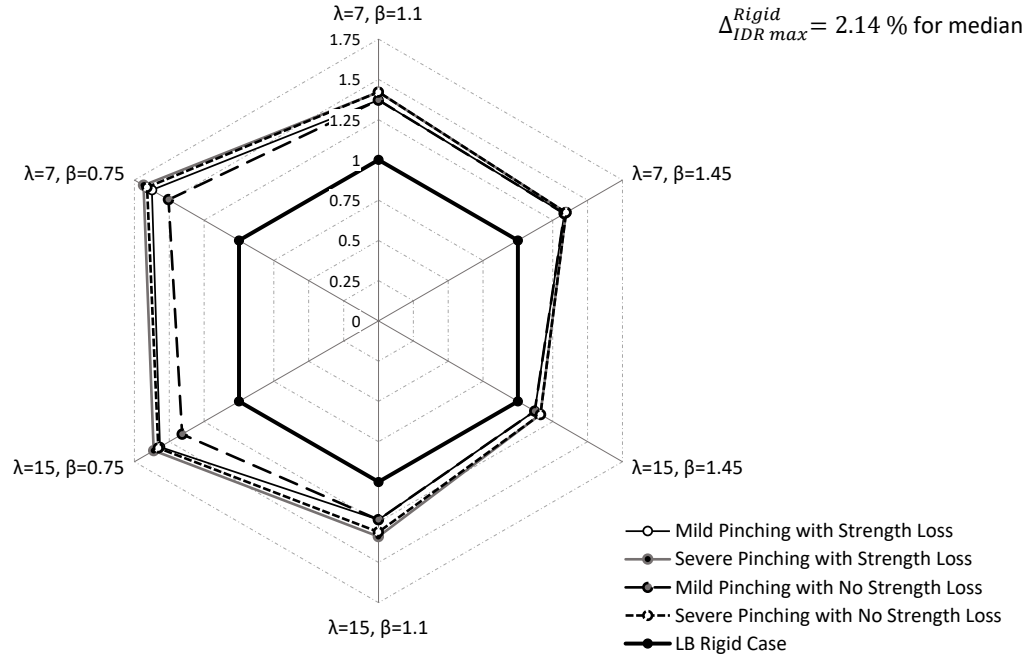

Figure 5.14: $\Delta_{IDR\,max}^{Model\,i}/\Delta_{IDR\,max}^{Rigid}$ for median IDR values in LB models

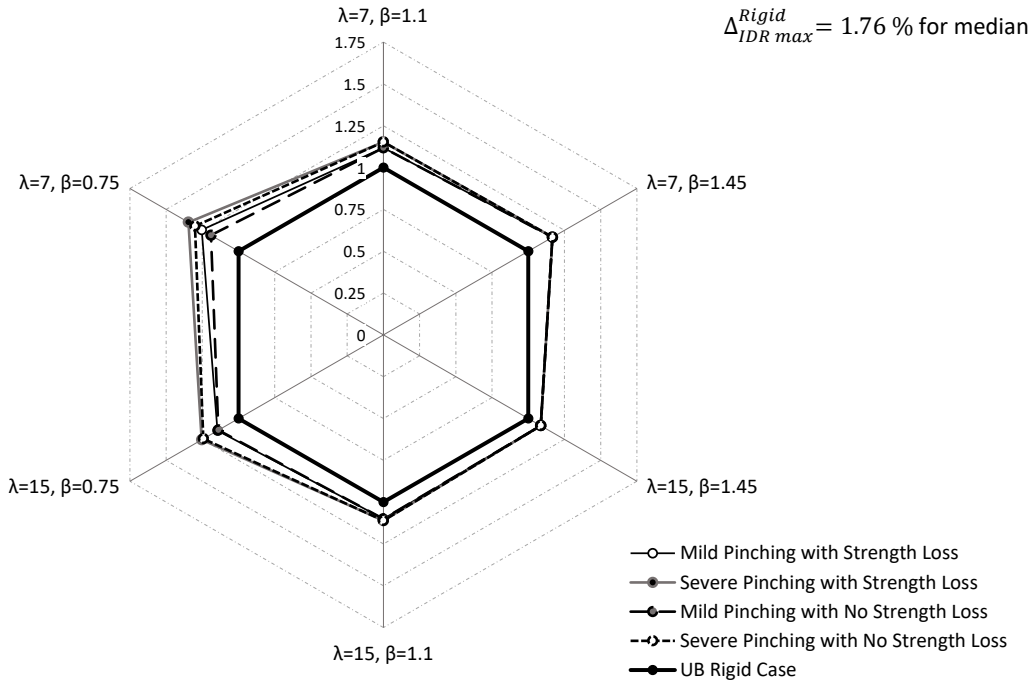

Figure 5.15: $\Delta_{IDR\,max}^{Model\,i}/\Delta_{IDR\,max}^{Rigid}$ for median IDR values in UB models

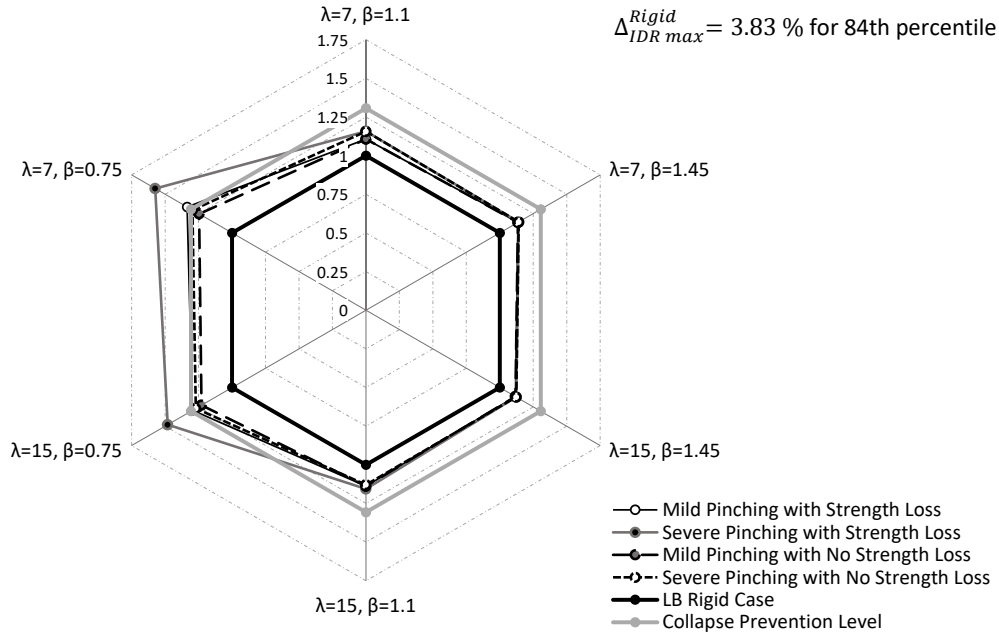

Figure 5.16: $\Delta_{IDR\,max}^{Model\,i}/\Delta_{IDR\,max}^{Rigid}$ for 84th percentile IDR values in LB models

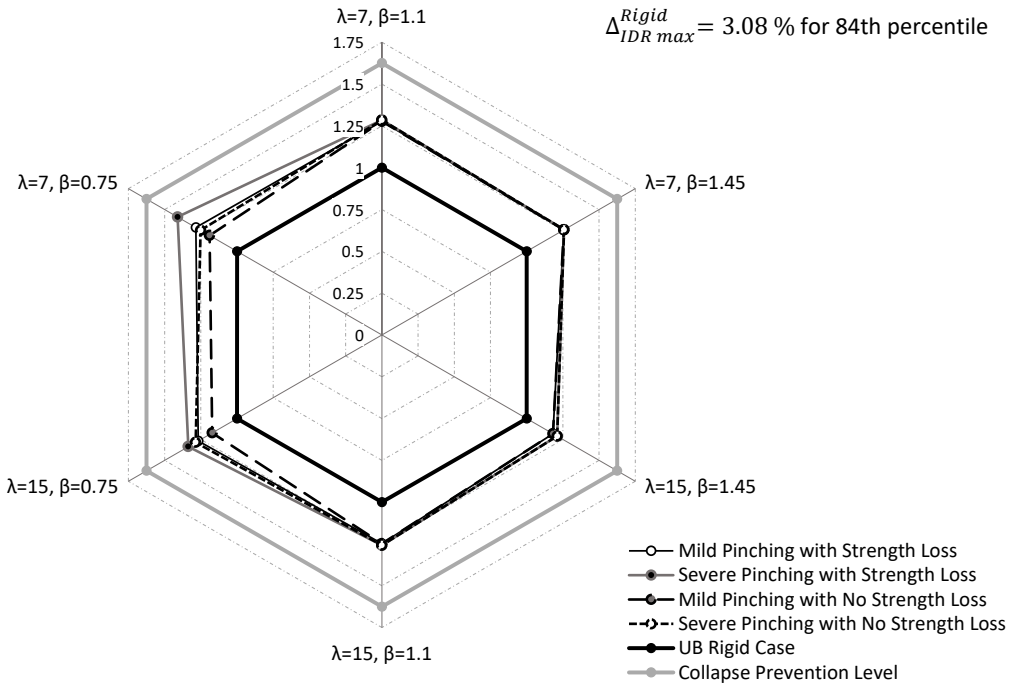

Figure 5.17: $\Delta_{IDR\,max}^{Model\,i}/\Delta_{IDR\,max}^{Rigid}$ for 84th percentile IDR values in UB models

When cases for median values in LB and UB structures are considered, the frames have relatively more deformations than the rigid case. Decrease in initial stiffness (λ in this study) makes a frame naturally more flexible and increases the displacement demands on a structure regardless of whether the frame is partial strength ($\beta = 0.75$) or full strength ($\beta = 1.1$ and $\beta = 1.45$ parameters in this study). Full strength connections show behavior closer to rigid case in both frame configurations as expected. The most critical cases among the results for LB and UB structures are observed in partial strength connections. Although the ratio of $\Delta_{IDR\,max}^{Model\,i}/\Delta_{IDR\,max}^{Rigid}$ is between 1.5 and 1.75 in LB structures with partial strength connections and approximately 1.25 in UB structures with partial strength connections, the responses are still safe in terms of CP level. The ratio representing CP level in Figure 5.14 and Figure 5.15 can be calculated as $\Delta^{CP\,Level}/\Delta_{IDR\,max}^{LB\,Rigid} = 5/2.14 = 2.34$ for LB structures and $\Delta^{CP\,Level}/\Delta_{IDR\,max}^{UB\,Rigid} = 5/1.76 = 2.84$ for UB structures, where the values are out of bounds these figures. This means that not only cases with partial strength, but also all cases for median values in LB and UB structures do not exceed the CP level of 5%. Even though a frame has connection responses with strength loss, but ensuring ductility of 0.04 rad at 80% of maximum connection strength as shown in Figure 4.9, it is still safe with regard to median IDR values, not exceeding CP level.

When cases for 84th percentile values in LB and UB structures are considered, the displacement demand in these cases is higher than the displacement demand in rigid case. For LB structures, the ratio of $\Delta_{IDR\,max}^{Model\,i}/\Delta_{IDR\,max}^{Rigid}$ in all cases in 84th percentile values is lower than that in median values for LB structures, but this is opposite for UB structures. A change in initial stiffness (λ) does not significantly affect the flexibility of a frame regardless of whether the frame is partial strength ($\beta = 0.75$) or full strength ($\beta = 1.1$ and $\beta = 1.45$) for 84th percentile values. The most critical cases among the results for LB and UB structures are observed in partial strength connections. The ratio representing CP levels in Figure 5.16 and Figure 5.17 can be calculated as $\Delta^{CP\,Level}/\Delta_{IDR\,max}^{LB\,Rigid} = 5/3.83 = 1.30$ for LB structures and $\Delta^{CP\,Level}/\Delta_{IDR\,max}^{UB\,Rigid} = 5/3.08 = 1.62$ for UB structures, where these limits are shown on these figures. In LB structures, the

cases other than the case with severe pinching with strength loss are safe since their ratios are under CP level, but the ratio in the case with severe pinching with strength loss exceeds CP level. When cases in UB structures are compared with CP level, all cases are safe with regard to 84th percentile IDR values.

All in all, in this section both results from median and 84th percentile values are gathered and compared with rigid cases of both frame configurations. If rigid case of a low-rise SMRF is designed compliant to ductility, stiffness and strength limitations of codes for higher period values (LB rigid frames), then the real behavior of connections are taken into account in the analysis for assessment of response, overall behavior of a structure can become critical in terms of drift demands, i.e. CP level can be exceeded. On the other hand, if rigid case of a low-rise SMRF is designed compliant to ductility, stiffness and strength limitations of codes for lower period values (UB rigid frames), then the real behavior of connections are taken into account in the analysis for assessment of response, overall behavior of a structure is not endangered in terms of increased drift demands, i.e. CP level is not exceed. This shows that UB design of structures provides more reliable structural response in the case when connection response demonstrates nonlinear behavior.

CHAPTER 6

CONCLUSION AND FUTURE RECOMMENDATIONS

6.1 Conclusion

In the scope of this thesis, the influence of several parameters to the nonlinear behavior of semi-rigid connections on general response of low-rise steel special moment resisting frames is studied. After a brief introduction and literature review in Chapter 1, modelling of frame members and semi-rigid connections are explained, and introduction on analysis types is done in Chapter 2. Then, a detailed information about post-Northridge 3-story SAC building is given along with material properties, loading conditions and steel section information in Chapter 3. In order to determine the precision of the model used in the analyses in terms of vibration characteristics and moment-rotation behavior of semi-rigid connections, preliminary comparison studies on vibration characteristics of a portal frame and post-Northridge 3-story SAC building are conducted, and the parameters to give desired hysteretic moment-rotation behaviors of semi-rigid connections are determined in Chapter 4. After the parameter group is selected to observe different behaviors on low-rise steel special moment resisting frame, modal, nonlinear static and nonlinear time history analysis are carried out, and results are discussed in Chapter 5.

The items listed below are the main conclusions in this thesis:

- The use of 4 force-based beam-column elements along a member is sufficient for a bare portal frame in order to capture fundamental period. When several bays and stories are present in a structure, the use of 1

force-based beam-column element along a member is sufficient in order to capture fundamental period within 1% error.

- The ratio of connection's initial stiffness to EI/L of the connecting beam, λ, is the only parameter that affects the modal analysis for the low-rise studied structures. When $\lambda = 7$, a difference up to 9% in period is observed with respect to rigid case in any frame configurations (LB or UB). When $\lambda = 15$, a difference up to 17% in period is observed with respect to rigid case in any frame configurations (LB or UB).

- For the low-rise studied structures, the influence of connection stiffness has the same level of period change for both lower bound (LB) or upper bound (UB) structures.

- When nonlinear behavior of connections are taken into account, it is observed that increased demands will be present compared to rigid case. However, if the requirements for stiffness, strength, ductility and energy dissipation are met in the codes, low-rise special moment resisting frames with semi-rigid connections can compensate more drift demands comparing rigid moment resisting frames.

- Among all investigated parameters, the frame configuration (LB or UB) and connection strength (Full or partial strength) have the most significant influence on the response of low-rise special moment resisting frames resulting into increased drift demands in excess of CP level. It is furthermore observed that pinching level (mild or severe) has less significance in this regards.

- In any frame configurations (LB or UB), mean and median of interstory drift ratios (IDR) are lower than collapse prevention (CP) level of 5%. 84th percentile of IDR does not exceed CP level of 5% for all cases except for LB cases with the parameters $\lambda = 7$ or $\lambda = 15$, $\beta = 0.75$, severe pinching with strength loss. On the other hand, 95th percentile of IDR exceeds CP level for all cases except for UB cases with the parameters $\lambda = 15$ and $\beta = 1.45$.

- UB design of structures provides more reliable structural response in the case when connection response demonstrates nonlinear behavior.

6.2 Future Recommendations

The following items listed below are the future recommendations in the field in order to give an insight to engineers and researchers:

- To conduct parametrical study on the influence of connection nonlinearity to the overall response of connection nonlinearity to the overall response of mid-rise and high-rise special moment resisting frames.
- To investigate parametrically studied influence of connection nonlinearity to the overall response of low-rise to high-rise special moment resisting frames in 3d including especially torsional effects.
- To investigate the connection influence on overall structural response under different earthquake levels and/or zones.

REFERENCES

[1] FEMA 356. Prestandard and Commentary for the Seismic Rehabilitation of Buildings. Technical report, American Society of Civil Engineers, Washington, DC, 2000.

[2] N. D. Aksoylar, A. S. Elnashai, and H. Mahmoud. The design and seismic performance of low-rise long-span frames with semi-rigid connections. *Journal of Constructional Steel Research*, 67(1):114–126, 2011.

[3] H. S. Al-Aasam and P. Mandal. Simplified Procedure to Calculate by Hand the Natural Periods of Semirigid Steel Frames. *Journal of Structural Engineering*, 139(6):1082–1087, 2013.

[4] R. Allahabadi and G. H. Powell. *DRAIN-2DX user guide*. University of California, Earthquake Engineering Research Center, 1988.

[5] American Institute of Steel Construction, Inc. *AISC 341-10. Seismic Provisions for Structural Steel Buildings*, 2010.

[6] American Institute of Steel Construction, Inc. *AISC 360-10. Specification for Structural Steel Buildings*, 2010.

[7] Ansys Inc. ANSYS Fluent UDF Manual. *Knowledge Creation Diffusion Utilization*, 15317(November):724–746, 2013.

[8] R. Bjorhovde, A. Colson, and J. Brozzetti. Classification System for Beam-to-Column Connections. *Journal of Structural Engineering (United States)*, 116(11):3059–3076, 1990.

[9] D. Bonowitz, M. Durkin, W. Gates, M. Morden, and N. Youssef. SAC 95-06. Surveys and Assessment of Damage to Buildings Affected by the Northridge Earthquake of January 17, 1994. Technical report, SAC Joint Venture, 1995.

[10] F. A. Charney, H. Iyer, and P. W. Spears. Computation of major axis shear deformations in wide flange steel girders and columns. *Journal of Constructional Steel Research*, 61(11):1525 – 1558, 2005.

[11] S.-J. Chen, C. H. Yeh, and J. M. Chu. Ductile Steel Beam-to-Column Connections for Seismic Resistance. *Journal of Structural Engineering*, 122(11):1292–1299, 1996.

[12] W.-F. Chen. *Practical Analysis for Semi-Rigid Frame Design.* Singapore ; River Edge, NJ : World Scientific, c2000., 2000.

[13] W.-F. Chen, N. Kishi, and M. Komuro. *Semi-Rigid Connections Handbook.* J. Ross Publishing civil & environmental engineering series. Ft. Lauderdale, FL : J. Ross Pub., c2011., 2011.

[14] G. G. Deierlein, A. M. Reinhorn, and M. R. Willford. Nonlinear structural analysis for seismic design. *NEHRP Seismic Design Technical Brief No*, 4, 2010.

[15] A. Elnashai, V. Papanikolaou, and D. Lee. Zeus-NL A system for inelastic analysis: User Manual. 2008.

[16] A. S. Elnashai and A. Y. Elghazouli. Seismic behaviour of semi-rigid steel frames. *Journal of Constructional Steel Research*, 29(1-3):149–174, 1994.

[17] European Committee for Standardization, Brussels, Belgium. *Eurocode 3: Design of Steel Structures*, 2005.

[18] D. A. Foutch. FEMA 355F. State of the Art Report on Performance Prediction and Evaluation of Steel Moment-Frame Buildings. Technical report, Fedral Emergency Management Agency (FEMA), 2000.

[19] A. Gupta and H. Krawinkler. Seismic demands for the performance evaluation of steel moment resisting frame structures. Technical report, The John A. Blume Earthquake Engineering Center, Department of Civil and Environmental Engineering, Stanford University. Report No. 132, 1999.

[20] Hibbett, Karlsson, and Sorensen. *ABAQUS/standard: User's Manual*, volume 1. Hibbitt, Karlsson & Sorensen, 1998.

[21] R. E. Holguin. Building department's response to EQ damage to steel frame buildings. *Journal of Performance of Constructed Facilities*, 12(4):199–201, 1998.

[22] B. Izzuddin and A. Elnashai. ADAPTIC-A Program for Adaptive Large Displacement Elastoplastic Dynamic Analysis of Steel, Concrete and Composite Frames. *Report No. ESEE*, 7:89, 1989.

[23] H. Krawinkler. FEMA 355C. State of the Art Report on Systems Performance of Steel Moment Frames Subject to Earthquake Ground Shaking. Technical report, Fedral Emergency Management Agency (FEMA), 2000.

[24] K. Lee and D. A. Foutch. SAC/BD-00/25. Performance Prediction and Evaluation of Steel Special Moment Frames for Seismic Loads. Technical report, SAC Joint Venture, 2000.

[25] E. Lui and W. Chen. Steel frame analysis with flexible joints. *Journal of Constructional Steel Research*, 8:161–202, 1987.

[26] E. M. Lui and W. F. Chen. Analysis and behaviour of flexibly-jointed frames. *Engineering Structures*, 8(2):107–118, 1986.

[27] S. A. Mahin. Lessons from Damage to Steel Buildings during the Northridge Earthquake. *Engineering Structures*, 20(4):261 – 270, 1998.

[28] B. F. Maison. *PC-ANSR: A computer program for nonlinear structural analysis*. National Information Service for Earthquake Engineering, 1992.

[29] B. F. Maison and K. Kasai. SAC/BD-99/16. Seismic Performance of 3 and 9 Story Partially Restrained Moment Frame Buildings. Technical report, SAC Joint Venture, 2000.

[30] B. F. Maison, K. Kasai, and A. Mayangarum. SAC/BD-99/17. Effects of Partially Restrained Connection Stiffness and Strength on Frame Seismic Performance. Technical report, SAC Joint Venture, 2000.

[31] S. Mazzoni, F. McKenna, M. H. Scott, G. L. Fenves, et al. OpenSees Command Language Manual. *Pacific Earthquake Engineering Research (PEER) Center*, 2006.

[32] T. Metin. A Parametric Study on the Influence of Semi-Rigid Connection Nonlinearity on Steel Special Moment Frames. Master's thesis, Middle East Technical University, Ankara, Turkey, February 2013.

[33] T. Metin and A. Saritas. A Parametric Study on the Influence of Semi-Rigid Connection Nonlinearity on Steel Special Moment Frames. In *11th International Congress on Advances in Civil Engineering, Istanbul, Turkey, October 21-25, 2014*, 2014.

[34] H. F. Ozel, A. Saritas, and T. Tasbahji. Consistent matrices for steel framed structures with semi-rigid connections accounting for shear deformation and rotary inertia effects. *Engineering Structures*, 2017.

[35] A. Pirmoz and M. M. Liu. Direct displacement-based seismic design of semi-rigid steel frames. *Journal of Constructional Steel Research*, 128:201 – 209, 2017.

[36] SAC Joint Venture Guidelines Development Committee and others. FEMA 267. Interim Guidelines: Evaluation, Repair, Modification and Design of Steel Moment Frames. Technical report, Report No. SAC-95-02, 1995.

[37] SAC Joint Venture Guidelines Development Committee and others. FEMA 267. Interim Guidelines Advisory No. 2 Supplement to FEMA-267 Interim Guidelines: Evaluation, Repair, Modification and Design of Welded Steel Moment Frame Structures. Technical report, Report No. SAC-99-01, 1999.

[38] A. Saritas and A. Koseoglu. Distributed inelasticity planar frame element with localized semi-rigid connections for nonlinear analysis of steel structures. *International Journal of Mechanical Sciences*, 96–97:216 – 231, 2015.

[39] A. Saritas and O. Soydas. Variational base and solution strategies for non-linear force-based beam finite elements. *International Journal of Non-Linear Mechanics*, 47(3):54 – 64, 2012.

[40] P. Somerville, N. Smith, S. Punyamurthula, and J. Sun. SAC/BD-97/04. Development of ground motion time histories for phase 2 of the FEMA/SAC steel project. Technical report, Report No. SAC/BD-97/04, 1997.

[41] E. L. Wilson and A. Habibullah. SAP2000 Structural Analysis Program. *Computers and Structures Inc., California*, 2002.